INTERNATIONAL ATOMIC ENERGY AGENCY
UNITED NATIONS EDUCATIONAL, SCIENTIFIC AND CULTURAL ORGANIZATION
INTERNATIONAL CENTRE FOR THEORETICAL PHYSICS
I.C.T.P., P.O. BOX 586, 34100 TRIESTE, ITALY, CABLE: CENTRATOM TRIESTE

H4.SMR/942-22

Third Workshop on
3D Modelling of Seismic Waves Generation
Propagation and their Inversion

4 - 15 November 1996

Upper Mantle Anisotropy from Surface Wave Studies

Jean-Paul Montagner

Institut Universitaire de France
Institute de Physique du Globe
Paris, France

Upper Mantle Anisotropy from Surface Wave Studies

Jean-Paul Montagner
Institut Universitaire de France
Département de Sismologie CNRS URA 195
Institut de Physique du Globe - Paris - France

November 5, 1996

Trieste
International Centre for Theoretical Physics
3rd Workshop on Three-Dimensional Modelling of Seismic Waves Generation, Propagation, and their Inversion

Introduction

I- Surface waves- normal modes

Presentation of surface waves

Importance of anisotropy

First order perturbation theory

II- Tomography of velocity and anisotropy

Forward problem

Inverse problem

III- Applications of anisotropy tomography

Global scale: mantle convection
(plate motion, continental root, flow pattern, detection of plumes, ...)

Regional scale: Tibet
(relationship with tectonics...)

Petrology

IV- Future Prospectives

Abstract

Global tomography has become very popular during the last 10 years and have provided 3-dimensional images from the surface of the Earth to its center. However, most of tomographic techniques are suffering severe limitations and approximations. A complete tomographic method usually includes the resolution of a forward problem and of an inverse problem. As far as the forward problem is concerned, it is shown in these notes how to take account of anisotropy of Earth's materials, and its influence on the phase of seismograms is explored. It is also shown that a tomographic model is not only a set of numerical values but that it is necessary to consider the structure of the data space (errors and correlations), the parameter space (*a posteriori* errors, covariance function, resolution) and the errors associated with the theoretical limitations.

With the increasing quality of seismograms provided by modern digital networks (GDSN, IDA, GEOSCOPE, IRIS), it will be possible in the future to obtain a whole family of reliable tomographic models, including V_P, V_S seismic wave velocity, anisotropic and anelastic parameters. Some applications of the anisotropic tomography are also presented.

1 Introduction

Ten years ago, the first global tomographic models were published (*Woodhouse and Dziewonski*, 1984; *Dziewonski*, 1984; *Clayton and Comer*, 1983; *Nakanishi and Anderson*, 1984; *Nataf, Nakanishi and Anderson*, 1984, 1986). Since that time, many new tomographic models were published, and a large family of techniques was made available. This important progress was made possible by the extensive use of computers which can handle very large datasets and by the availability of good quality digital seismograms recorded by seismic networks such as the International Deployment of accelerometers (*Agnew et al.*, 1976), the Global Digital Seismograph Network (*Peterson et al.*, 1977) and more recently GEOSCOPE (*Romanowicz et al.*, 1984) and IRIS (*Smith*, 1986). However, most of tomographic techniques only make use of the phase information in seismograms and very few of the amplitude, even when one works on seismic waveform (*Woodhouse and Dziewonski*, 1984). We will show in this paper, from a theoretical and practical point of view, why it is much easier to explain the phase of seismic signals than amplitude.

Therefore, global tomographic models have been improved over years by an increase in the number of data and by more general parameterizations, now including anisotropy (Radial anisotropy in *Nataf et al.* (1986); general slight anisotropy in *Montagner and Tanimoto* (1990, 1991) and to a less extent anelasticity (*Tanimoto*, 1989; *Romanowicz*, 1991; Roult et al., 1991), but there is still a major step to perform, in taking a complete account of amplitude anomalies in the most general case. There were some attempts to do so on global scale (*Tanimoto*, 1984b; *Wong*, 1989) and on a regional scale, following the works of *Snieder* (1988a,b). But, from a practical point of view, it induces inverse problems of very large size and it made it necessary to limit the parameter space to its isotropic part. We make a review of the theoretical limitations of present tomographic techniques and propose to get more insight in the investigation of anisotropy. Contrarily to the common belief, the anisotropy is not a second order effect and must be taken into account to avoid any bias on seismic velocities V_P and V_S. In order to make this paper useful for students, the different calculations are detailed in the simplest case.

The reader is referred to other authors when the generalization of this simple case is available. Finally, the practical implementation of the inverse problem is presented as well as how one can take account of errors on data and how to calculate the resolution and *a posteriori* covariance functions of parameters.

2 Presentation of surface waves and normal modes

3 An anisotropic Earth

3.1 Seismic anisotropy at all scales

The evidence of anisotropy is steadily growing during the last 30 years. It turns out that it is present at all scales. Different geophysical fields are involved in the investigation of the manifestations of anisotropy of Earth materials, mineral physics and geology for the study of the microscopic scale, and seismologists for scales larger than typically one kilometer. The different observations related to anisotropy, at different scales will be briefly reviewed.

• *Microscopic scale.*

The different minerals present in the upper mantle are anisotropic (*Peselnick et al.*, 1974). The main constituent, olivine, is strongly anisotropic; the difference of velocity between the fast axis and the slow axis is larger than 20%. Other important constituents such as orthopyroxene or clinopyroxene are anisotropic as well (> 10%) (see for example *Christensen and Lundquist*, 1982 and *Anderson*, 1989, for a review). Some other constituents such as garnet display a cubic crystallographic structure which presents a small anisotropy. Consequently, the petrological models which are assemblages of different minerals are less anisotropic than pure olivine. The amount of anisotropy is largely dependent on the percentage of these different minerals and on the mechanisms which will align the crystallographic axes according to preferred orientations. For example, the anisotropy of the pyrolitic model, mainly composed of olivine (*Ringwood*, 1975) and orthopyroxene, will depend on the relative orientation of their crystallographic axes (*Christensen and Lundquist*, 1982). However, through the mechanisms of lattice preferred orientation, its anisotropy can be larger than 10 % (*Montagner and Anderson*, 1989a). For competing petrological models such as piclogite (*Anderson and Bass*, 1984, 1986), where the percentage of olivine is smaller, and of garnet larger, the amount of anisotropy will be smaller (about 5%).

As depth is increasing, the minerals will undergo phase transformations. It is now widely recognized that with increasing pressure and temperature, the crystallographic structure evolves towards a more closely packed structure, more isotropic, such as cubic structure. For example, olivine transforms towards β-spinel and then γ-spinel in the upper transition zone (400-660km of depth) and towards perovskite and magnesiowustite in the lower mantle. The ideal structure of perovskite is cubic, but can display some important distortion, which can induce some anisotropy at least in the uppermost lower mantle. Therefore, at microscopic scales, we can conclude that earth materials in the upper mantle are strongly anisotropic, but that the anisotropy tends to decrease as depth is increasing.

At slightly larger scales, the scale of rock samples, several studies of anisotropy were undertaken. Dunite, which is also pure olivine displays a large anisotropy (*Peselnick and Nicolas*, 1978). Moreover, this anisotropy is coherent in whole massifs of ophiolites over several tens of kilometers (*Nicolas*, 1993; *Vauchez and Nicolas*, 1991). At larger wavelengths, anisotropy is also present and can be investigated from seismic observations.

• *Macroscopic scale*:

Different and independent seismic datasets make evident that the effect of anisotropy is not negligible for explaining the propagation of seismic waves inside the Earth.

From a seismological point of view, the evidence that the upper mantle is anisotropic is steadily growing resulting from an increased number of observations implying anisotropy. The early

evidence was the discrepancy between Rayleigh and Love wave dispersion (*Anderson*, 1961; *Aki and Kaminuma*, 1963) and the azimuthal dependence of P_n velocities (*Hess*, 1964). Azimuthal variations are now well documented for different areas in the world for body waves and surface waves.

Body waves:

For body waves, this kind of informations results from the investigation of the splitting in teleseismic shear waves such as SKS (*Vinnik et al.*, 1984; 1989a,b; 1991; 1992), ScS [*Ando*, 1984; *Fukao*, 1984) and S (*Ando and Ishikawa*, 1982; *Bowman and Ando*, 1987). These waves are shown to provide an excellent lateral resolution, if we restrict to the deep upper mantle (i.e. below crust). And among these different observations, the splitting information derived from SKS is the less ambiguous and has been extensively used in teleseismic anisotropy investigations (*Silver and Chan*, 1988; *Vinnik et al.*, 1989a,b; *Ansel and Nataf*, 1989...). The drawback of this technique is that it is almost impossible to locate at depth the anisotropic area.

Surface waves:

Surface waves are also well suited for investigating upper mantle anisotropy. Two kinds of observable anisotropy can be considered. The first one results from the well-known discrepancy between Love and Rayleigh waves (*Aki and Kaminuna*, 1961; *Anderson*, 1961). The so-called "polarization" anisotropy or radial anisotropy. In order to remove this discrepancy, it is necessary consider a transversely isotropic model with a vertical symmetry axis. This kind of anisotropy is characterized by 5 anisotropic parameters plus density (*Anderson*, 1961). **However, *Levshin and Ratnikova* (1984) showed that lateral heterogeneity can lead to a Rayleigh-Love discrepancy and that we must be cautious about the interpretation of this discrepancy in terms of anisotropic model. (On a global scale, *Nataf et al.* (1984; 1986) have derived by the simultaneous inversion of Rayleigh and Love wave dispersion, the geographical distributions of S-wave anisotropy at different depths assuming transverse isotropy with vertical symmetry axis.**

The second kind of observable anisotropy is the azimuthal anisotropy which was directly derived from the azimuthal variation of phase velocity. It was observed for the first time on surface waves by *Forsyth* (1975) in Nazca plate. Since these pioneering studies, global and regional models have been derived for both kinds of anisotropy (*Mitchell and Yu*, 1980; *Montagner*, 1985). *Tanimoto and Anderson* (1985) obtained a global distribution of the Rayleigh wave azimuthal anisotropy at different periods. On a regional scale, several tomographic investigations report the existence of azimuthal anisotropy in the Indian Ocean (*Montagner*, 1986a), in the Pacific ocean (*Suetsugu and Nakanishi*, 1987; *Nishimura and Forsyth*, 1987, 1988) and in Africa (*Hadiouche et al.*, 1988). *Lévêque and Cara* (1985), *Cara and Lévêque* (1988) used higher mode data to display anisotropy under the Pacific Ocean and North America down to at least 300km.

However, the "polarization" anisotropy (or radial anisotropy) and the azimuthal anisotropy are two different manifestations of a same phenomenon, the anisotropy of the upper mantle. *Montagner and Nataf* (1986) derived a technique which makes it possible to explain simultaneously these two forms of seismically observable anisotropy. The principles of this technique will be described in section 2.5, for the most general case of anisotropy (at the condition that it is small). The method can be slightly simplified by introducing only one symmetry axis (7 independent

anisotropic parameters) and it was coined "Vectorial tomography" (*Montagner and Nataf*, 1988). It was applied to the investigation of the Indian Ocean (*Montagner and Jobert*, 1988). Moreover, they showed that, paradoxically, in order to explain their data in the Indian Ocean, a parameterization with anisotropy requires less parameters than a parameterization with only isotropic terms. Therefore, contrarily to body waves, surface waves enable to locate at depth anisotropy but, so far, its lateral resolution (several thousands kilometers) is very poor.
Finally, anisotropy has not only an effect on the phase of seismograms, but also an effect on its amplitude. Due to the coupling between surface wave modes, one of the less ambiguous effect is the fact that Love waves can be present on the vertical and the radial component (*Park and Yu*, 1993).
Therefore, there is no doubt on the existence of anisotropy and it cannot be considered as a second order effect. It is present at different scales and at different depths. We note that it tends to decrease as wavelength is increasing, from 20% at microscopic scale down to $1-2\%$ at very large wavelengths. Several conditions must be encountered in order to get an observable anisotropy at long period and large wavelength. The material must be microscopically anisotropic, there must be some efficient mechanism of preferred orientation, which aligns fast axis (or slow axis) of minerals. There must be in addition an efficient strain field, with a long wavelength coherency, for spatial wavelengths Λ_S such that $\Lambda_S \gg \lambda$ (where λ is the wavelength of the wavè under consideration). This kind of condition is usually encountered in tectonically active areas.
Several questions arise:
- How biased are models when anisotropy is not taken into account?
- How can we simultaneously explain the different observations of surface wave anisotropy, radial anisotropy and azimuthal anisotropy?
- How can it be related to body wave anisotropy?

3.2 First order perturbation theory

The basic equation which governs the displacement $\mathbf{u}(\mathbf{r},t)$ is the elasto-dynamic equation (*Woodhouse and Dahlen* , 1978):

$$\rho_0 \frac{d^2 u_i}{dt^2} = \sum_j \sigma_{ij,j} + f_{Si} + f_{Ei} \tag{1}$$

f_{Si} et f_{Ei} represent respectively the whole ensemble of applied internal and external forces. Generally, by neglecting advection terms, this equation is written:

$$(\rho_0 \partial_{tt} - L)\mathbf{u}(\mathbf{r},t) = \mathbf{f}(\mathbf{r},t) \tag{2}$$

where L is an integro-differential operator and f expresses all internal forces applied in r at time t. We assume that f is equal to 0 for $t < 0$. In the elastic case, there is a linear relationship between σ_{ij} and the strain tensor ϵ_{kl}. $\sigma_{ij} = \sum_{kl} \Gamma_{ijkl}\epsilon_{kl}$ (+ terms related to the initial stress). Γ_{ijkl} is a 4^{th}-order tensor. By using the different

symmetry conditions $\Gamma_{ijkl} = \Gamma_{jikl} = \Gamma_{ijlk} = \Gamma_{klij}$, it is easily shown that the tensor Γ has 21 independent elastic moduli.
Let us assume that the solution $\mathbf{u}(\mathbf{r}, t)$ of the equation is known for a reference Earth model M_0, with its corresponding operator L_0.

$$\rho_0 \partial_{tt} \mathbf{u}(\mathbf{r}, t) = L_0 \mathbf{u}(\mathbf{r}, t) \tag{3}$$

In the simple plane case (fundamental modes, no coupling between branches of Rayleigh and Love waves), the frequency shift, for a constant wavenumber k can be rewritten:

$$\delta\omega|_k = -\frac{1}{2\omega} \frac{\langle \mathbf{k}|\mathbf{E}^{\mathbf{T}}\, \mathbf{\Gamma}\, \mathbf{E}|\mathbf{k}\rangle}{\langle \mathbf{k}|\mathbf{k}\rangle} \tag{4}$$

Instrumental Point of view

- short period seismology

$T < 1\,s \Leftrightarrow f > 1\,Hz$

- Long period seismology

$T > 20\,s \Leftrightarrow f < 0.05\,mHz$

Revolution

- Broadband Seismology

$0.05\,s. < T < 3600\,s.$

$20\,Hz. > f > 0.3\,mHz$

well calibrated seismogram

Chile Earthquake

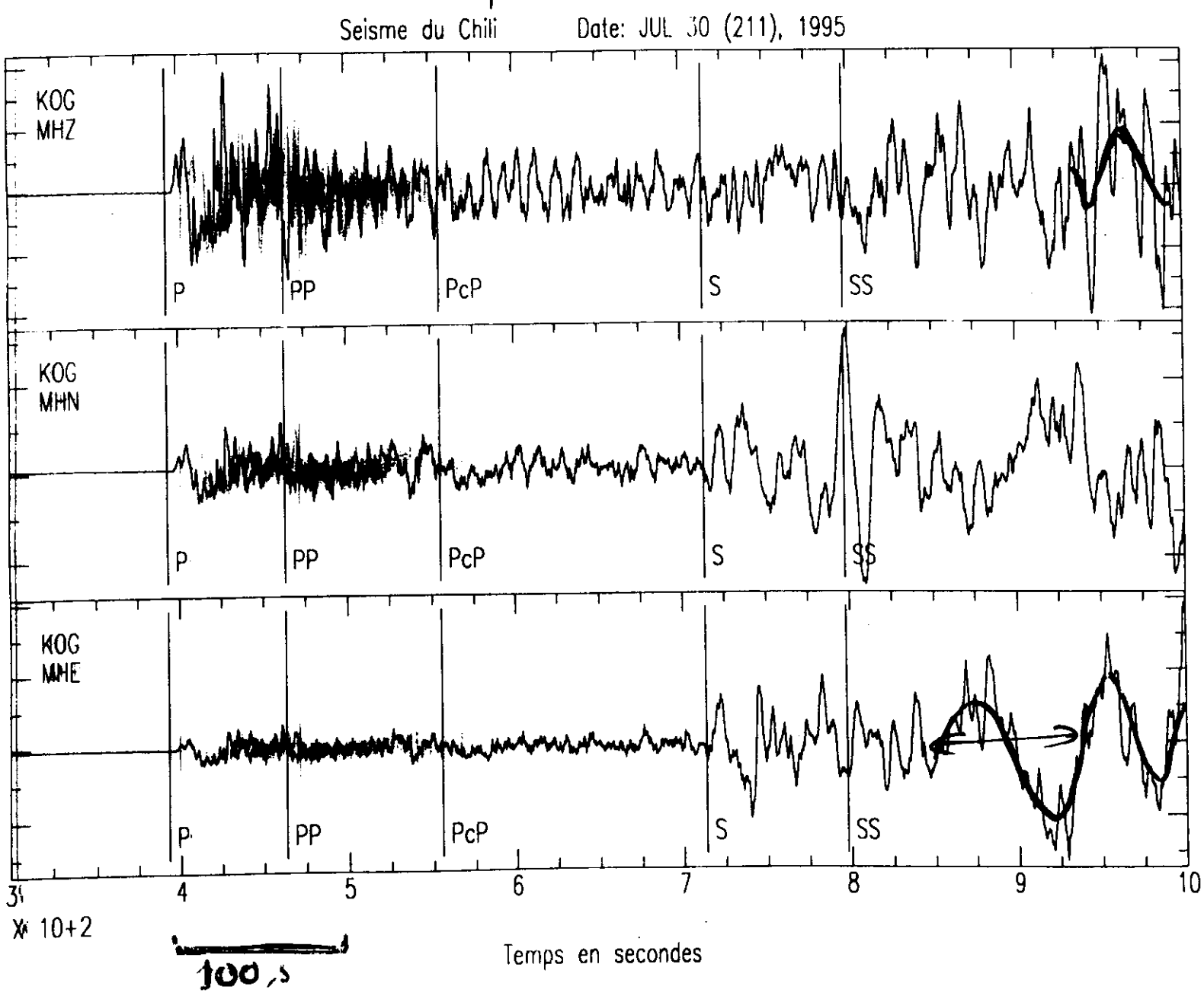

Macquarie Earthquake - May 1989

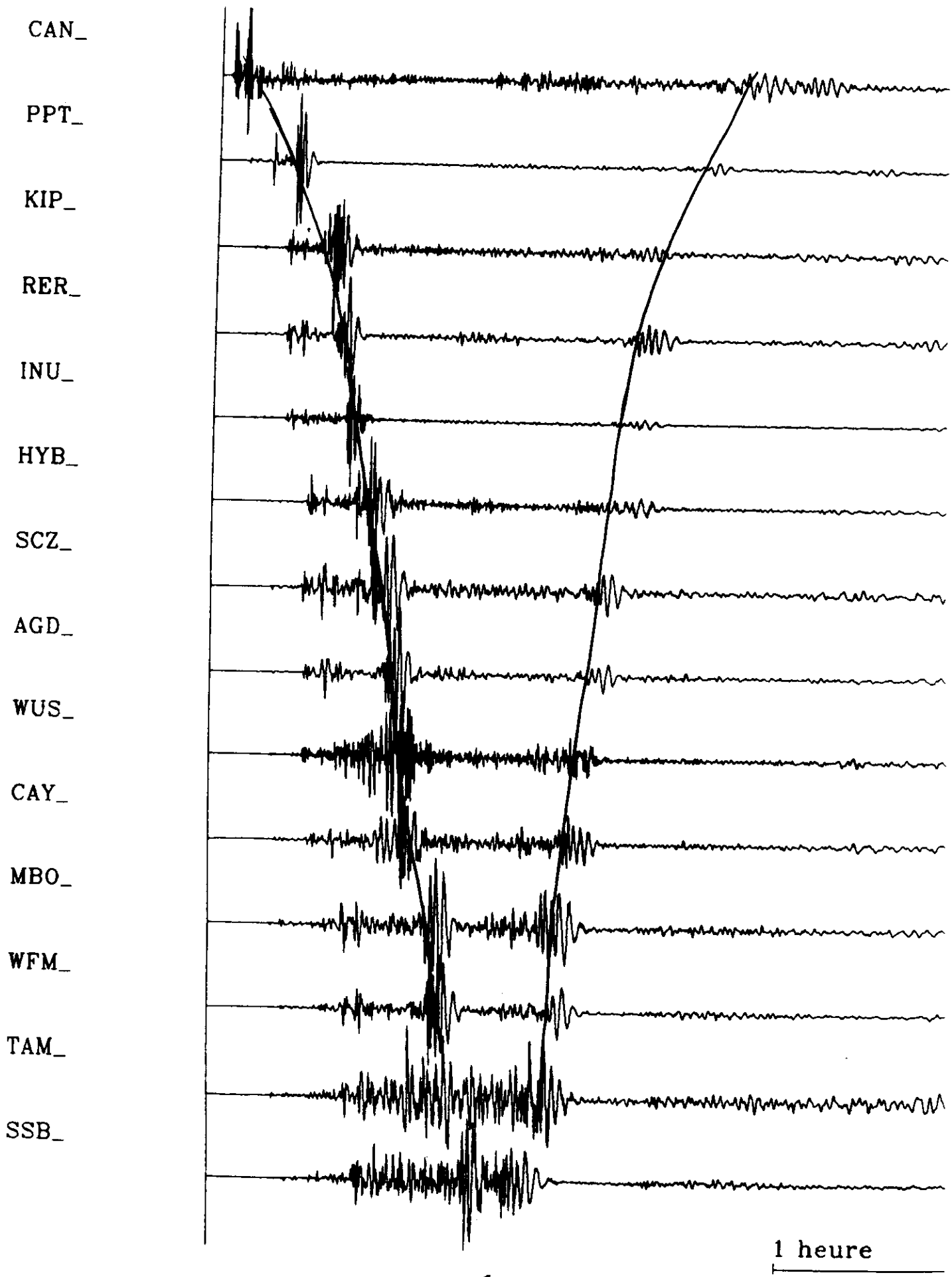

u displacement

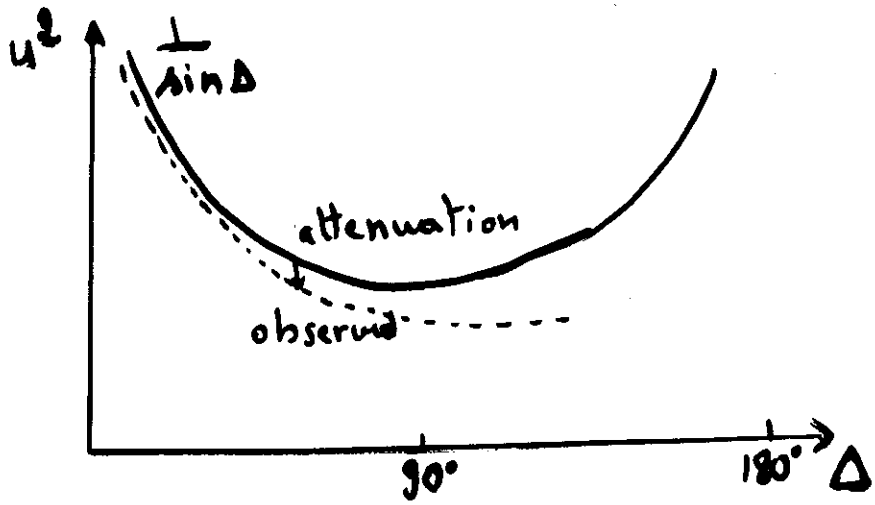

$$u \propto \frac{1}{\sqrt{\sin\Delta}}$$

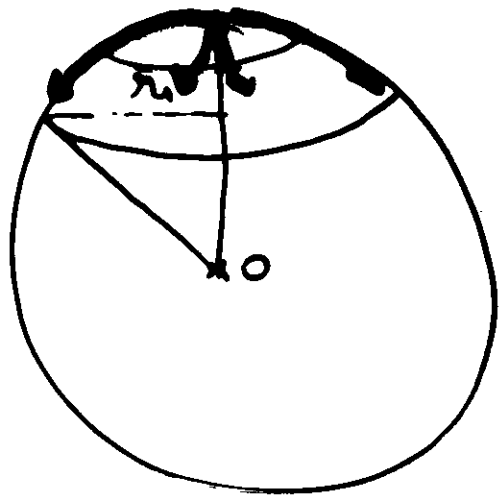

$$u_1^2 \cdot 2\pi r_1 = u_2^2 \cdot 2\pi r_2 = \text{const}$$

$$u_1^2 \propto \frac{1}{r_1}$$

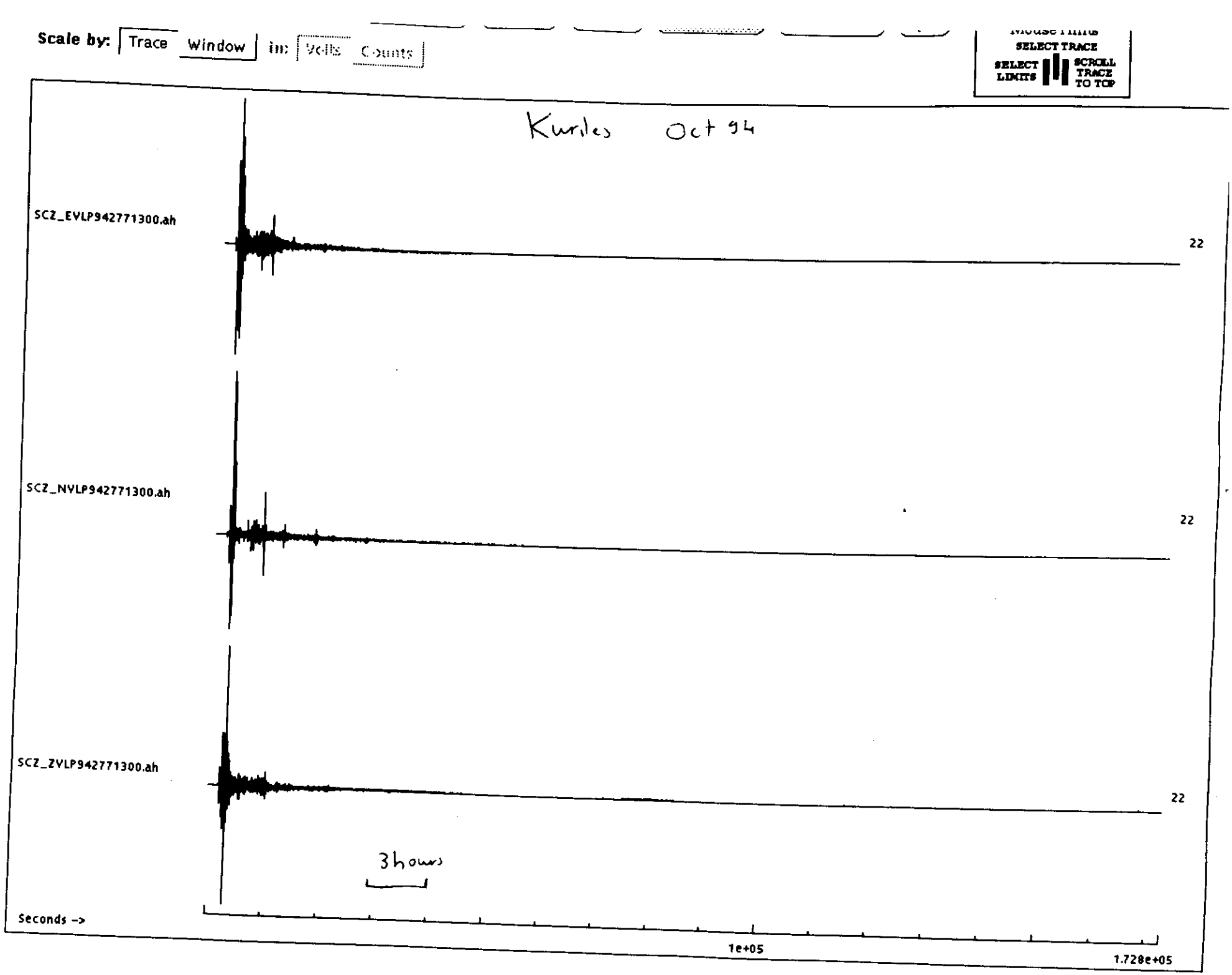
Scale by:
Trace
Window
in:
Volts
Counts
SELECT TRACE
SELECT LIMITS
SCROLL TRACE TO TOP
Kurile Oct 94
SCZ_EVLP942771300.ah
22
SCZ_NVLP942771300.ah
22
SCZ_ZVLP942771300.ah
22
3hours
Seconds ->
1e+05
1.728e+05

Horizontal Plane

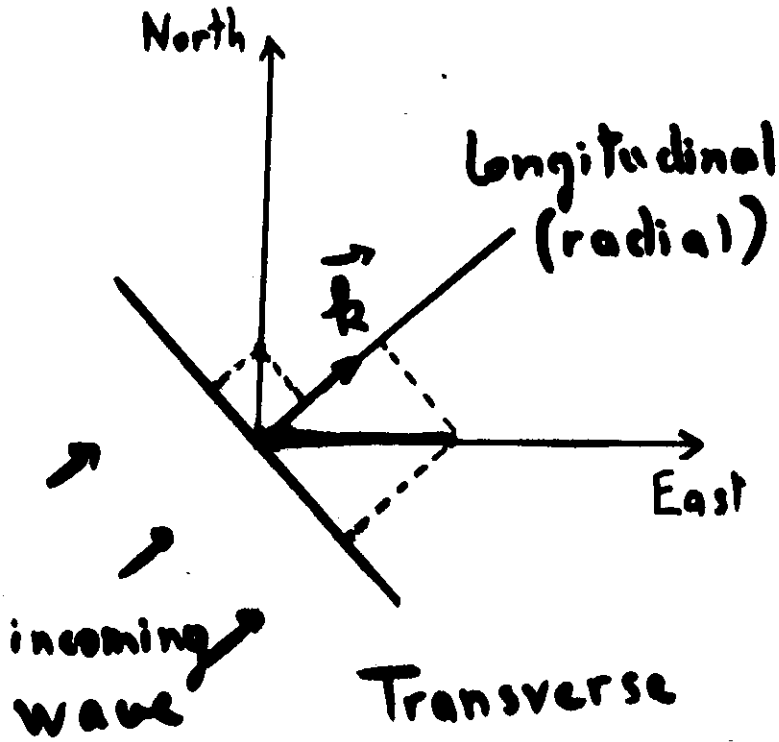

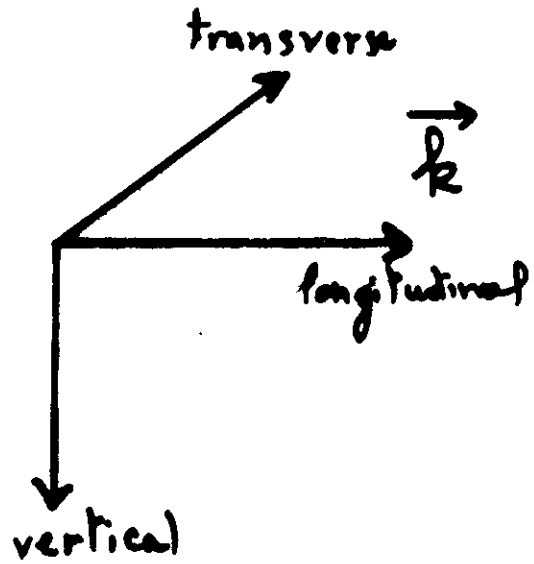

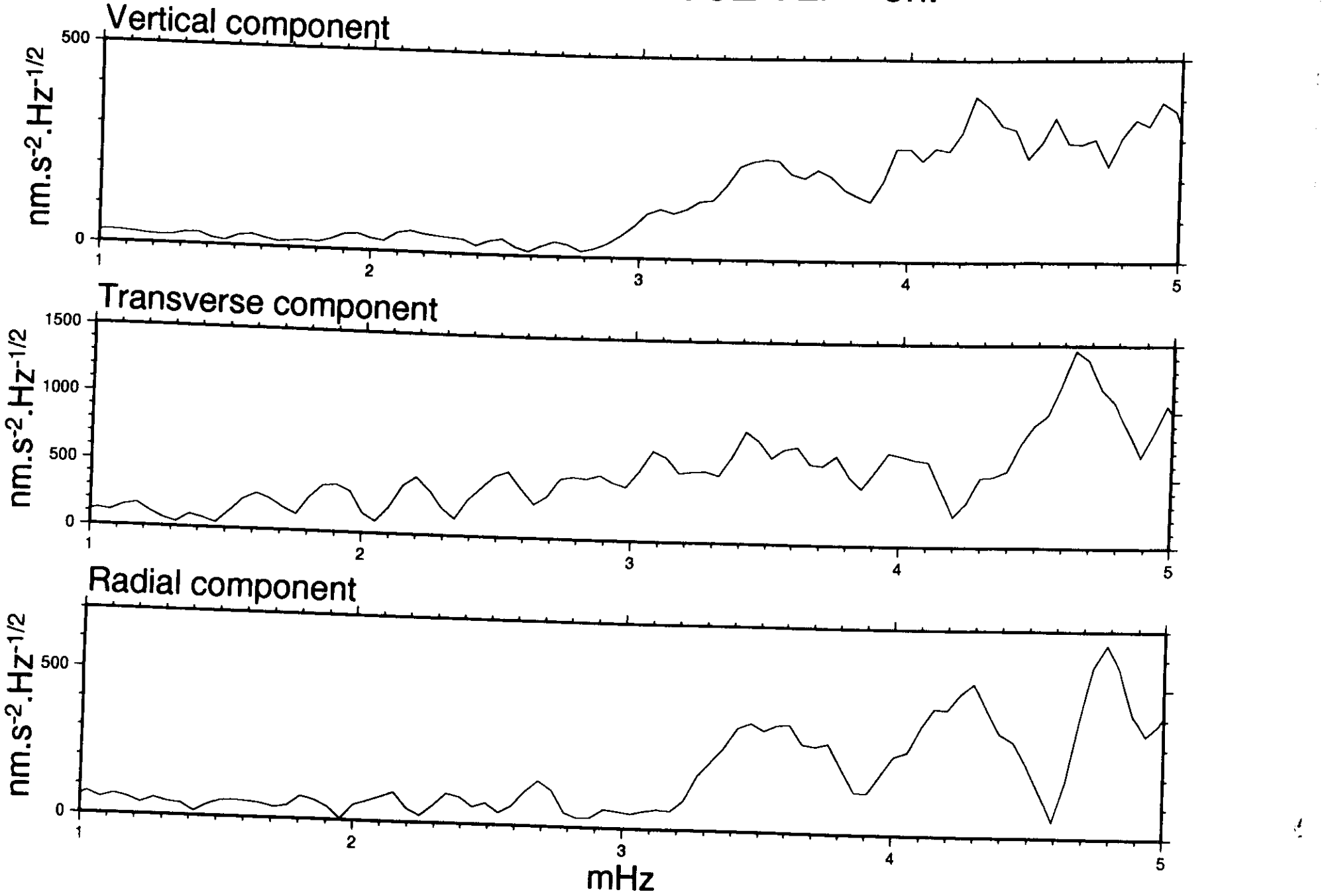
KURIL 94 277 - SCZ VLP - 3h.
Vertical component
nm.s-2.Hz-1/2
500
0
1
2
3
4
5
Transverse component
nm.s-2.Hz-1/2
1500
1000
500
0
1
2
3
4
5
Radial component
nm.s-2.Hz-1/2
500
0
1
2
3
4
5
mHz

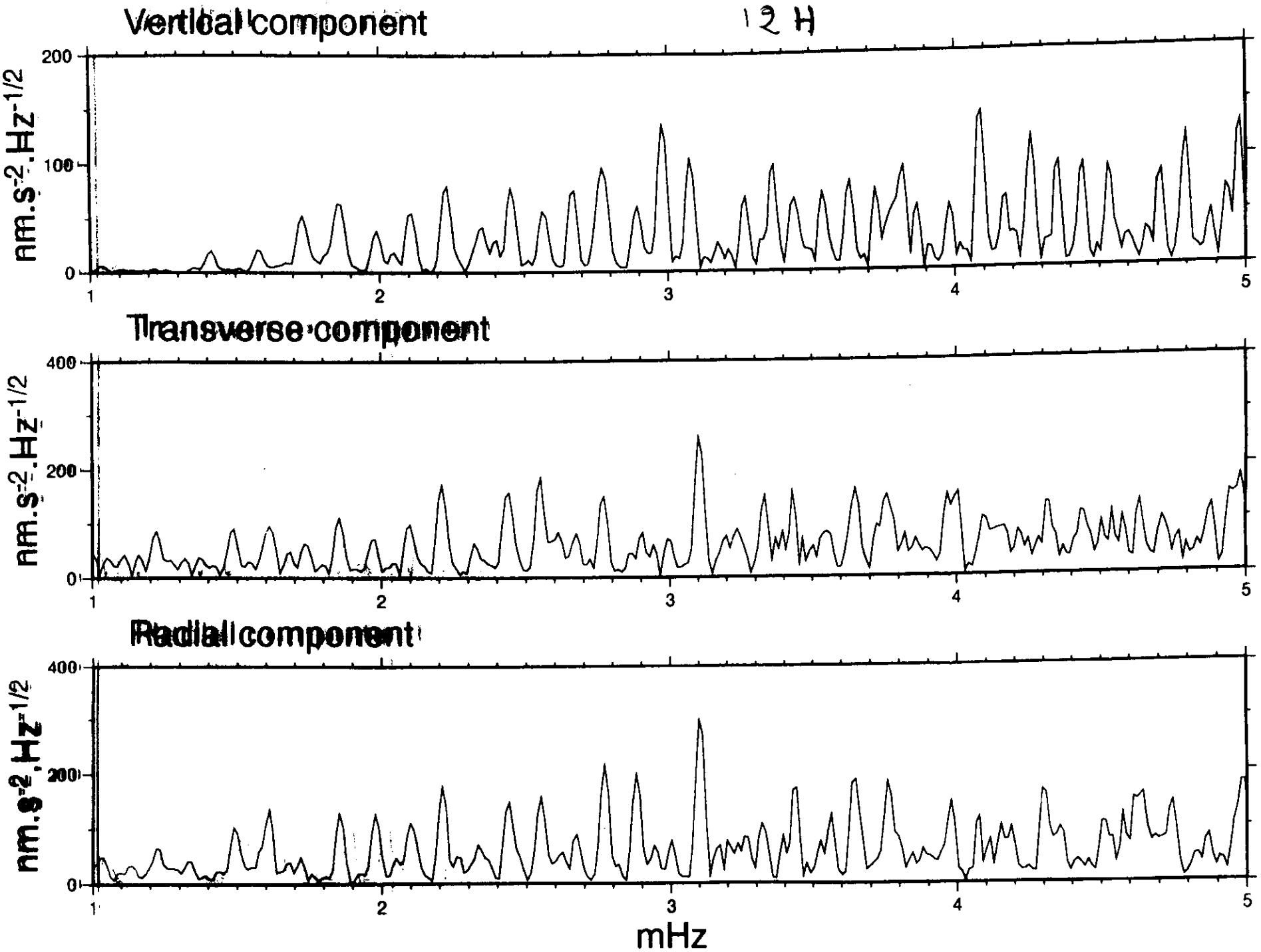
Vertical component
12 H
200
100
0
nm.s-2.Hz-1/2
1
2
3
4
5
Transverse component
400
200
0
nm.s-2.Hz-1/2
Radial component
400
200
0
nm.s-2.Hz-1/2
mHz

KURIL 94 277 - SCZ VLP - 36h.

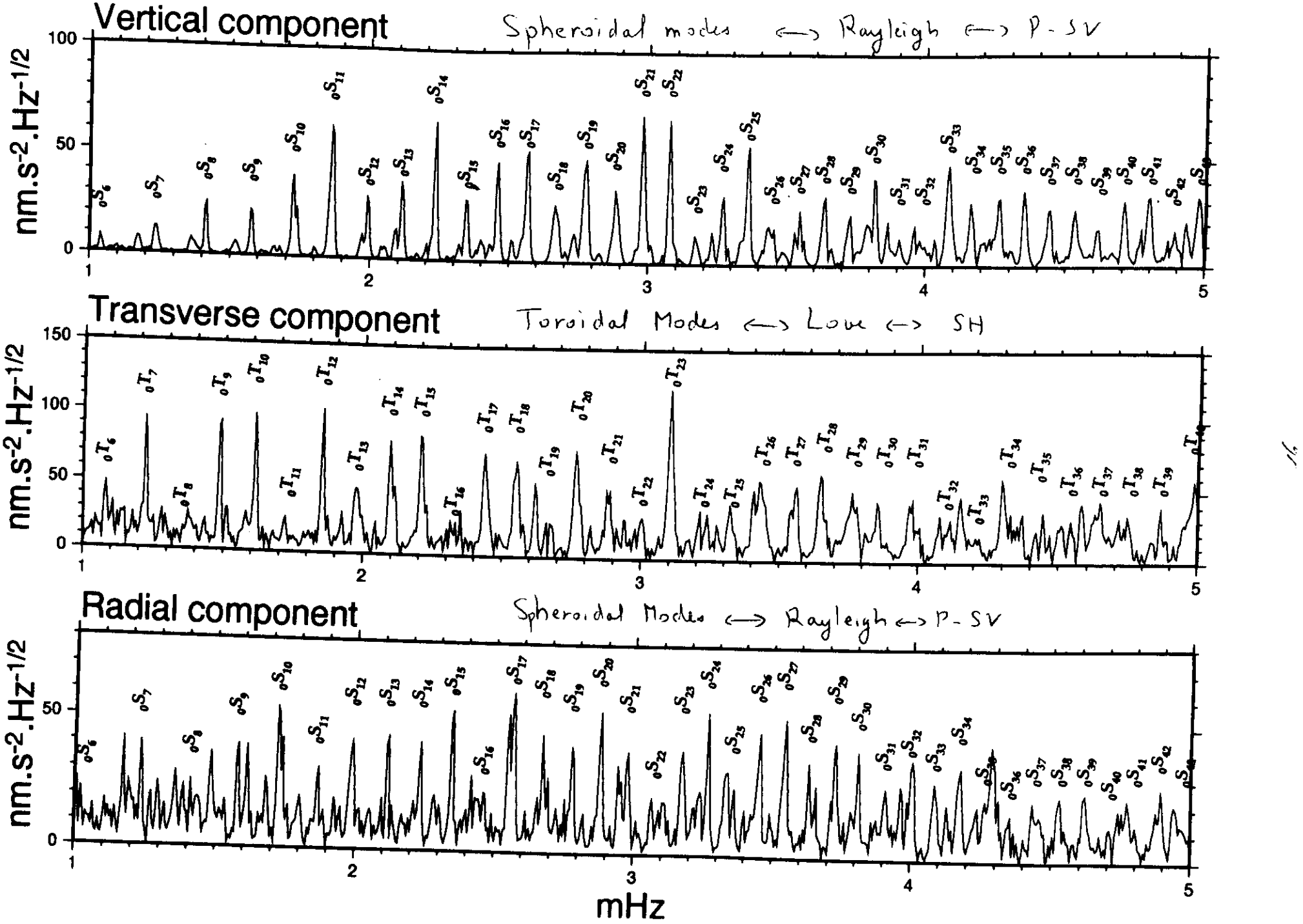

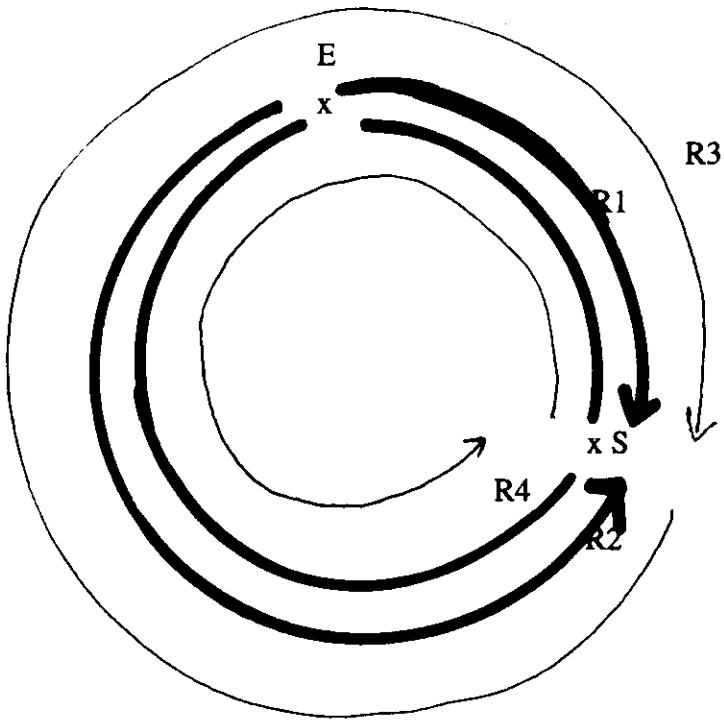

Eigenperiods $_{n}T_{l}^{m}$

n radial order

l angular order

m azimuthal order (but degeneracy of periods in a spherically symmetric reference Earth Model)

Spheroidal Modes ⟺ Rayleigh Waves ⟺ P, SV

$_{0}S_{2}$ 3000s. $_{0}S_{40}$ 210s

Toroidal Modes ⟺ Love Waves ⟺ SH

$_{0}T_{2}$ 2600s. $_{0}T_{40}$ 200s

Elasto-dynamic equation

$$\rho \frac{\partial^2 u_i}{\partial t^2} = \sum_{j=1}^{3} \frac{\partial}{\partial x_j} \sigma_{ij} + \rho g_i \; (+ f_i + \ldots)$$

ρ density
u_i displacement
σ_{ij} stress tensor
ρg_i gravity
f_i external forces

$$\rho \ddot{u} = \nabla \sigma + f$$

Ⓗ Elastic medium

$$\sigma_{ij} = c_{ijkl}\, \varepsilon_{kl} \quad \text{(Hooke's law)}$$

Anelasticity ?

$$c_{ijkl} = c^{elast}_{ijkl} \left(1 + i\, Q^{-1}_{ijkl}\right)$$

C_{ijkl} 81 elements

Symmetries of σ_{ij}, ε_{kl} : $c_{ijkl} = c_{jikl} = c_{ijlk}$

Symmetry of strain energy $W = \frac{1}{2} \sigma_{ij} \varepsilon_{ij} = \frac{1}{2} c_{ijkl} \varepsilon_{kl} \varepsilon_{ij}$

$$c_{ijkl} = c_{klij}$$

21 independent elements

Surface waves in isotropic medium

2 independent solutions

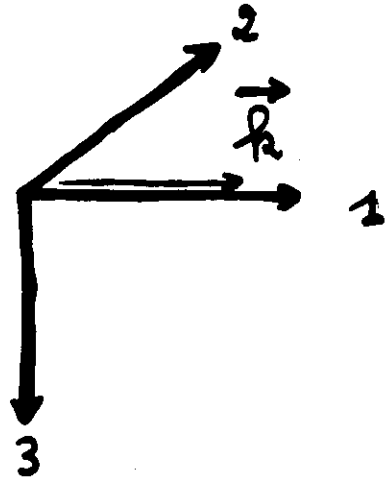

Rayleigh waves

$$\vec{u}_R(r,t) = \begin{pmatrix} V(z) \\ 0 \\ iU(z) \end{pmatrix} e^{i(k_R x - \omega t)}$$

Love waves

$$\vec{u}_L(r,t) = \begin{pmatrix} 0 \\ W(z) \\ 0 \end{pmatrix} e^{i(k_L x - \omega t)}$$

Dispersed waves $C(\omega) = \frac{\omega}{k}$

$T_2 > T_2$

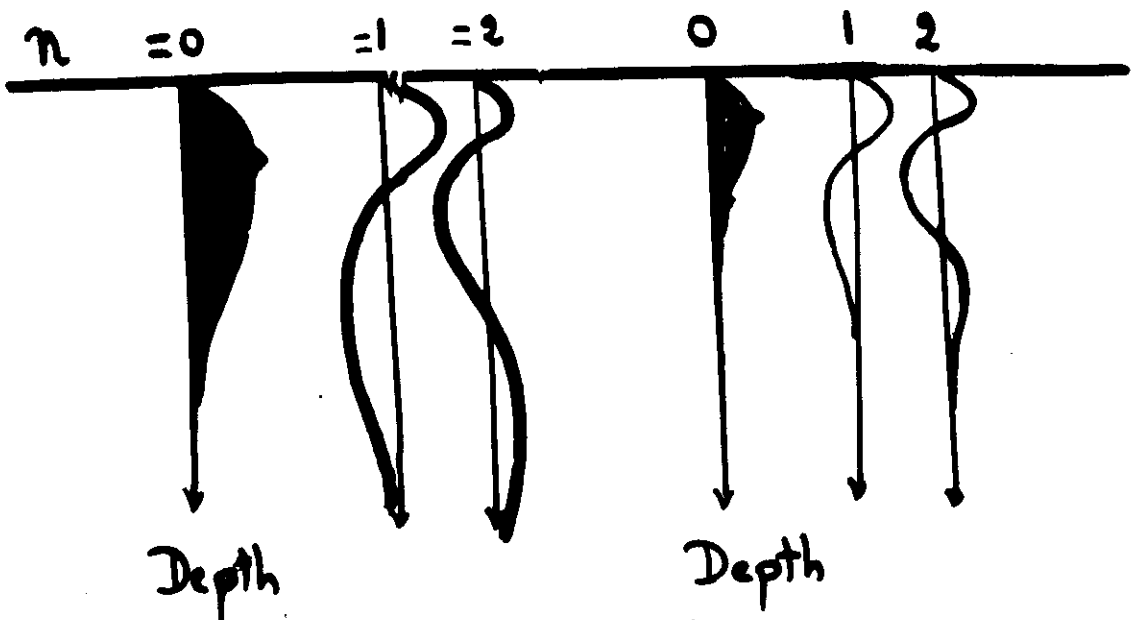

$$\rho \ddot{u}_i = \frac{\partial}{\partial x_j}\left(c_{ijkl}\,\varepsilon_{kl}\right) + \rho g_i$$

(H) $c_{ijkl} = \overset{\circ}{c}_{ijkl} + \delta c_{ijkl}$

$\overset{\circ}{c}_{ijkl}$ → isotropic

δc_{ijkl} → small

(or transversely isotropic with vertical symmetry axis)

Approach.

1 - We solve the equation for the isotropic part

$$\rho \ddot{u}_i = \frac{\partial}{\partial x_j}\left(\overset{\circ}{c}_{ijkl}\,\varepsilon_{kl}\right) + \rho g_i \Leftrightarrow \underline{\rho \ddot{\vec{u}} = \overset{\circ}{\mathcal{L}}\vec{u} + \rho \vec{g}}$$

Decoupling P-SV → **Rayleigh** ; SH → **Love**

2. We apply first order perturbation theory to anisotropy

$\mathcal{L}_\circ + \delta\mathcal{L}$

Why do we need step 2 ?

IMPORTANCE OF ANISOTROPY

It is present at all scales.

It is the rule not the exception

- Microscopic scale
- Macroscopic scale

  Body waves

  Surface waves

Mechanisms of preferred orientation

Anisotropy is not a second order effect

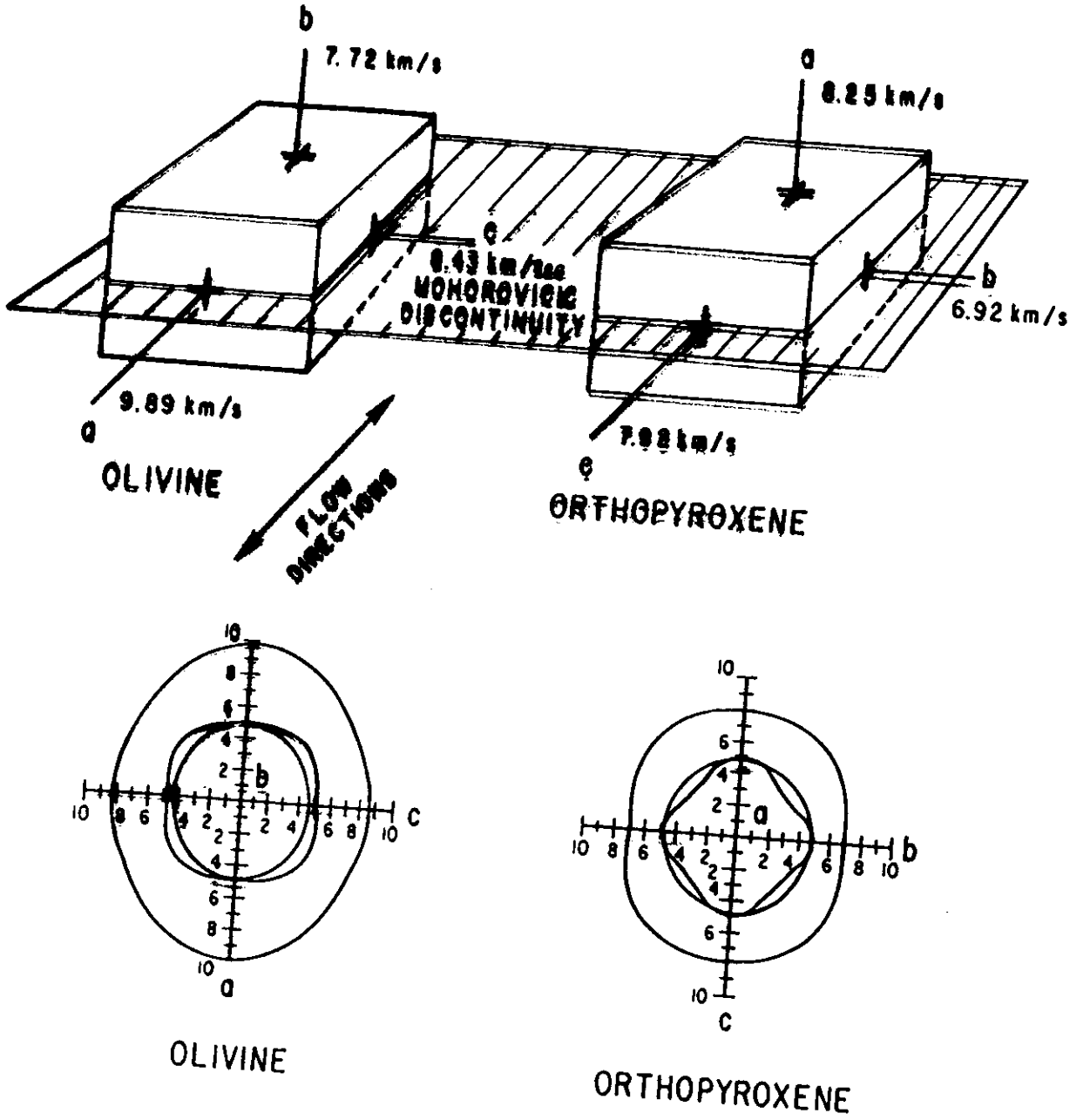

Olivine and orthopyroxene orientations within the upper mantle showing compressional velocities for the three crystallographic axes, and compressional and shear velocities in the olivine *a*-*c* plane and orthopyroxene *b*-*c* plane (after Christensen and Lundquist, 1982).

(Anderson, 1989)

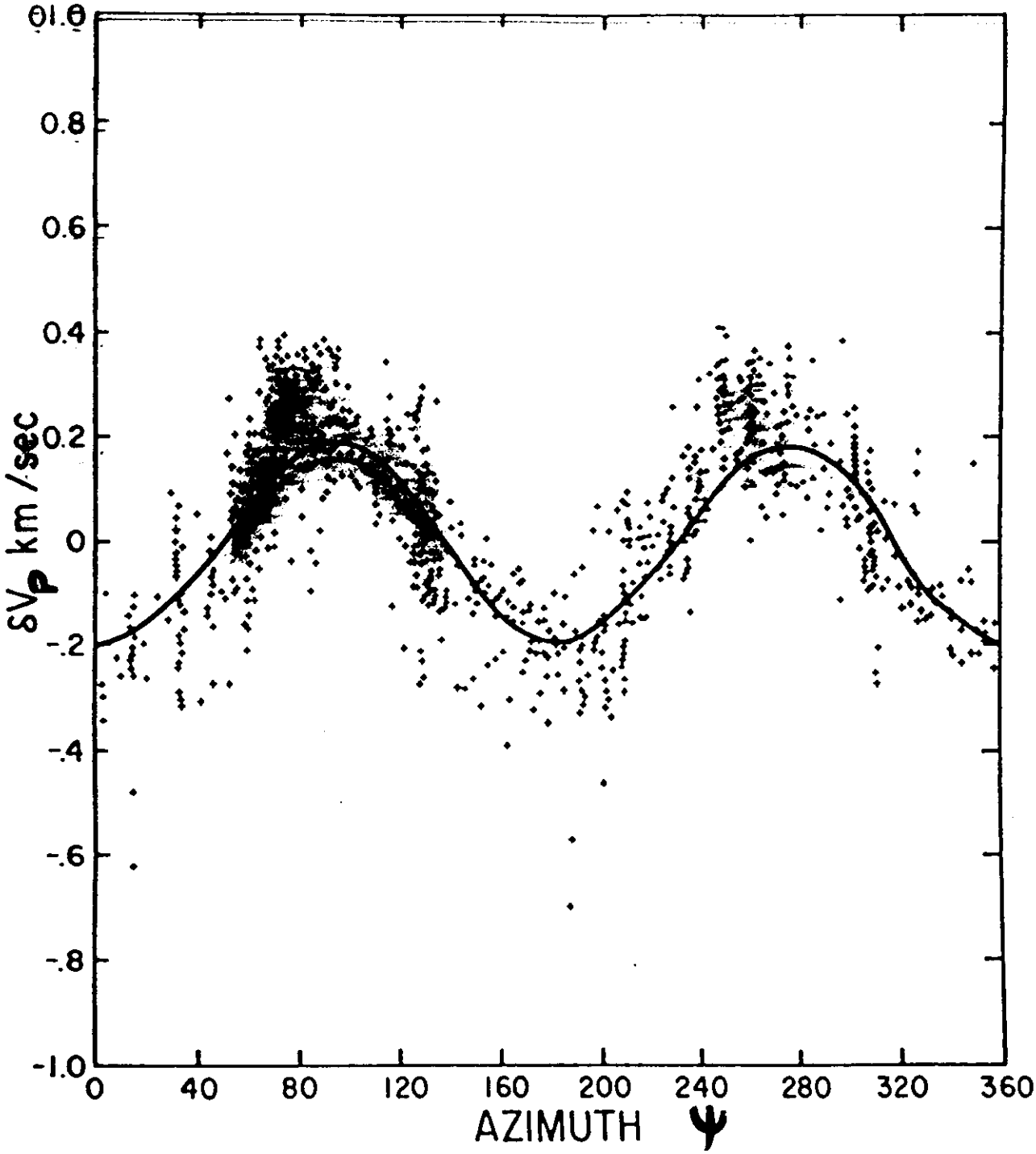

Azimuthal anisotropy of Pn waves in the Pacific upper mantle. Deviations are from the mean velocity of 8.159 km/s. Data points from seismic-refraction results of Morris and others (1969). The curve is the velocity measured in the laboratory for samples from the Bay of Islands ophiolite (Christensen and Salisbury, 1979).

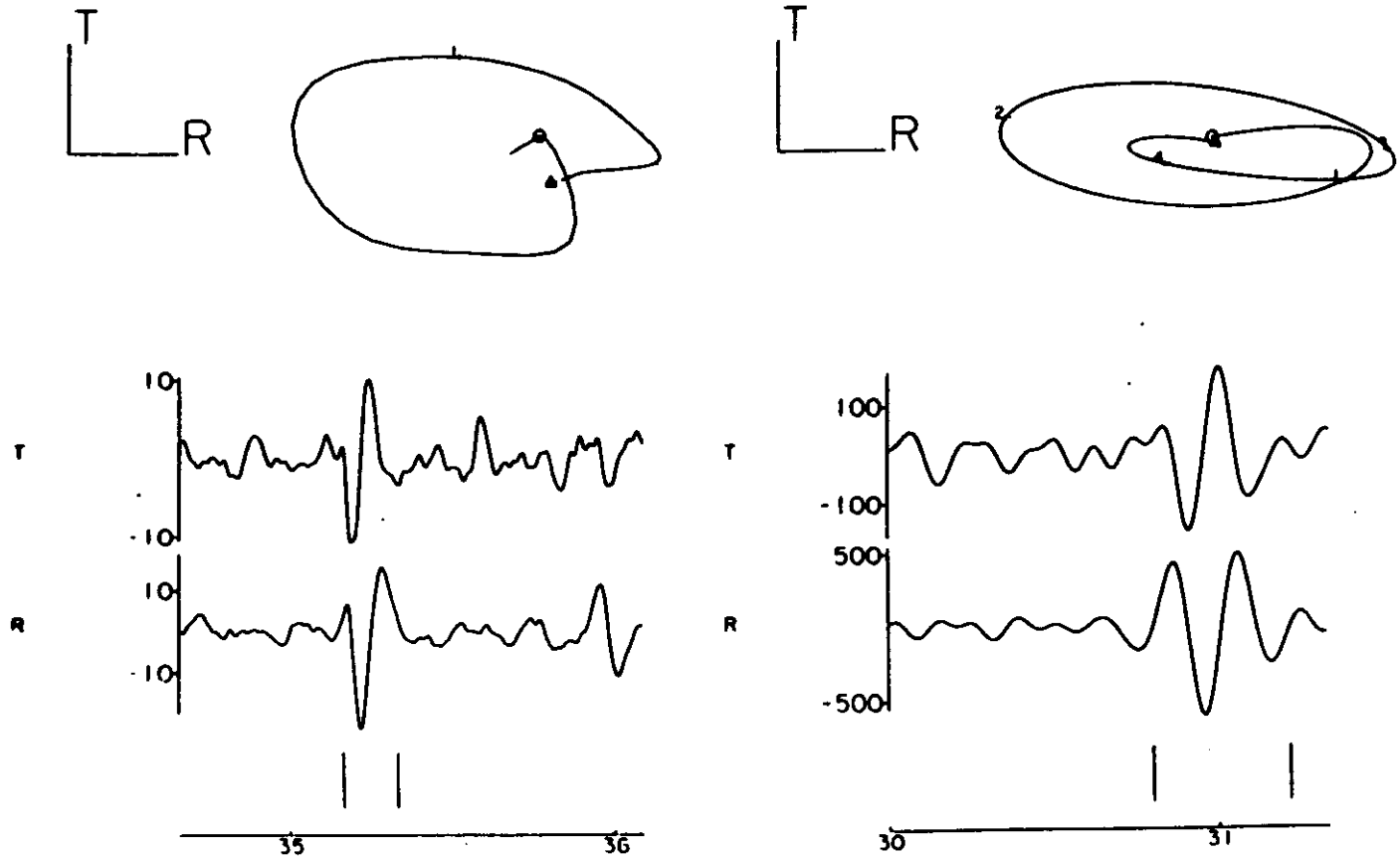

Two examples of SKS splitting observations at station SSB (France). The particle motion plots corresponding to the transverse (T) and radial (R) components are given for each case.
Event (2) occurred on May 26, 1986 at 19h 06mn 15.9 sec in the Fidji Tonga area (depth 538 km, epicentral distance 154.5°).
Event (22) occurred on May 1, 1988 at 23 hours 06mn and 30.7 sec in the Sandwich Island region (depth 114 km, epicental distance 104.6°) . From Vinnik et al., 1989.

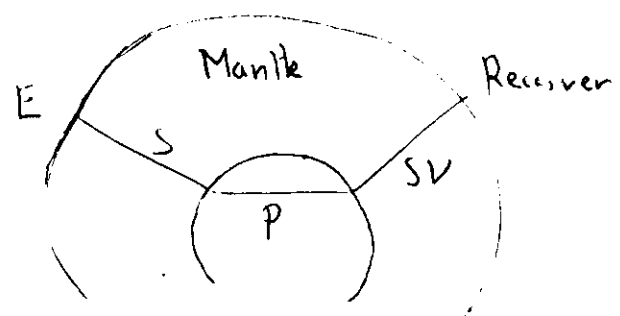

"POLARIZATION" ANISOTROPY

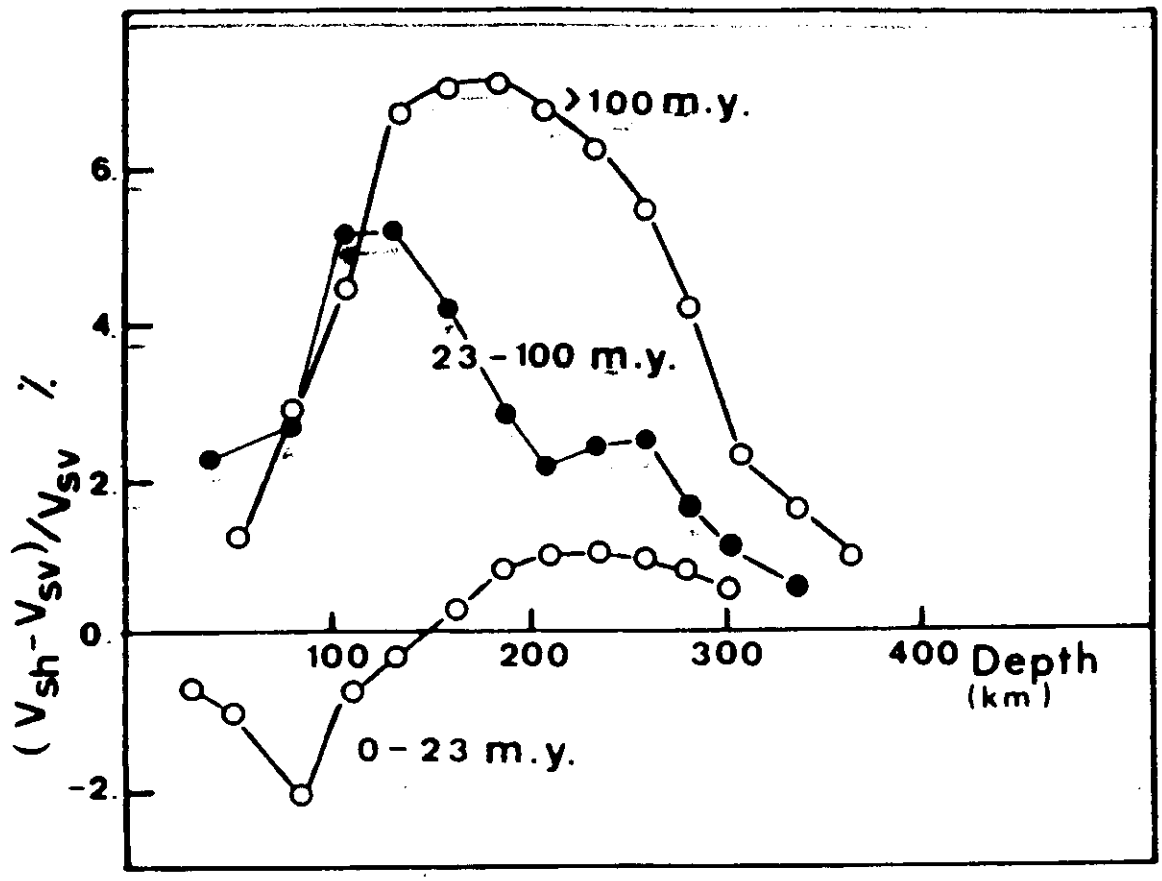

Fig. 11. Variation of polarization anisotropy with the age of the sea floor and with depth.

(Montagner, 1985)

Rayleigh $\longrightarrow V_{SV}(r)$

Love $\longrightarrow V_{SH}(r)$

In an isotropic medium $V_{SV}(r) = V_{SH}(r)$

$V_R \equiv V_{R_0} + x_1 \cos 2(\psi - \psi_2)$ of period T

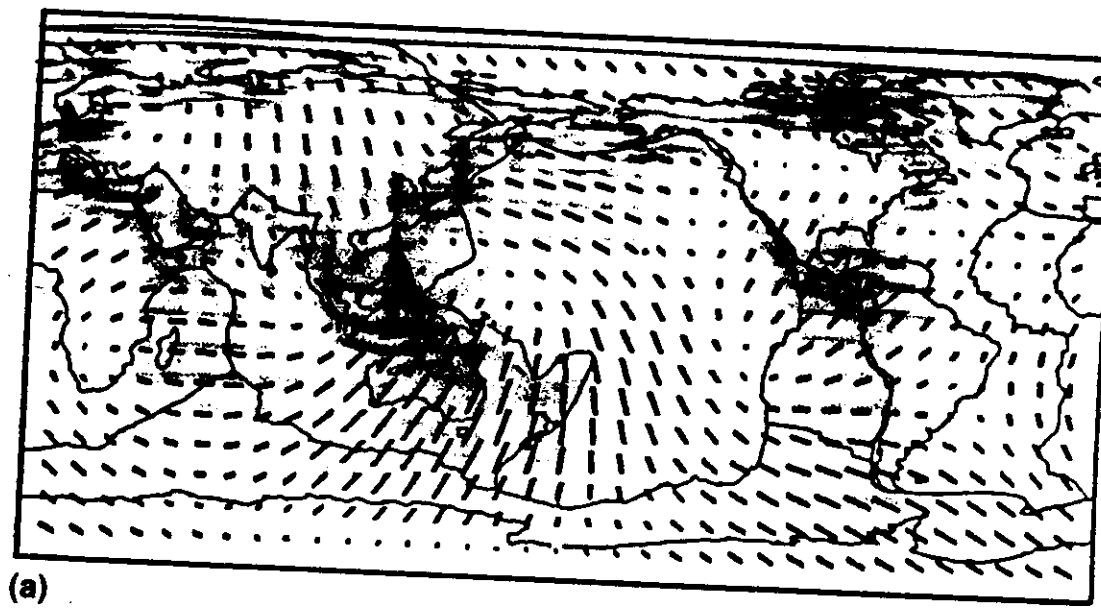

(a)

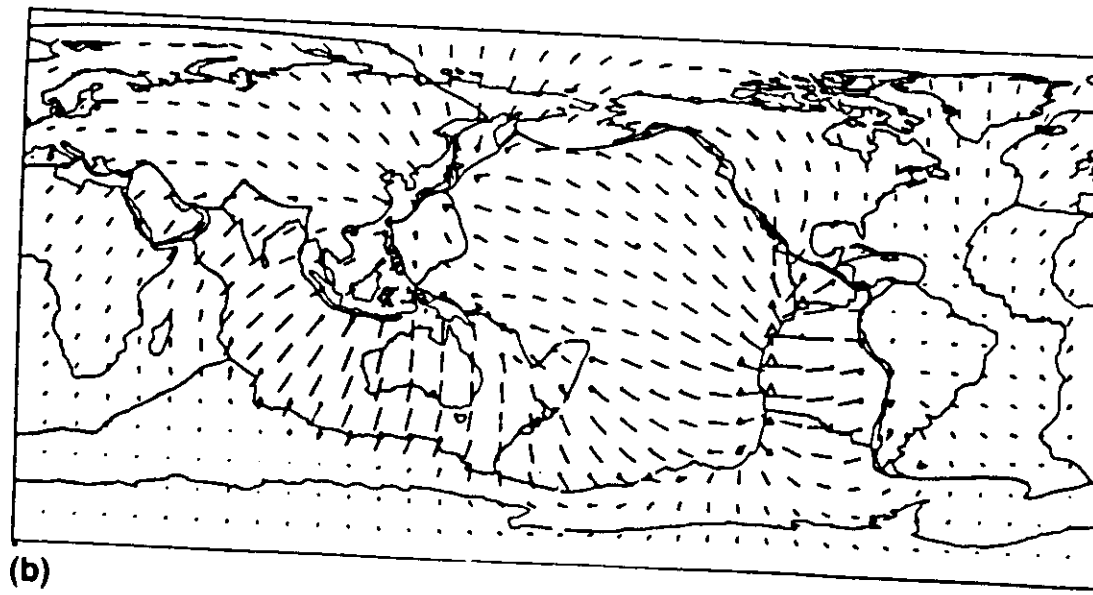

(b)

FIGURE 15-12
(a) Azimuthal anisotropy of 200-s Rayleigh waves. The map includes cos 2Θ, sin 2Θ and $l = 1, 2$ and 3 terms. The lines indicate the fast phase velocity direction. The length of the lines is proportional to the anisotropy (Tanimoto and Anderson, 1984). (b) Flow lines at 260 km depth for the upper-mantle kinematic flow model of Hager and O'Connell (1979). The model includes a low-viscosity channel (10^{19} poises) in the upper mantle.

(Tanimoto & Anderson 1984)

A8

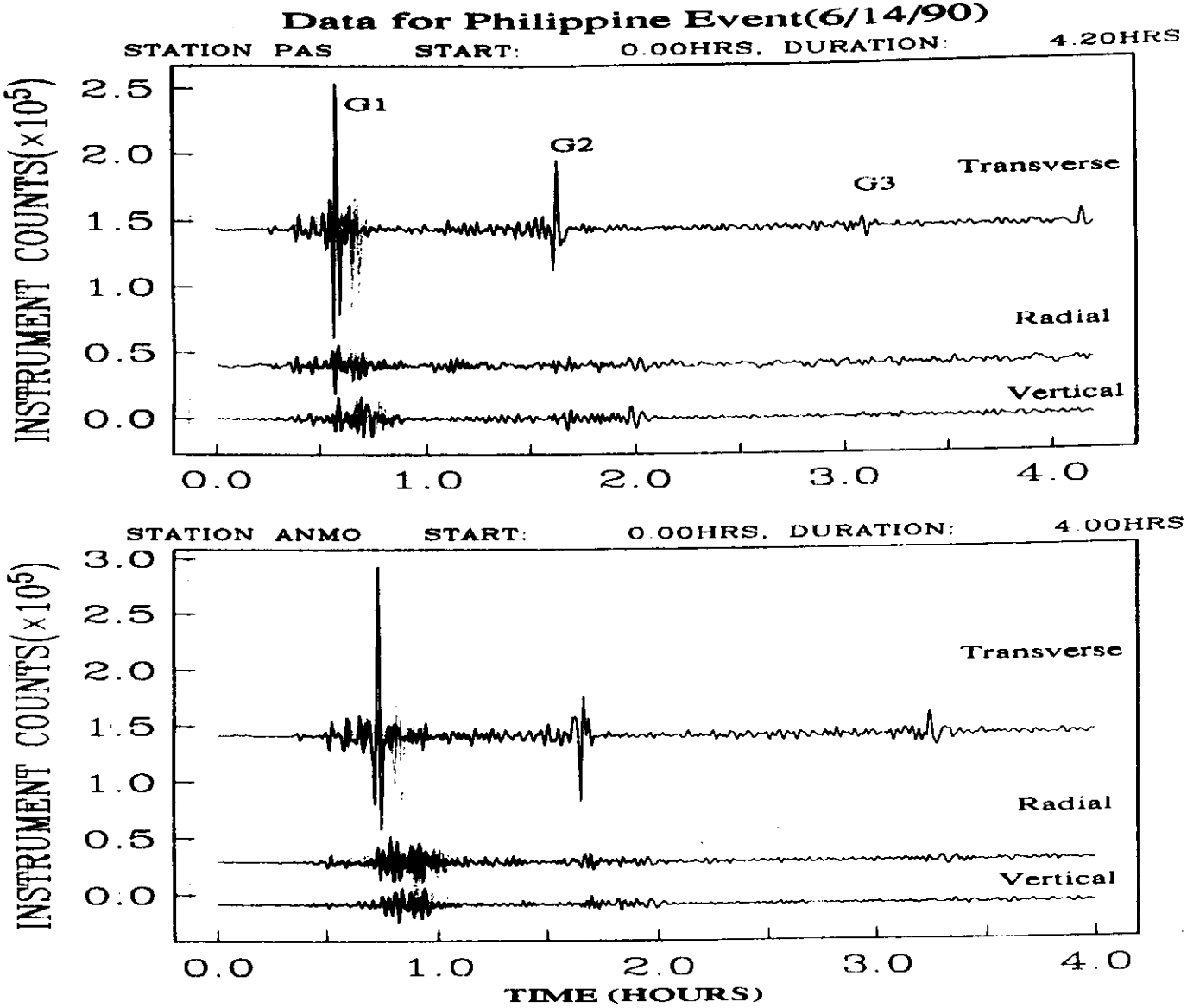

Park et al. (1991)

First Order Perturbation Theory
(non degenerate case)

$$\mathcal{L} \longrightarrow \mathcal{L}^\circ + \delta\mathcal{L}$$

(105) $\mathcal{L}^\circ y_n^\circ = -\lambda_n^\circ y_n^\circ$ **Step 1**

$$(197)\quad \lambda_n = \lambda_n^{(0)} + \lambda_n^{(1)}$$

$$(198)\quad y_n = y_n^{(0)} + \sum_m a_{nm}^{(1)} y_m^{(0)}$$

$$(201)\quad \lambda_n - \lambda_n^{(0)} = \frac{\langle y_n^\circ | \delta\mathcal{L} | y_n^\circ \rangle}{\langle y_n^\circ | y_n^\circ \rangle} + O(\delta\mathcal{L}^2)$$ **Step 2**

$$(204)\quad y_n - y_n^\circ = \sum_{m \neq n} \frac{\langle y_m^\circ | \delta\mathcal{L} | y_n^\circ \rangle}{\lambda_n^\circ - \lambda_m^\circ} y_m^\circ$$

Plane case

$$\lambda_n \longrightarrow \rho_\circ \delta\omega^2|_k$$

$$\delta\mathcal{L} \longrightarrow E^T \delta c\, E$$

$E^T \delta c\, E$ → strain operator: $E\vec{u} = \frac{1}{2}(\nabla\vec{u} + u^T\nabla^T) = \varepsilon$

δc ↓ anisotropic elastic tensor

$$\rho\, \delta(\omega^2)|_k = \frac{\langle u_k | E^T \delta c E | u_k \rangle}{\langle u_k | u_k \rangle}$$

$$\frac{\delta\omega}{\omega}\Big|_k = \frac{1}{2\omega^2} \frac{\int_\circ^\infty \varepsilon_{ij}^* \, \delta c_{ijkl} \, \varepsilon_{kl} \, dz}{\int_\circ^\infty \rho\, u_k^* u_k \, dz}$$

Physical meaning

Kinetic energy $K = \frac{1}{2} \rho \dot{u}^2 = \frac{1}{2} \rho \omega^2 u^2$

Potential strain energy

$$W = \frac{1}{2} \varepsilon_{ij}^* C_{ijkl} \varepsilon_{kl}$$

$$C_{ijkl} \longrightarrow C_{ijkl} + \delta c_{ijkl} \Longrightarrow dW = \langle u | E^T \delta c E | u \rangle$$

$$dK = \frac{1}{2} \rho \, \delta(\omega^2) \, u^2$$

$$dK = dW$$

In the following $\delta c_{ijkl} = \gamma_{ijkl}$

1 Plane Case

In this section, we will follow the same approach as *Montagner and Nataf* (1986) for calculating $\delta\omega|_k$. Let us consider the propagation of the fundamental modes ofLove and Rayleigh waves in an arbitrarily stratified half- space in which a right-handed Cartesian coordinate system (x, y, z) is defined by:

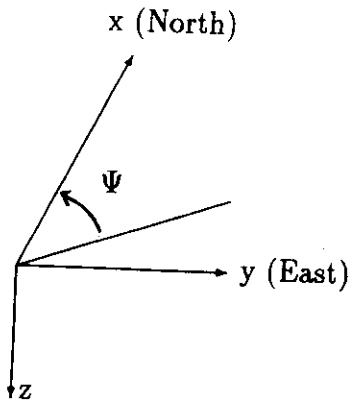

Figure 1: Definition of the Cartesian coordinate system (x, y, z) used in the calculations. Ψ is the azimuth with respect to North of the wavevector.

The half-space is assumed to be homogeneous and may be described by its density $\rho(z)$ and its 4th-order elastic tensor $\Gamma(z)$ with 21 independent elastic coefficients, all quantities independent of x and y coordinates. The unperturbed medium is assumed isotropic with an elastic tensor $\Gamma_0(z)$. In that medium, the two cases of Love and Rayleigh wave dispersion can be successively considered.
The unperturbed Love wave displacement is of the form:

$$\mathbf{u}(\mathbf{r},t) = \begin{pmatrix} -W(z)\sin\Psi \\ W(z)\cos\Psi \\ 0 \end{pmatrix} exp(i[k(x\cos\Psi + y\sin\Psi) - \omega t]) \tag{1}$$

where $W(z)$ is the scalar depth eigenfunction for Love waves, k is the horizontal wave number, and Ψ is the azimuth of the wave number k measured clockwise from the North.
The unperturbed Rayleigh wave displacement is of the form:

$$\mathbf{u}(\mathbf{r},t) = \begin{pmatrix} V(z)\cos\Psi \\ V(z)\sin\Psi \\ iU(z) \end{pmatrix} exp(i[k(x\cos\Psi + y\sin\Psi) - \omega t]) \tag{2}$$

where $V(z)$ and $U(z)$ are the scalar depth eigenfunctions for Rayleigh waves. The associated strain tensor $\epsilon(\mathbf{r},\mathbf{t})$ is defined by:

$$\epsilon_{ij}(\mathbf{r},t) = 1/2(u_{i,j} + u_{j,i}) \tag{3}$$

where $,j$ denotes the differentiation with respect to the j-th coordinate. The medium is perturbed from $\Gamma_0(z)$ to $\Gamma_0(z) + \gamma(z)$, where $\gamma(z)$ is small compared to $\Gamma_0(z)$ but quite general

in the sense that there is no assumption on the kind of anisotropy. This means that we are in the approximation where we can still consider quasi-Love modes and quasi-Rayleigh modes (*Crampin*, 1984). From Rayleigh's principle, the first order perturbation $\delta C(\mathbf{k})$ in phase velocity dispersion is (*Smith and Dahlen*, 1973, 1975):

$$\delta C(\mathbf{k}) = \frac{C}{2\omega^2} \frac{\int_0^\infty \gamma_{ijkl}\epsilon_{ij}\epsilon_{kl}^* dz}{\int_0^\infty \rho_0 u_k u_k^* dz} \tag{4}$$

where u_i and ϵ_{ij} are the displacement and the strain for the unperturbed half-space and the asterisk denotes complex conjugation.
The equation (..) is completely equivalent to equation (..). For a given wavenumber k, $\frac{\delta C}{C}|_k = \frac{\delta \omega}{\omega}|_k$
Now because of the symmetry of the tensors $\gamma(z)$ and ϵ, we use the simplified index notation c_{ij} and ϵ_i for the elements γ_{ijkl} and ϵ_{ij}, but we must take account of the number n_{ij} of coefficients γ_{ijkl} for each c_{ij}. The simplified index notation for the elastic tensor γ_{ijkl} is defined in a coordinate system (x_1, x_2, x_3) by:

$$\gamma_{ijkl} \longrightarrow c_{pq} \begin{cases} \text{if } i = j \Rightarrow & p = i \\ \text{if } k = l \Rightarrow & q = k \\ \text{if } i \neq j \Rightarrow & p = 9 - i - j \\ \text{if } k \neq l \Rightarrow & q = 9 - k - l \end{cases} \tag{5}$$

This kind of transformation enables to relate the 4^{th} order tensor Γ (3x3x3x3) to a matrix c (6x6). The same simplified index notation can be applied to the components of the strain tensor ϵ_{ij}, transforming the 2^{nd} order tensor ϵ (3x3) into a vector with 6 components. However, it is necessary to be careful, because to a given c_{pq} corresponds several γ_{ijkl}, therefore γ_{ijkl} must be replaced by $n_{pq}c_{pq}$, where n_{pq} is the number of γ_{ijkl} giving the same c_{pq}. Therefore, the equation (..) expressing Rayleigh's principle can be rewritten as:

$$\delta C(\mathbf{k}) = \frac{C}{2\omega^2} \frac{\int_0^\infty \sum_{ij} n_{ij}c_{ij}\epsilon_i\epsilon_j^* dz}{\int_0^\infty \rho_0 u_k u_k^* dz} \tag{6}$$

We detail only the calculations for Love waves.
• Love waves.
By using previous expressions for $\mathbf{u}(\mathbf{r}, t)$ and $\epsilon_{ij}(\mathbf{r}, \mathbf{t})$, the various expressions of strain are:

$$\begin{cases} \epsilon_1 &= -i\cos\Psi\sin\Psi.kW \\ \epsilon_2 &= i\cos\Psi\sin\Psi.kW \\ \epsilon_3 &= 0 \\ \epsilon_4 &= 1/2\cos\Psi.W' \\ \epsilon_5 &= -1/2\sin\Psi.W' \\ \epsilon_6 &= 1/2(\cos^2\Psi - \sin^2\Psi).kW \end{cases} \tag{7}$$

where $W' = \frac{dW}{dr}$. In table 1, the different terms $n_{ij}c_{ij}\epsilon_i\epsilon_j^*$ are given. We note that when $c_{ij}\epsilon_i\epsilon_j^*$ is a purely imaginary complex, its contribution to $\delta C(k, \Psi)$ is null. When all the contributions are summed, the different terms $\cos\Psi^k \sin\Psi^l$ present are such that $k + l$ is even, which is not surprising in the light of the reciprocity principle. Therefore, each term can be developed as a Fourier series in Ψ with only even terms. Finally it is found:

$$\begin{aligned}\delta C_L(k,\Psi) = \frac{C}{2\omega^2 L_0} \int_0^\infty dz\{k^2W^2[\frac{1}{8}(c_{11}+c_{22}-2c_{12}+4c_{66}] + W'^2[\frac{1}{2}(c_{44}+c_{55})] \\ + \cos 2\Psi.W'^2[\frac{1}{2}(c_{44}-c_{55})] - \sin 2\Psi.W'^2 c_{45} \\ - \cos 4\Psi.k^2W^2[\frac{1}{8}(c_{11}+c_{22}-2c_{12}-4c_{66})] \\ + \sin 4\Psi.k^2W^2[\frac{1}{2}(c_{26}-c_{16})]\}\end{aligned} \quad (8)$$

In the particular case of a transversely isotropic medium with vertical symmetry axis (also named radial anisotropy), we have: $c_{11} = c_{22} = \delta A$, $c_{33} = \delta C$, $c_{12} = \delta(A-2N)$, $c_{13} = c_{23} = \delta F$, $c_{44} = c_{55} = \delta L$, $c_{66} = \delta N$ and $c_{14} = c_{24} = c_{15} = c_{25} = c_{16} = c_{26} = 0$, where we have used the classical notations of *Takeuchi and Saito*. The azimuthal terms vanish and the previous equation (..) reduces to:

$$\delta C_L(k,\Psi) = \frac{1}{2C_L L_0}\int_0^\infty dz\{W^2\delta N + \frac{W'^2}{k^2}\delta L\}dz \quad (9)$$

Therefore, the same expresions as *Takeuchi and Saito* (1972, p. 268) are found in the case of radial anisotropy. By keeping only the constant term of equation (..), which corresponds to the averaging over azimuth Ψ,one obtains an equivalent transversely isotropic model with vertical symmetry axis by setting:
$\delta N = \frac{1}{8}(c_{11}+c_{22}) - \frac{1}{4}c_{12} + \frac{1}{2}c_{66}$
$\delta L = \frac{1}{2}(c_{44}+c_{55})$
If we call C_{ij} the elastic coefficients of the total elastic tensor, we can set:
$N = \rho V_{SH}^2 = \frac{1}{8}(C_{11}+C_{22}) - \frac{1}{4}C_{12} + \frac{1}{2}C_{66}$
$L = \rho V_{SV}^2 = \frac{1}{2}(C_{44}+C_{55})$
According to equation (..), the first order perturbation in Love wave phase velocity $\delta C_L(k,\Psi)$ can then be expressed as:

$$\delta C_L(k,\Psi) = \frac{1}{2C_{0_L}(k)}[L_1(k) + L_2(k)\cos 2\Psi + L_3(k)\sin 2\Psi + L_4(k)\cos 4\Psi + L_5(k)\sin 4\Psi \quad (10)$$

where

$$\begin{aligned}L_0(k) &= \int_0^\infty \rho W^2 dz \\ L_1(k) &= \frac{1}{L_0}\int_0^\infty (W^2\delta N + \frac{W'^2}{k^2}\delta L)dz \\ L_2(k) &= \frac{1}{L_0}\int_0^\infty -G_c(\frac{W'^2}{k^2})dz \\ L_3(k) &= \frac{1}{L_0}\int_0^\infty -G_s(\frac{W'^2}{k^2})dz \\ L_4(k) &= \frac{1}{L_0}\int_0^\infty -E_c.W^2 dz \\ L_5(k) &= \frac{1}{L_0}\int_0^\infty -E_s.W^2 dz\end{aligned}$$

• Rayleigh waves.
The same procedure holds for Rayleigh wave phase velocity perturbation δC_R , starting from the displacement given previously (*Montagner and Nataf*, 1986).

$$\delta C_R(k,\Psi) = \frac{1}{2C_{0_R}(k)}[R_1(k) + R_2(k)\cos 2\Psi + R_3(k)\sin 2\Psi + R_4(k)\cos 4\Psi + R_5(k)\sin 4\Psi \quad (11)$$

where

$$R_0(k) = \int_0^\infty \rho(U^2 + V^2)dz$$
$$R_1(k) = \frac{1}{R_0}\int_0^\infty [V^2.\delta A + \frac{U\cdot^2}{k^2}.\delta C + \frac{2U\cdot V}{k}.\delta F + (\frac{V\cdot}{k} - U)^2.\delta L]dz$$
$$R_2(k) = \frac{1}{R_0}\int_0^\infty [V^2.B_c + \frac{2U\cdot V}{k}.H_c + (\frac{V\cdot}{k} - U)^2.G_c]dz$$
$$R_3(k) = \frac{1}{R_0}\int_0^\infty [V^2.B_s + \frac{2U\cdot V}{k}.H_s + (\frac{V\cdot}{k} - U)^2.G_s]dz$$
$$R_4(k) = \frac{1}{R_0}\int_0^\infty E_c.V^2dz$$
$$R_5(k) = \frac{1}{R_0}\int_0^\infty E_s.V^2dz$$

The 13 depth-functions $A, C, F, L, N, B_c, B_s, H_c, H_s, G_c, G_s, E_c, E_s$ are linear combinations of the elastic coefficients C_{ij} and are explicitly given as follows:

Constant term (0 Ψ -azimuthal term: independent of azimuth)

$$A = \rho V_{PH}^2 = \frac{3}{8}(C_{11} + C_{22}) + \frac{1}{4}C_{12} + \frac{1}{2}C_{66}$$
$$C = \rho V_{PV}^2 = C_{33}$$
$$F = \frac{1}{2}(C_{13} + C_{23})$$
$$L = \rho V_{SV}^2 = \frac{1}{2}(C_{44} + C_{55})$$
$$N = \rho V_{SH}^2 = \frac{1}{8}(C_{11} + C_{22}) - \frac{1}{4}C_{12} + \frac{1}{2}C_{66}$$

2 Ψ -azimuthal term:

$\cos 2\Psi$	$\sin 2\Psi$
$B_c = \frac{1}{2}(C_{11} - C_{22})$	$B_s = C_{16} + C_{26}$
$G_c = \frac{1}{2}(C_{55} - C_{44})$	$G_s = C_{54}$
$H_c = \frac{1}{2}(C_{13} - C_{23})$	$H_s = C_{36}$

4 Ψ -azimuthal term:

$\cos 4\Psi$	$\sin 4\Psi$
$E_c = \frac{1}{8}(C_{11} + C_{22}) - \frac{1}{4}C_{12} - \frac{1}{2}C_{66}$	$E_s = \frac{1}{2}(C_{16} - C_{26})$

where indices 1 and 2 refer to horizontal coordinates (1: North; 2: East) and index 3 refers to vertical coordinate. ρ is the density, V_{PH}, V_{PV} are respectively horizontal and vertical P-wave velocities, V_{SH}, V_{SV} horizontal and vertical S-wave velocities.
If we consider the constant terms L_1 and R_1, five independent combinations of the C_{ij} are involved. They correspond to the case of a transversely isotropic medium with a vertical symmetry axis (or radial anisotropy) after averaging over all azimuths. The elastic coefficients of this kind of medium were defined by *Love* (1927) and *Takeuchi and Saito* (1972). It is also recalled that A, C, L, N can be retrieved from measurements of the P- and S- wave velocities propagating perpendicular or parallel to the axis of symmetry. Some of the previous combinations were already derived in the expressions that describe the azimuthal dependence of body waves (see *Crampin et al.* (1984) for example) in a weakly anisotropic medium.

$$\rho V_P^2 = A + B_c \cos 2\Psi + B_s \sin 2\Psi + E_c \cos 4\Psi + E_s \sin 4\Psi$$

$$\rho V_{SP}^2 = N - E_c \cos 4\Psi - E_s \sin 4\Psi$$

$$\rho V_{SR}^2 = L + G_c \cos 2\Psi + G_s \sin 2\Psi$$

Therefore, the equations (..) and (..) define the forward problem in the framework of a first order perturbation theory. We will see in the next section how to solve the inverse problem. That means that, ideally, surface waves have the ability for providing 13 elastic parameters, which emphasizes the enormous potential of surface waves in terms of geodynamical and petrological implications. However, from a practical point of view, data do not have the resolving power for inverting for so many parameters. *Montagner and Anderson* (1989a) proposed to use constraints from petrology in order to reduce the parameter space. Actually, they found that some of these parameters display large correlations independent of the petrological model used. Two extreme models were used to derive these correlations, the pyrolite model (*Ringwood*, 1975) and the piclogite model (*Anderson and Bass*, 1984, 1986; *Bass and Anderson*, 1984). In the inversion process, the smallest correlations between parameters of both models are kept. This approach was already followed by *Montagner and Anderson* (1989b) to derive an average reference earth model. These simple linear combinations of the elastic tensor components were first displayed by *Montagner and Nataf* (1986). They are sufficient to describe the two seismically observable effects of anisotropy on surface waves, the "polarization" anisotropy (*Schlue and Knopoff*, 1977) and the azimuthal anisotropy (*Forsyth*, 1975).
In conclusion, the 0-Ψ term corresponds to the average over all azimuths and involves 5 independent parameters, A, C, F, L, N, which express the equivalent transverse isotropic medium with vertical symmetry axis (more simply named radial anisotropy). The other azimuthal terms (2-Ψ and 4-Ψ) depend on 4 groups of 2 parameters, B, G, H, E respectively describing the azimuthal variation of A, L, F, N. Therefore, the different azimuthal terms present in equations (..) and (..), depend on three- dimensional parameters, which are assumed independent.
The other important point in these expressions is that they provide the partial derivatives for the radial and azimuthal anisotropy of surface waves. These partial derivatives can be easily calculated by using a radial anisotropic medium, such as the one used in *PREM* (*Dziewonski and Anderson*, 1981). The corresponding kernels for the fundamental mode are detailed and their variation at depth was discussed in *Montagner and Nataf* (1986). They are shown in figures 2 for Love and Rayleigh waves at 2 different periods.
T and **R** stand respectively for toroïdal and spheroïdal modes. The partial derivatives of the eigenperiod ${}_0T_l$ with respect to parameter p, $\frac{p}{T}\frac{\partial T}{\partial p}$ are computed for a spherical Earth but they can easily be converted into phase velocity partial derivatives by using:

$$\frac{p}{C}\left(\frac{\partial C}{\partial p}\right)_T = -\frac{C}{U}\frac{p}{T}\left(\frac{\partial T}{\partial p}\right)_k$$

In parentheses, the azimuthal parameters which are sensitive to the same partial derivatives are displayed. For example, the parameter G has the same kernel as parameter L (related to V_{SV}). This figure shows that Love waves are almost insensitive to V_{SV} and Rayleigh waves to V_{SH}. Rayleigh waves are the most sensitive to SV-waves. However, as pointed out by *Anderson and Dziewonski* (1982), the influence of P-waves (through parameters A and C) can be very large in an anisotropic medium. The influence of density is also very large for Love and Rayleigh waves,

but as shown by *Takeuchi and Saito* (1972), it is largely decreased when seismic velocities are inverted for, instead of elastic moduli and density. According to equations (..) and (..) any azimuthal term δC_q appearing in these equations, can be related to the different elastic anisotropic parameters defined as linear combinations of elastic moduli:

$$(\delta C_q)_T = \sum_{i=1}^{n_p} \frac{C}{U} \int_0^\infty (\frac{\partial C}{\partial p})_{k,p_{j=i}} \delta p_i \frac{dz}{\Delta h}$$

where Δh is the normalizing thickness for the partial derivatives and n_p the number of parameters.

Table 1: Calculation of the various $c_{ij}\epsilon_i\epsilon_j$ for Love waves, with the simplified index notation. $\alpha = \cos\Psi$; $\beta = \sin\Psi$

n	ij	$c_{ij}\epsilon_i\epsilon_j$
1	11	$c_{11}\alpha^2\beta^2.k^2W^2$
1	22	$c_{22}\alpha^2\beta^2.k^2W^2$
1	33	0
2	12	$-c_{12}\alpha^2\beta^2.k^2W^2$
2	13	0
2	23	0
4	14	$c_{14}(-i\alpha^2\beta).\frac{kWW\cdot}{2}$
4	15	$c_{15}(i\alpha^2\beta).\frac{kWW\cdot}{2}$
4	16	$c_{16}(-\alpha\beta)(\alpha^2-\beta^2).\frac{k^2W^2}{2}$
4	24	$c_{24}(-i\alpha^2\beta).\frac{kWW\cdot}{2}$
4	25	$c_{25}(-i\alpha\beta^2).\frac{kWW\cdot}{2}$
4	26	$c_{26}(\alpha\beta)(\alpha^2-\beta^2).\frac{k^2W^2}{2}$
4	34	0
4	35	0
4	36	0
4	44	$c_{44}\alpha^2.\frac{W\cdot^2}{4}$
8	45	$c_{45}(-\alpha\beta).\frac{W\cdot^2}{4}$
8	46	$c_{46}(-i\alpha)(\alpha^2-\beta^2).\frac{kWW\cdot}{2}$
4	55	$c_{55}\beta^2.\frac{W\cdot^2}{4}$
8	56	$c_{56}(i\beta)(\alpha^2-\beta^2).\frac{kWW\cdot}{2}$
4	66	$c_{66}(\alpha^2-\beta^2).\frac{k^2W^2}{4}$

Therefore, we have shown that it is possible to calculate the effect of a general slight anisotropy on the phase of surface waves. The effect of anisotropy on the amplitude of waves is much more complex and makes it necessary to take account of coupling with other modes. However, it can be calculated by using the expression of displacement given by equation (..). We will now show how to implement such a theory from a practical point of view, and design a tomographic technique in order to invert for the 13 different anisotropic parameters, which arise as well in the plane case as in the spherical case.

0Ψ term	$A = \frac{3}{8}(C_{11} + C_{22}) + \frac{1}{4}C_{12} + \frac{1}{2}C_{66}$ → V_{PH}	
	$C = C_{33}$ → V_{PV}	
	$F = \frac{1}{2}(C_{13} + C_{23})$	
	$L = \frac{1}{2}(C_{44} + C_{55})$ → V_{SV}	
	$N = \frac{1}{8}(C_{11} + C_{22}) - \frac{1}{4}C_{12} + \frac{1}{2}C_{66}$ → V_{SH}	
	cos	sin
2Ψ term	$B_c = \frac{1}{2}(C_{11} - C_{22})$	$B_s = C_{16} + c_{26} \rightarrow B$
	$G_c = \frac{1}{2}(C_{55} - C_{44})$	$G_s = C_{54} \rightarrow G$
	$H_c = \frac{1}{2}(C_{13} - C_{23})$	$H_s = C_{36} \rightarrow H$
4Ψ term	$E_c = \frac{1}{8}(C_{11} + C_{22}) - \frac{1}{4}C_{12} - \frac{1}{2}C_{66}$	$E_s = \frac{1}{2}(C_{16} - C_{26}) \rightarrow E$

1: horizontal direction East

2: horizontal direction perpendicular to 1-axis

3: vertical direction

$$B = \sqrt{B_c^2 + B_s^2}$$

$$G = \sqrt{G_c^2 + G_s^2}$$

$$H = \sqrt{H_c^2 + H_s^2}$$

$$E = \sqrt{E_c^2 + E_s^2}$$

Average over azimuth of $\delta c \Rightarrow$ only 0-4 term

5 independent parameters $\Rightarrow$ equivalent tranversely isotropic medium with vertical Symmetry axis

A, C, F, L, N (PREM)

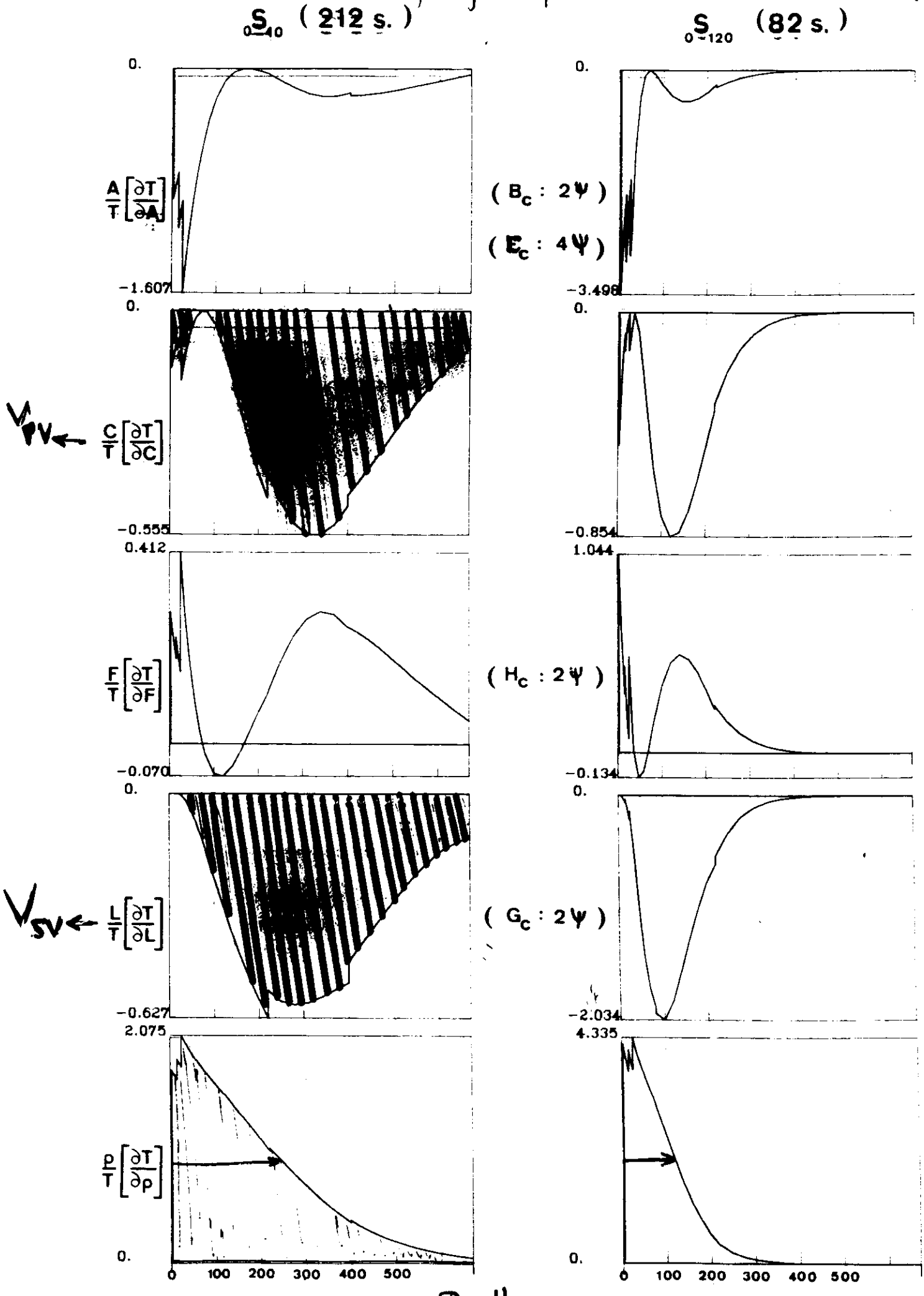
S_{0-40} (212 s.)
S_{0-120} (82 s.)
0.
$\frac{A}{T}\left[\frac{\partial T}{\partial A}\right]$
−1.607
(B_c : 2Ψ)
(E_c : 4Ψ)
−3.498
V_{PV}
$\frac{C}{T}\left[\frac{\partial T}{\partial C}\right]$
−0.555
−0.854
0.412
$\frac{F}{T}\left[\frac{\partial T}{\partial F}\right]$
−0.070
1.044
(H_c : 2Ψ)
−0.134
V_{SV}
$\frac{L}{T}\left[\frac{\partial T}{\partial L}\right]$
−0.627
−2.034
2.075
$\frac{\rho}{T}\left[\frac{\partial T}{\partial \rho}\right]$
4.335
(G_c : 2Ψ)
0
100
200
300
400
500
Depth

LOVE - Toroidal modes

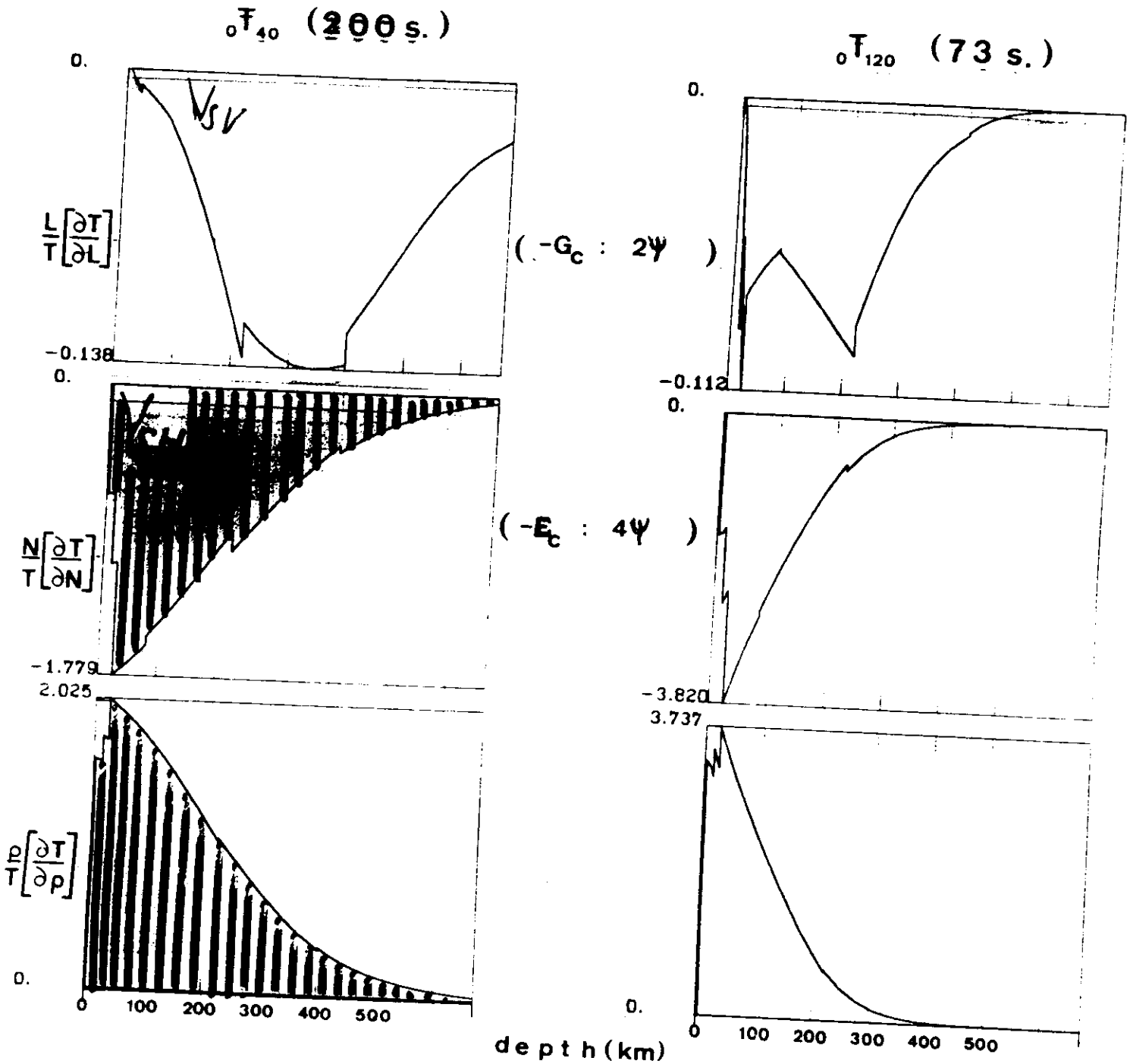

Forward Modeling

Asthenospheric Anisotropy: 2.5%
(140 - 400 km)

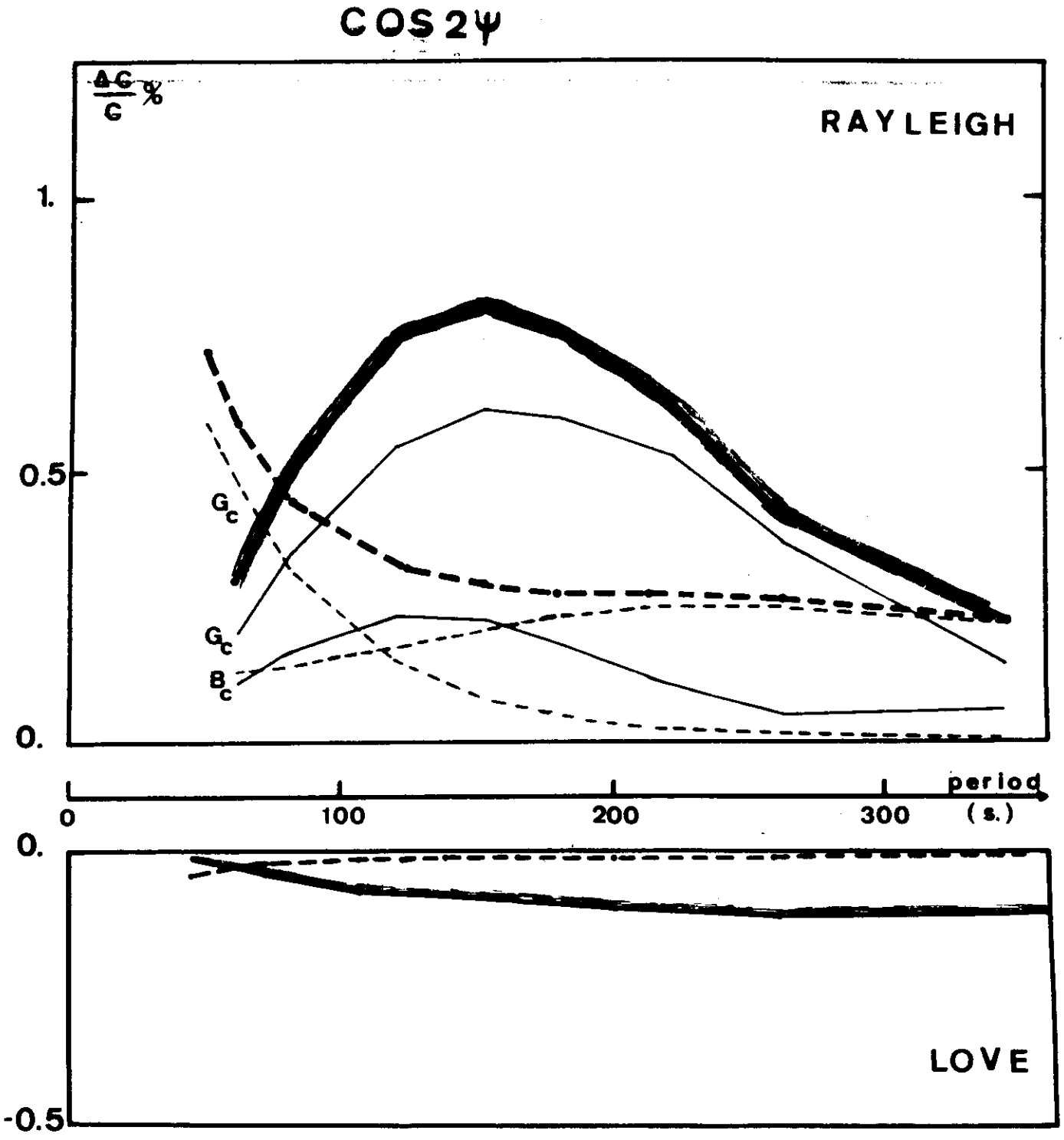

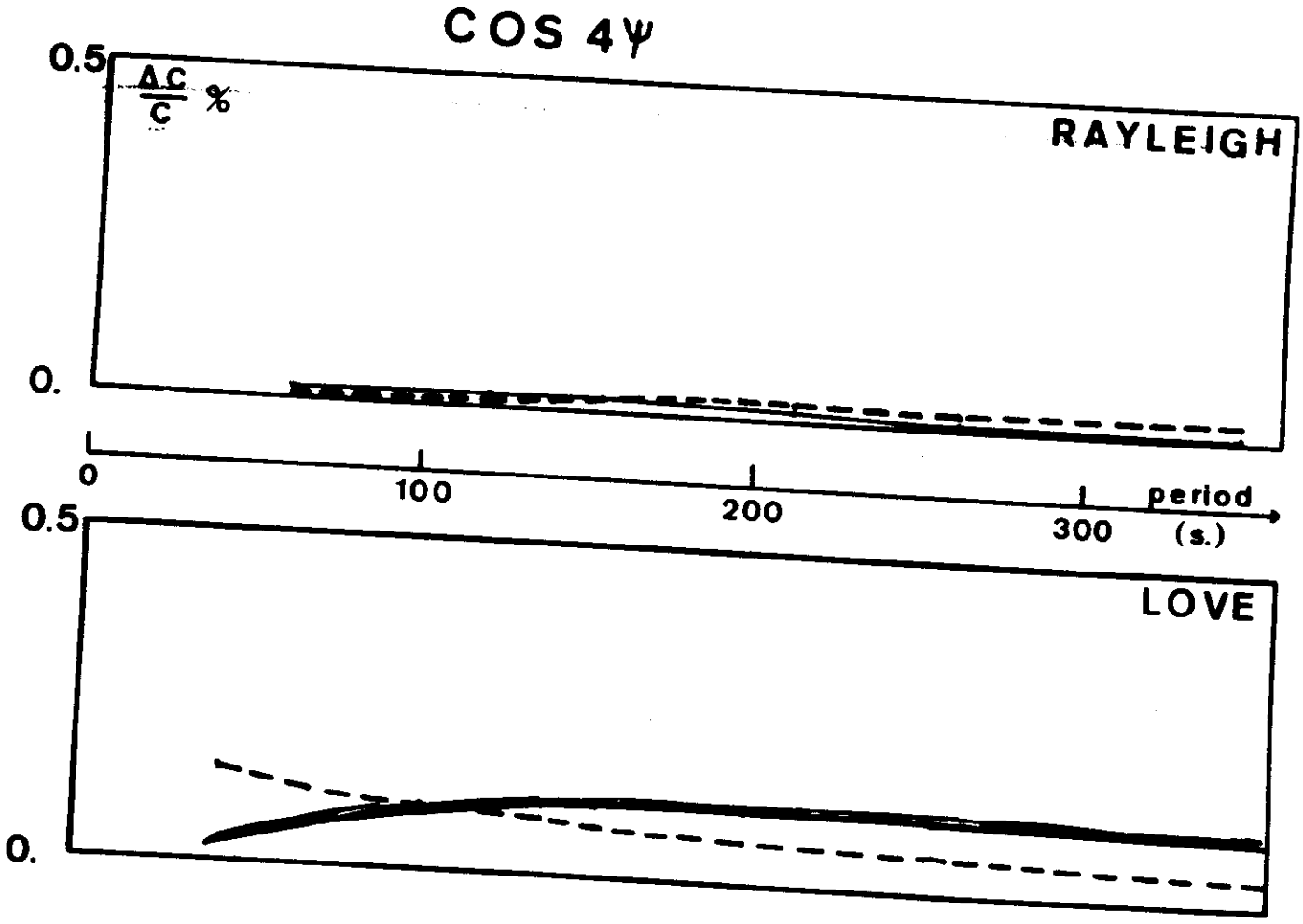
COS 4ψ
0.5
ΔC/C %
RAYLEIGH
0.
0
100
200
300
period
(s.)
0.5
LOVE
0.

SURFACE WAVES

Fundamental, higher modes

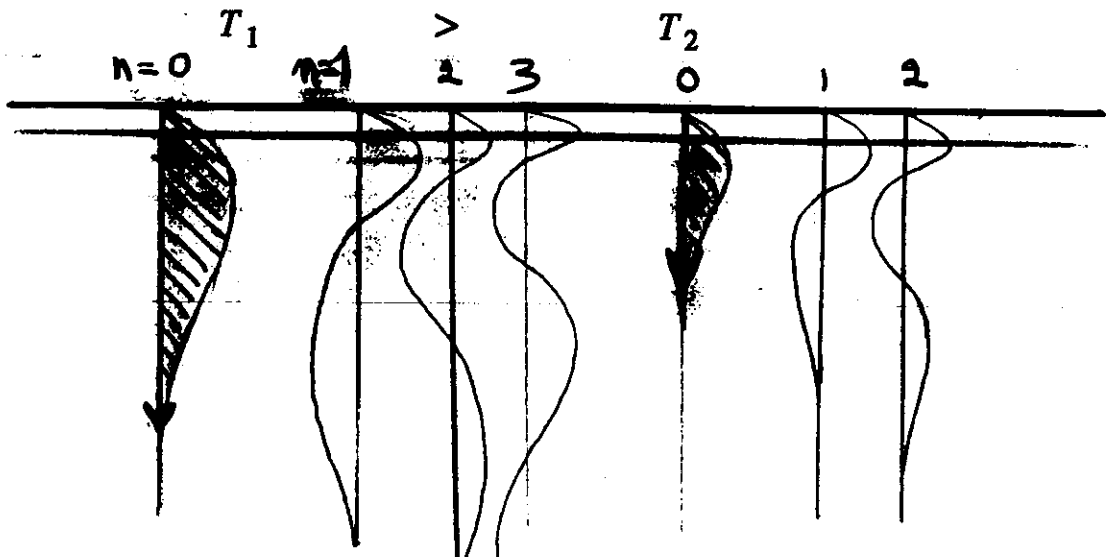

Local phase velocity C at point r, ψ azimuth along the ray.

$$C(\omega,\psi)=A_0(\omega)+A_1(\omega)\cos(2\psi)+A_2(\omega)\sin(2\psi)+A_3(\omega)\cos(4\psi)+A_4(\omega)\sin(4\psi)$$

0ψ, 2ψ, 4ψ

ρV_{PH}^2 = A Bc Bs Ec Es

ρV_{PV}^2 = C

F Hc Hs

ρV_{SV}^2 = L Gc Gs

ρV_{SH}^2 = N Ec Es

Tomographic Technique:

$$\delta C(T,\theta,\phi) = \int_{r_1}^{r_2} \frac{\partial C}{\partial \beta}\,\delta\beta(r,\theta,\phi) + \int_{r_1}^{r_2} \frac{\partial C}{\partial p}\,\delta p(r,\theta,\phi) + \cdots \Rightarrow \delta\beta(r,\theta,\phi),\ \delta p(r,\theta,\phi)$$

Data Parameters

3 Tomography of anisotropy

Tomography is a generic term which means that it describes the structure of an object. It is usually recovered by illuminating a 3D object by rays, waves andor through an inversion procedure. The correct description of this object implies that we are able to find its location in space and its physical properties. A tomographic technique usually necessitates to define at the same time a forward problem and an inverse problem. We will successively consider how to set the forward problem, and how it is used to calculate the partial derivatives of data with respect to parameters, for retrieving these parameters.

3.1 Forward problem

We must make the following hypotheses: let us assume that a data space d and a parameter space p can be defined. We also assume that a theory exists, which enables to define a functional g relating d and p such that:
$d = g(p)$, where d is the set of data (which samples the data space), and p the set of parameters. The next point is now how to define both spaces.

Data Space: d
It is sampled by a set of seismograms. The choice of seismograms is very important because it will condition the quality of the inversion. For example, if we look for the structure of a given area, it is necessary to have a very dense and uniform coverage of the area. If in addition, we look for the anisotropy of this area, it will be necessary to have anywhere a very good azimuthal coverage. We can either take the seismogram $u(t)$, and try to directly match the waveform in the time domain, or work in the Fourier domain, by separating phase and amplitude on each component:

$$u_i(t) = \int_{-\infty}^{\infty} A_i(\omega) e^{i(\omega t - \phi_i)} d\omega$$

The approach consisting in fitting seismic waveform is quite general but does not necessarily correspond from a practical point of view, to the simplest choice. As presented in the previous section, it was shown that in a heterogeneous medium, the calculation of amplitude effects makes it necessary to calculate the coupling between different multiplets, which is very time consuming. When working in Fourier domain. different time windows can be considered and we can try in a first time to separately match the phase of different seismic trains, body waves and surface waves. Figure 3 shows an example of data seismogram and synthetic seismograms obtained by normal mode summation. The different monomode seismograms corresponding to different higher modes are displayed. The fundamental wavetrain is at large epicentral distance well separated from other modes. The part of the seismogram corresponding to higher modes is more complex and shows a mixing of these modes in the time domain. Therefore, from a practical point of view, the fitting of the fundamental mode wavetrain will not cause any problem and has been widely used in global mantle tomography.
The use of higher mode wavetrain and the separation of overtones is much more difficult. The first attempts were performed by *Nolet* (1975), *Cara* (1978), *Okal and Bong-Jo* (1985) and *Dost* (1990) by applying a spatial filtering method. Different techniques based on waveform inversion

of fundamental and higher-mode surface waves were also designed in the following years (*Lerner-Lam*, 1983; *Nolet*, 1990; *Lévêque et al.*, 1991). Unfortunately, all these techniques can only be applied to areas where dense arrays of seismic stations are present, i.e. in North America and Europe. By using a set of seismograms either recorded in one station but corresponding to several earthquakes located in a small source area, *Stutzmann and Montagner* (1993) showed how to separate the different higher modes. This technique might be easily applied as well, to seismograms originating from one seismic source recorded in an array of stations. Since it is necessary to fit higher mode wave packet, it is shown that it is necessary to recalculate the eigenfunctions at each iteration of the inversion process. We will only detail the technique which was designed for fitting the fundamental mode wavetrain and the reader is referred for example to *Stutzmann and Montagner* (1993, 1994) for recovering the higher mode dispersion properties.

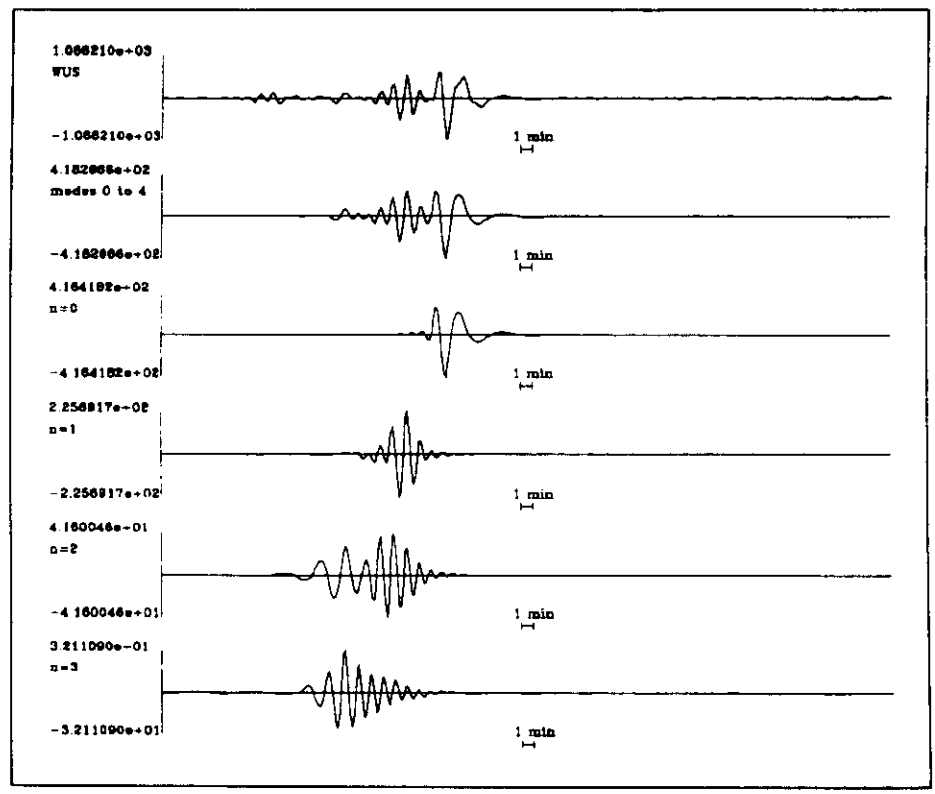

Figure 3: An example of data seismogram (top) and synthetic seismogram, obtained by normal mode summation. The bottom 4 figures corresponds to monomode synthetic seismograms, calculated for PREM. The maximum of amplitude for each mode is reported on the left. The seismogram was recorded in the GEOSCOPE station of Wushi (China). It corresponds to a Japan earthquake (date: 92/08/29, time: 19:19:11.4, lat: 33.40N., long: 138.09E, depth= 309km).

We take advantage of the fact that, according to the Fermat's principle, the phase velocity perturbation is only dependent to second order on path perturbations, whereas amplitude perturbation are dependent, at first order, to these perturbations. That is completely equivalent to the simple case described in section 2.3 where the eigenfrequency perturbation can be easily

computed by using the corresponding eigenfuntion (equation 11) whereas the calculation of amplitude perturbation necessitates to take account of the coupling with other modes (equation 12).

The phase is a more robust observable than the amplitude. The amplitude $A(\omega)$ depends in a complex manner upon seismic moment tensor, attenuation, scattering, focusing effects, station calibration and near-receiver structure whereas the phase $\phi(\omega)$ is readily related to lateral heterogeneities of seismic velocity and anisotropies. The next section will detail how it is possible to separate these different effects on amplitude in order to obtain attenuation.

The dataset that we will consider. is composed of propagation times (or phase velocity measurements) along paths:
$d = \{\frac{\Delta}{c(T)}\}$.

The second important ingredient which has to be defined in any inverse problem is the structure of the data space. It is expressed through its covariance function (continuous case) or covariance matrix (discrete case) of data C_d. When data d_i are independent, C_d is diagonal and its elements are the square of the errors on data σ_{d_i}.

The phase of a seismogram at time t is decomposed as follows: $\phi = k.r + \phi'_0$, where k is the wave vector, ϕ'_0 is the initial phase which can be decomposed as follows: $\phi'_0 = \phi_0 + \phi_S + \phi_I$, ϕ_S is the initial source phase, ϕ_0 is related to the number of polar phase shifts, ϕ_I is the instrumental phase. ϕ can be measured on seismograms by Fourier transform and it can be assumed that ϕ_S is correctly given from the Centroid moment tensor solution (*Dziewonski et al.*, 1981). For a path between a source S and a receiver R with an epicentral distance Δ, the phase ϕ at period T is given by (*Nakanishi and Anderson*, 1984):

$$\phi(T) = \frac{\omega\Delta}{\bar{C}(T)} + \phi_0 + \phi_S + \phi_I \tag{39}$$

or

$$\phi = \phi'_0 + \int_S^R \frac{\omega ds}{C(T,\theta,\phi)} \tag{40}$$

where $\bar{C}(T)$ is the average of the local phase velocity $C(T,\theta,\phi)$ along the path $S \rightarrow R$.

Following the results of the previous section, different approximations are considered when using this expression of the phase:

- large angular order $\ell \gg 1$, but not too large because we know that at periods smaller than 50s, the scattering problems can be very important (*Snieder*, 1988a,b; *Friederich et al.*, 1994). From a practical point of view, that means that we work in the period range 50s. $< T <$ 300s.
- geometrical optics approximation:

If λ is the wavelength of the surface wave at period T, and Λ_S the spatial wavelength of heterogeneity: $\Lambda_S \gg \lambda = CT \Rightarrow \Lambda_S \gtrsim 2,000km$.

- slight anisotropy and heterogeneity: $\frac{\delta C}{C} \ll 1$. According to *Smith and Dahlen* (1973) for the plane case (equations 31 and 32 of section 2.5) and equation 37 in the section 2.6 for the spherical case (*RS*, 1988), the local phase velocity can be decomposed as a Fourier series of the azimuth Ψ:

$$\frac{\delta C(T,\theta,\phi)}{C} = A_0 + A_1 \cos 2\Psi + A_2 \sin 2\Psi + A_3 \cos 4\Psi + A_4 \sin 4\Psi \tag{41}$$

And every azimuthal term A_i can be related to a set of anisotropic parameters p_i.

$$\frac{\Delta}{\bar{C}(T)} - \frac{\Delta}{C_0(T)} = -\sum_{j=0}^{2}\sum_{i=1}^{13} \int_E^R \frac{ds}{C_0}\int_0^a \left[\left(\frac{p_i}{C}\frac{\partial C}{\partial p_i}\right)_j \frac{\delta p_i(\vec{r})}{p_i}\cos(2j\Psi) + \left(\frac{p_i}{C}\frac{\partial C}{\partial p_i}\right)_j \frac{\delta p_i(\vec{r})}{p_i}\sin(2j\Psi)\right]\frac{dz}{\Delta h} \quad (42)$$

Following the approach of *Snieder* (this issue), that means that we consider that the perturbation is at the same time smooth and weak.

Parameter space: $p(r)$

Again, it is quite important to thoroughly think of the structure of the parameter space. First of all, it is necessary to define how many physical parameters can be inverted for, in the framework of the theory that is considered. For example, if it is assumed that the Earth is elastic, laterally heterogeneous but isotropic, we can only invert for 3 independent physical parameters, V_P, V_S and density ρ, or the elastic moduli λ, μ plus density ρ. In a transversely isotropic medium with a vertical symmetry axis (*Anderson*, 1961; *Takeuchi and Saito*, 1972), the number of independent physical parameters is now 6 (5 elastic moduli + density). In the most general case of a slight anisotropy, we can invert for 14 physical parameters (13 combinations of elastic moduli + density). Therefore, the number of "physical" parameters p_i is dependent on the underlying theory which is used for explaining the dataset.
Once the number of "**physical**" independent parameters is defined, we must be able to define how many "**spatial**" parameters are necessary to describe the 3D distributions $p_i(r,\theta,\phi)$. That is a difficult problem because the number of "spatial" parameters which can be solved from the dataset is not necessarily sufficient to provide a correct description of $p_i(r,\theta,\phi)$. In any case, it is necessary to assess the range of possible variations for $p_i(r,\theta,\phi)$ in order to provide some bounds on the parameter space. This is done through a covariance function of parameters in the continuous case (or a covariance matrix in the discrete case). These *a priori* constraints can be provided by other fields of geosciences, geology, mineral physics, geochemistry, geodynamics, numerical modeling...
Consequently, a tomographic technique must not be restricted to the inversion of parameters $p = \{p_i(r,\theta,\phi)\}$ that are searched for, but must include the calculation of the final covariance function (or matrix) of parameters C_p. That means that the correct interpretation of tomographic models is contingent to the resolution and the errors of the final parameters and is largely dependent on the resolving power of data (*Backus and Gilbert*, 1967, 1968, 1970).
Finally, the functional g which expresses the theory relating the data space to the parameter space is also subject to uncertainty. In order to be completely consistent, it should be necessary to be able to define the domain of validity of the theory and to assess the error σ_T associated with the theory. *Tarantola and Valette* (1982) showed that the error σ_T is simply added to the error on data σ_d.

3.2 Inverse problem

The equation (42) expressing the first order perturbation theory of the forward problem can be simply written:

$$d = Gp$$

where G is a matrix (or a linear operator) composed of Fréchet derivatives of d with respect to p. which has the dimensions $n_d \times n_p$ (number of data $\times$ number of parameters). This matrix usually is not square and many different techniques in the past have been used for inverting G. In any case, the inverse problem will consist in finding an inverse for the functional g, that we will write $\tilde{g}^{-1}$, notwithstanding the way it is obtained. Different strategies can be followed to invert for the 3D-models $p(r)$. This point can be illustrated by presenting 2 different approaches, respectively coined 1-step and 2-step inversions.

• **One step inversion**: The equation (42) is directly used for retrieving $\frac{\delta p_i(r)}{p_i}$

$$p = \tilde{g}^{-1}(d) \tag{43}$$

In dividing the upper mantle into 5 independent layers, a *minimum* parameter space will be composed of 13 (+density) physical parameters multiplied by 5 layers. If geographical distributions of parameters are searched for up to degree 12, that implies $\approx$ 10000 parameters. The problem will be almost impossible to handle from a computational point of view.

• **Two step inversion.**
In order to decrease the size of the matrix to be inverted, it is possible to divide the inversion scheme into two steps:

First step: Regionalization of phase velocity dataset at different periods.

The inverse problem consists in obtaining the geographical distributions of the local phase (or group velocity) and their azimuthal terms at different periods. This step is often named regionalization. The forward problem is obtained by combining equations (39) and (40):

$$\frac{\Delta}{C(T)} = \int_S^R \frac{\omega ds}{C(T,\theta,\phi)}$$

It can be formally written:

$$d = g_1(p_1) \tag{44}$$

And the inverse problem by:

$$p_1 = \tilde{g}_1^{-1}(d) \tag{45}$$

The first parameter space is defined by parameters $p_1 = \{\delta C(T,\theta,\phi)\}$, and its *a posteriori* covariance function C_{p_1}.

Second step: Inversion at depth of local phase velocity and azimuthal anisotropy terms.

The data d_1 used in this second step are the final parameters $p_1(T,\theta,\phi)$ determined by the first step and the covariance function of data is $C_{d_1} = C_{p_1}$. For example, the forward problem for Love waves in the plane case is given by equation (31) and in the spherical case by equation (38). The second parameter space p_2 is defined by the 13 elastic parameters (+eventually density) $p_2 = \{p_i(r,\theta,\phi), i\epsilon[1,14]\}$ derived in section 2.5 , and its *a posteriori* covariance function C_{p_2}. The forward and inverse problems can be formally written:

$$d_1 = p_1 = g_2(p_2) \Rightarrow p_2 = \tilde{g}_2^{-1}(p_1) \tag{46}$$

By combining equations (44), (45) and (46), both steps give:

$$d = g_1 \circ g_2(p_2) \Rightarrow p_2 = \tilde{g}_2^{-1} \circ \tilde{g}_1^{-1} d \tag{47}$$

It can be demonstrated that both approaches are equivalent (*Montagner*, 1986b) if vertical and horizontal variations are decoupled, and if we take care to take for the second step $C_{d_1} = C_{p_{1_{final}}}$. In the second approach, we save space memory by solving, firstly a 2D-problem, and then a 1D-problem.

For the 2-step approach, the general procedure can be summarized as follows:

• Extraction of 3-component data seismograms, calculation of synthetic seismograms for a given path between epicenter S and receiver R.

$\Downarrow$

• Calculation of average phase velocity between S and R, $\bar{C}(T, S \rightarrow R)$ at different periods T, for Rayleigh and Love waves.

$\Downarrow$ Continuous Regionalization

• $A_i(T, \theta, \phi)$, $i \epsilon [1, 5]$ for Rayleigh and Love waves.

$\Downarrow$ Inversion at depth.

• $A, C, F, L, N, B_c, B_s, G_c, G_s, H_c, H_s, E_c, E_s$

To solve both inverse problems, different algorithms can be used. We detail in appendix C the particular technique of *Montagner* (1986b) based on the algorithm of *Tarantola and Valette* (1982). The choice of the parameterization is also very important and different possibilities can be considered:

• Discrete basis of functions:

For a global study, the natural basis is composed of the spherical harmonics function for the lateral variations in θ, ϕ. For the radial variations, polynomial expansions can be used (see for example *Dziewonski and Woodhouse*, (1987) for Tshebyshev polynomials). Another possibility is to divide the Earth into cells of various size according to the resolution we can expect from the path coverage. The cell decomposition is valid as well for global investigations as for regional studies.

• Continuous function $p(r)$:

In that case, we directly invert for the function p. However, the number of parameters is then infinite and it is necessary to define a covariance function of parameters $C_{p_0}(r, r')$ in order to reduce the number of independent parameters. For the lateral variations in θ, ϕ, we can make use of a Von Mises distribution (*Fisher*, 1953; *Montagner*, 1986b) for initial parameters $p_0(r)$:

$$C_{p_0}(r, r') = \sigma_p(r)\sigma_p(r') \exp \frac{\cos \Delta_{rr'} - 1}{L_{cor}^2}$$

where L_{cor} is the correlation factor defining the smoothness of the final model. This kind of distribution is well suited for studies on a sphere and is asymptotically equivalent to a Gaussian

distribution when $L_{cor} \ll 2\pi$. Then the covariance function of parameters reduces to:

$$C_{p_0}(r,r') = \sigma_p(r)\sigma_p(r') \exp -\frac{\Delta^2 - 1}{2L_{cor}^2}$$

In that case, L_{cor} is named the angular correlation length.
When different azimuthal terms distributions are searched for, it is possible to define cross-correlated covariance functions of parameters $C_{p_i,p_j}(r,r')$, but it can be assumed that the different terms of the Fourier expansion in azimuth are independent and these terms can be taken equal to zero.
For the inversion at depth, since the number of physical parameters is very large (13), it is difficult to assume that physical parameters are uncorrelated. Then, the different terms of the covariance function C_p between parameters p_1 and p_2 at radii r_i and r_j can be defined as follows:

$$C_{p_1,p_2}(r_i,r_j) = \sigma_{p_1}\sigma_{p_2}\zeta_{p_1,p_2} e^{\frac{(r_i-r_j)^2}{2L_{r_i}L_{r_j}}} \qquad (48)$$

Where ζ_{p_1,p_2} is the correlation between physical parameters p_1 and p_2 inferred for instance from different petrological models (*Montagner and Anderson*, 1989a) and L_{r_i}, L_{r_j} are the radial correlation lengths which enable to smooth the inverse model.
It is interesting to note, that the local resolution of parameters is imposed by both the correlation length and the path coverage, contrarily to the *Backus-Gilbert* (1967, 1968) approach, which primarily depends on the path coverage. But the effect of a damping factor in order to smooth the solution, is equivalent to the introduction of a simple covariance function. When the correlation length is chosen very small, the algorithms of *Backus-Gilbert* (1968, 1970) and *Tarantola- Valette* (1982) are quite similar.

3.3 Practical implementation.

This complete 2-step procedure was implemented for making different regional and global studies. From petrological and mineralogical considerations, *Montagner and Nataf* (1988) and *Montagner and Anderson* (1989a,b) showed that the predominant terms of phase velocity azimuthal expansion are the 0-Ψ and 2-Ψ for Rayleigh waves, and 0-Ψ and 4-Ψ for Love waves. *Montagner and Nataf* (1988) showed that the best resolved parameters are $L = \rho V_{SV}^2$, $N = \rho V_{SH}^2$ and G_c, G_s, E_c, E_s which respectively express the azimuthal variations of V_{SV} and V_{SH}.
Another important point emphasized by *Montagner and Jobert* (1988) and *Montagner and Tanimoto* (1991) is the importance of shallow layers (oceanic - continental crusts, bathymetry - topography, sedimentary thicknesses...) on phase velocity. In order to avoid the deep structure to be biased by an improper account of shallow layers, it is necessary to correct phase velocity measurements along each path. This correction is not negligible, and contrarily to the common belief, it tends to increase the amplitude of lateral heterogeneities below the crust (*Montagner and Tanimoto*, 1991).
This technique has made it possible to simultaneously explain the "Rayleigh-Love discrepancy" (*Schlue and Knopoff*, 1977) and the azimuhal anisotropy, firstly displayed in the Nazca plate by *Forsyth* (1975). However, the main limitation of this technique applied to the fundamental mode of surface waves is that the radial resolution is limited to the first 500km of the upper mantle. In order to go further, it is necessary to use seismic waves sensitive to deeper structure.

Principles of tomography

To retrieve 3D structure of seismic parameters

Data

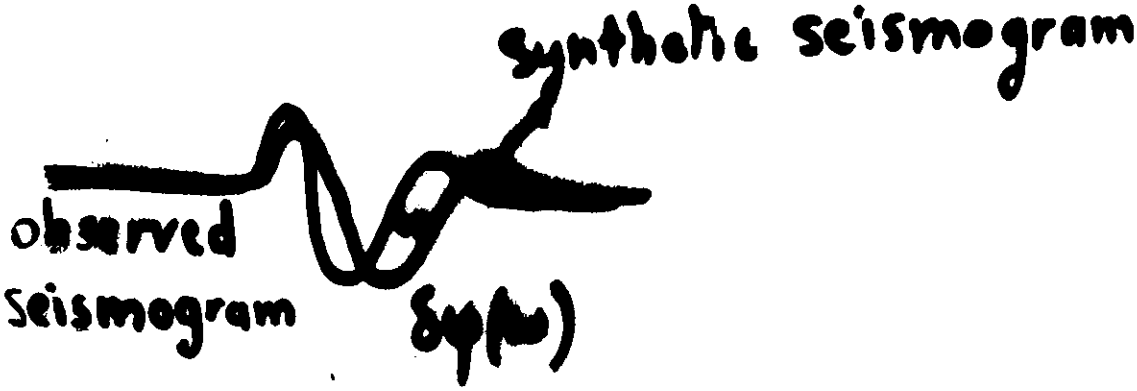

Phase: more robust observable

$$\text{Phase} \quad \varphi(\omega) = \int_E^R \frac{\omega \, ds}{c(\omega)}$$

$c(\omega)$ ↳ phase velocity

$c = c_0(\omega) + \delta c(\omega, \theta, \varphi)$ 1st order perturbation

$$\delta\varphi(\omega) = \int_E^S \frac{\omega \, ds}{c_0(\omega)} \underbrace{\left(- \frac{\delta c(\omega, \theta, \varphi)}{c_0} \right)}_{\text{local phase velocity}}$$

to

When anisotropy is taken into account:

$$\frac{\delta c}{c_0} = A_0(\omega,\theta,\varphi) + A_1(\omega,\theta,\varphi)\cos 2\psi + A_2(\omega,\theta,\varphi)\sin 2\psi + A_3(\omega,\theta,\varphi)\cos 4\psi + A_4(\omega,\theta,\varphi)\sin 4\psi$$

$$\frac{\delta c}{c_0} = \sum_{j=0}^{4} A_j(\omega,\theta,\varphi)\, F_j(\psi)$$

$$\downarrow$$

$$\sum_{j=0}^{4}\sum_{i=1}^{13}\int_0^a \left(\frac{\rho_i}{c}\frac{\partial c}{\partial \rho_i}\right) F_j(\psi)\frac{dz}{\Delta h}\,\delta p_i(r,\theta,\varphi)$$

$$\delta\varphi(\omega) = \int_E^S \sum_j \sum_i \frac{\omega\, ds}{c_0(\omega)} \int_0^a \left(\frac{\rho_i}{c}\frac{\partial c}{\partial \rho_i}\right) f_j(\psi)\frac{dz}{\Delta h}\,\delta p_i(r,\theta,\varphi)$$

data

parameters

Forward Problem

$$\vec{d} = g(\vec{p})$$

$\vec{d} = \{\delta\varphi(\omega)\}$ C_d data space

$\vec{p} = \{p_i(r,\theta,\varphi)\}$ C_{p_0} parameter space

a priori covariance function of parameters

Inverse Problem

$$\vec{p} = \tilde{g}^{-1}(\vec{d})$$

C_{P_F} Final covariance function of parameters

Limitations

- slight anisotropy
- geometrical optics approximation

  λ wavelength of surface wave

  Λ_s spatial wavelength of heterogeneity

  $\Lambda_s \gg \lambda$
- long period (scattering effects)

  $40s < T < 300s$

Practical limitations

- Distribution of seismic sources non uniform
- Poor coverage of the Earth by stations

$\Rightarrow$ Some oceanic areas are not well covered.
Lateral resolution > 1000 km

$\Rightarrow$ Transition zone poorly resolved

INSTITUT DE PHYSIQUE DU GLOBE DE PARIS
Département de Sismologie

Global seismicity 1928-1993

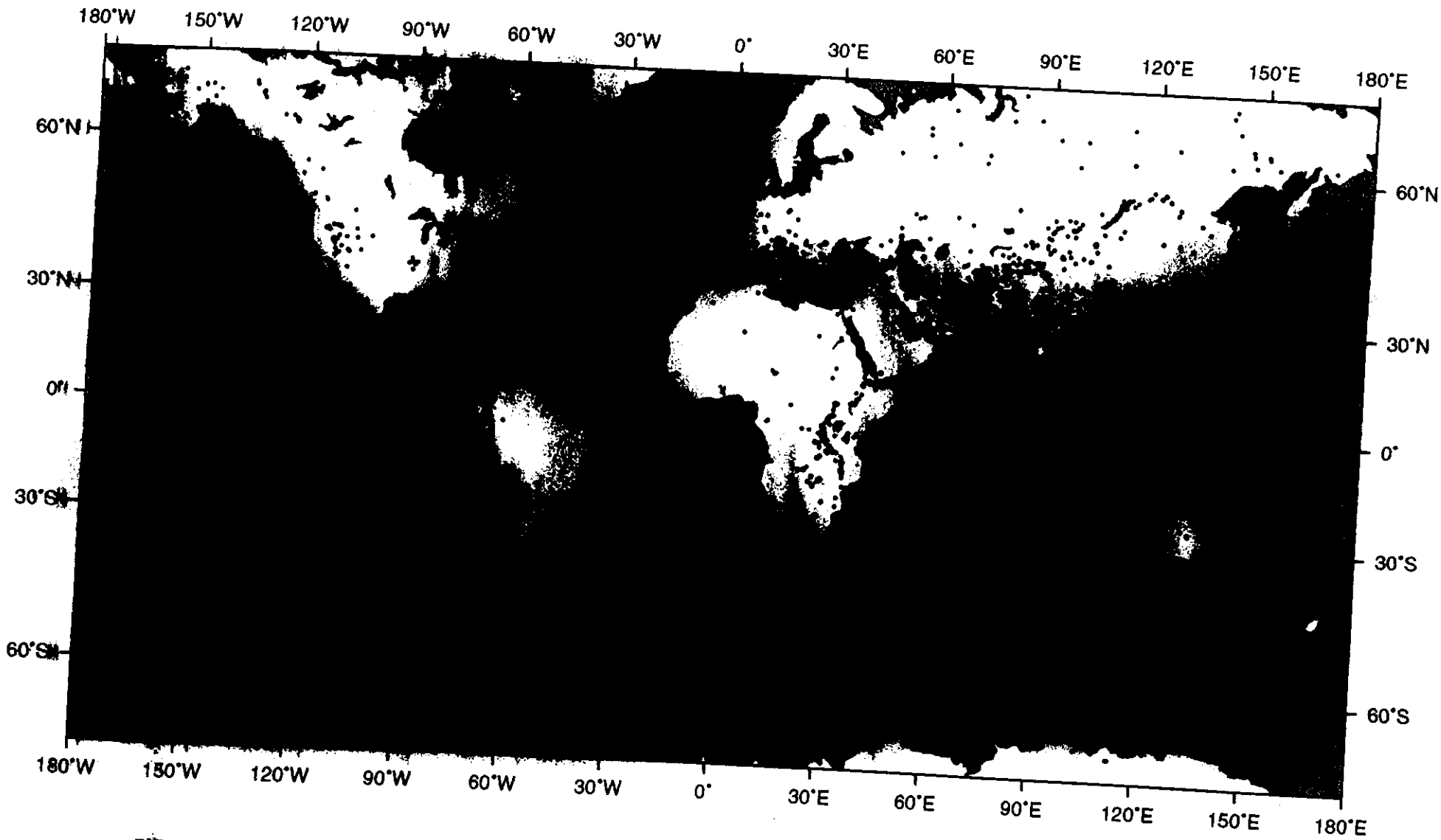

Magnitude Mb or Ms >= 5.0

Genevieve Patau,
Fri Jan 6 08:35:53 MET 1995

Broadband Digital stations

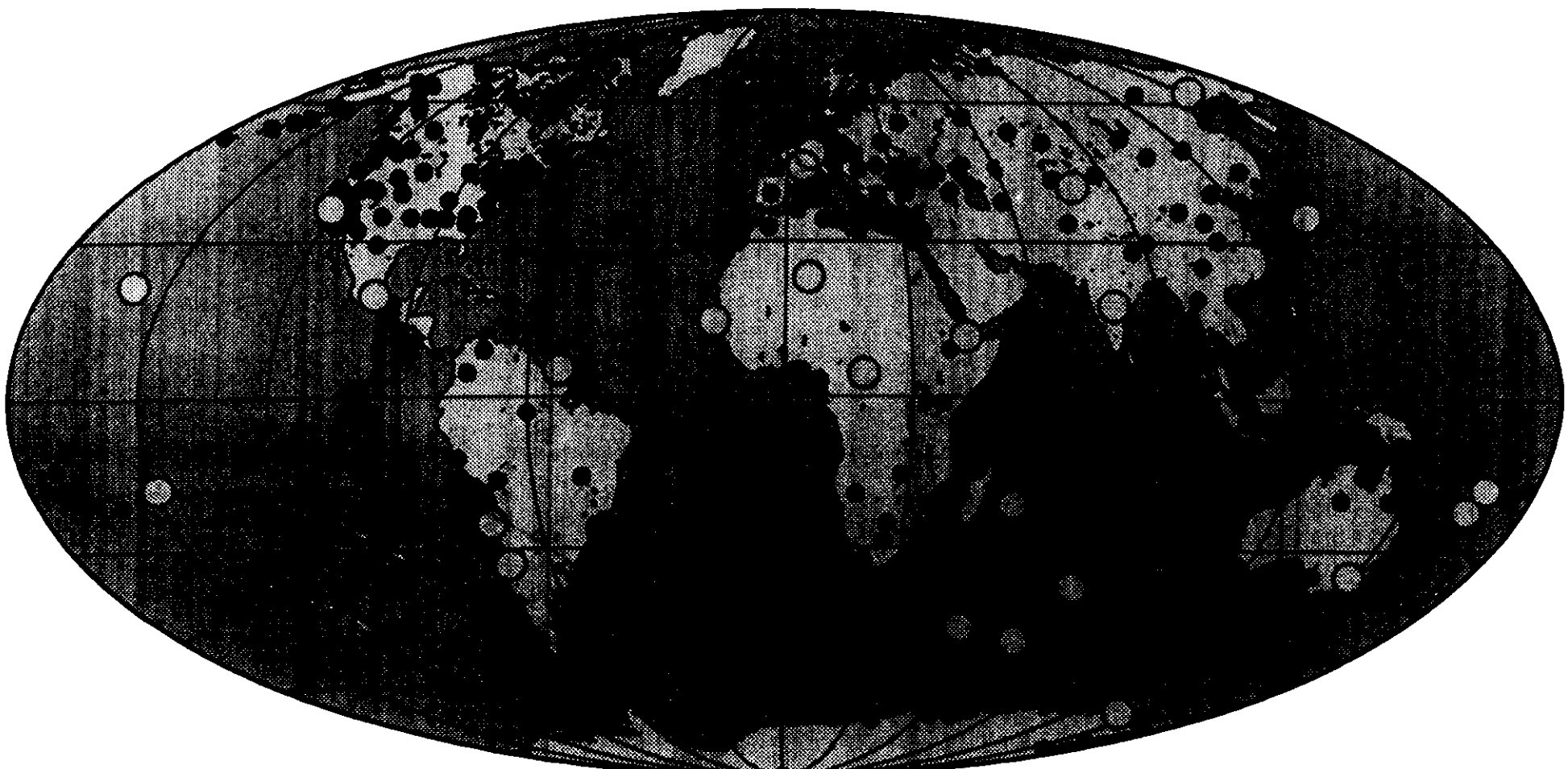

● *Broadband Digital stations*
○ *Geoscope stations*

October 8th, 1995
Genevieve Roult

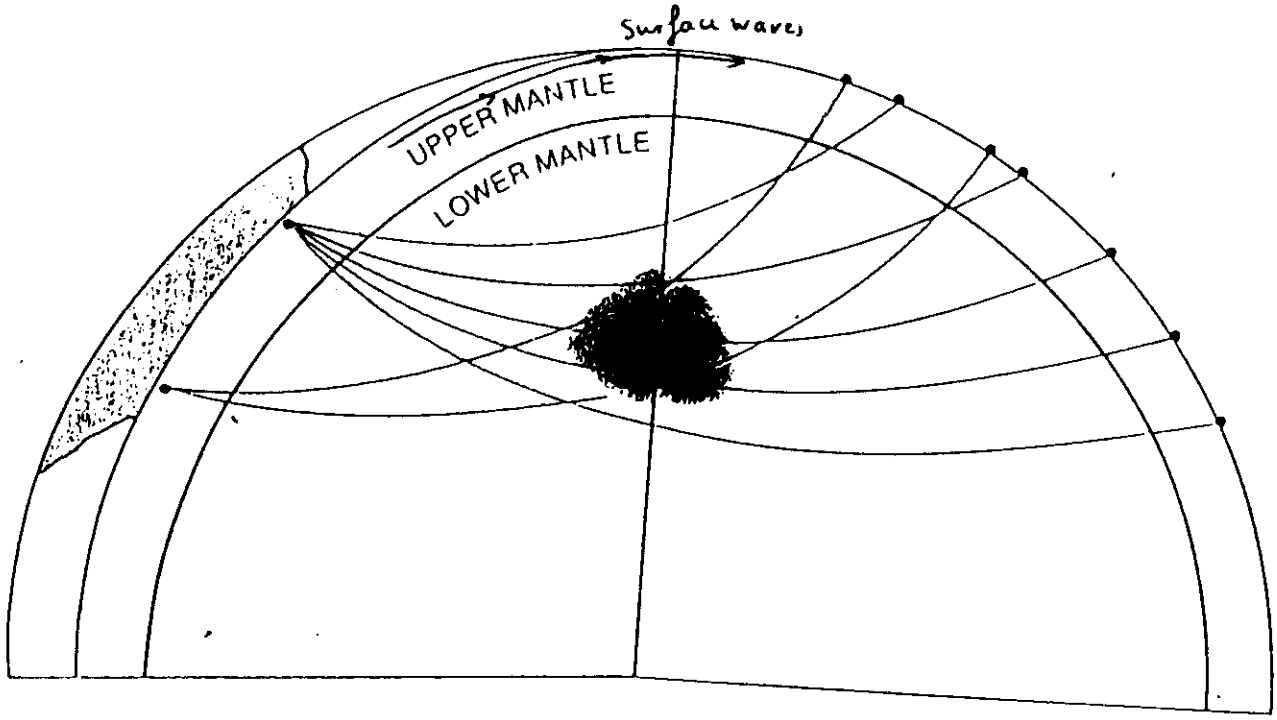
Surface waves
UPPER MANTLE
LOWER MANTLE

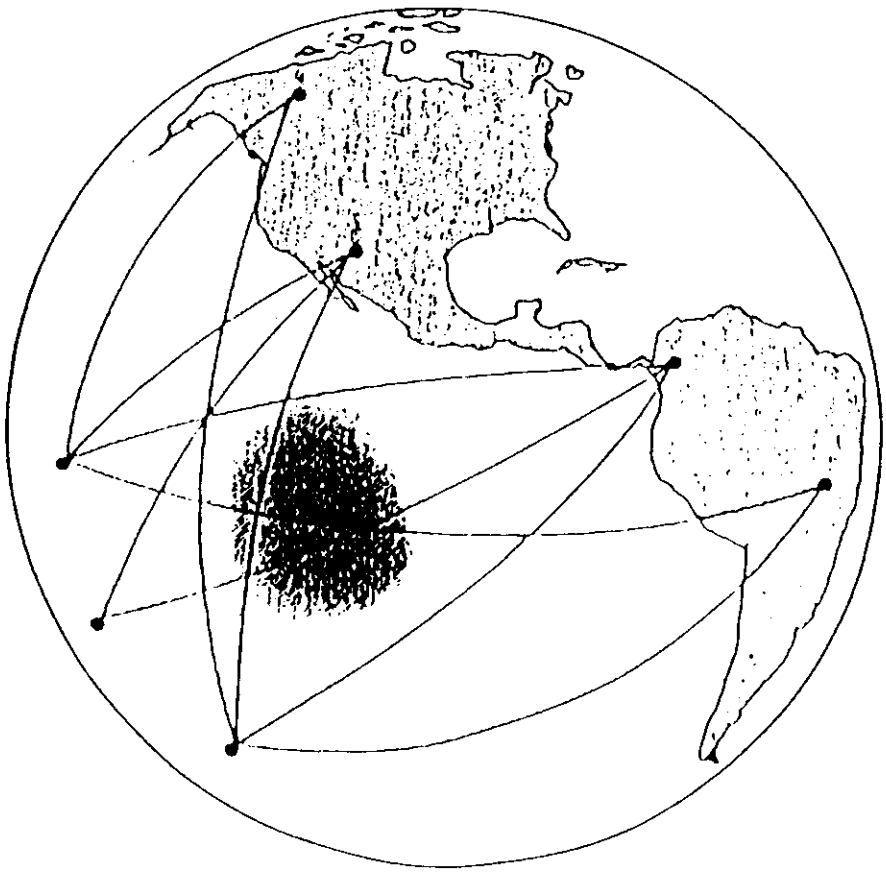

LOVE 0+4-PSI

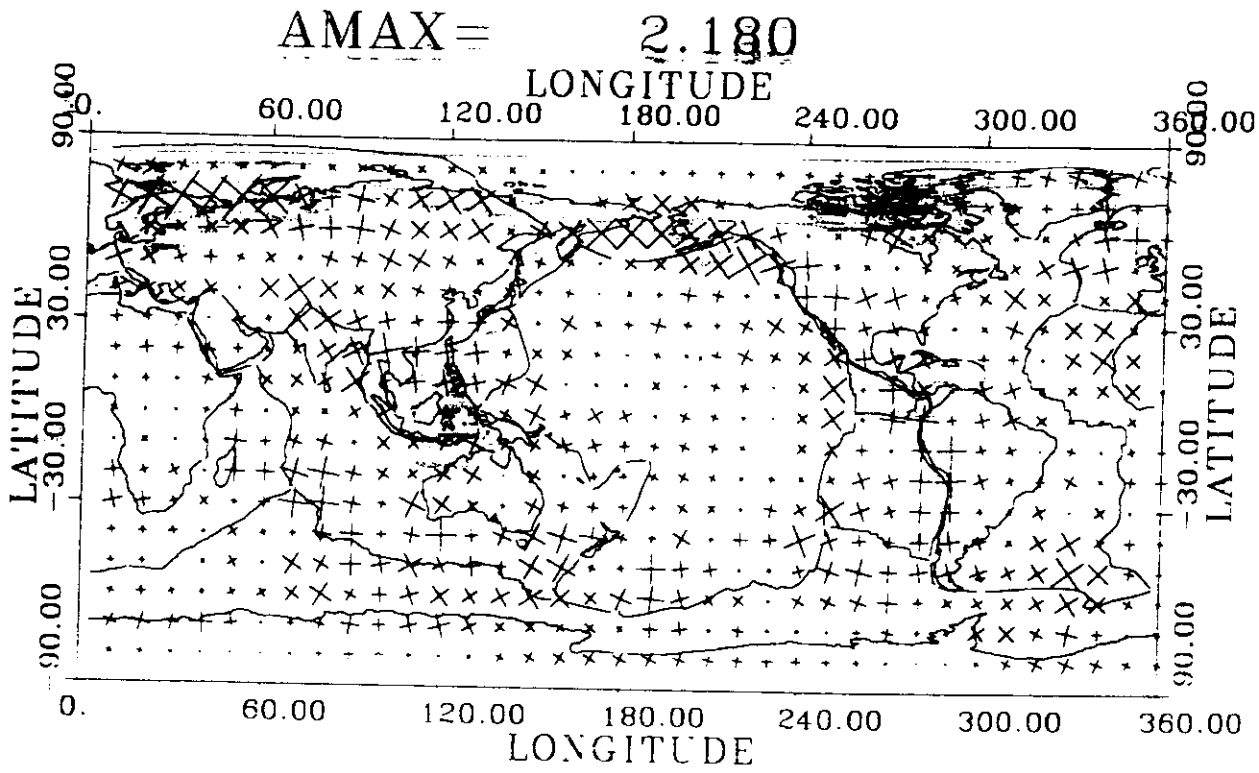

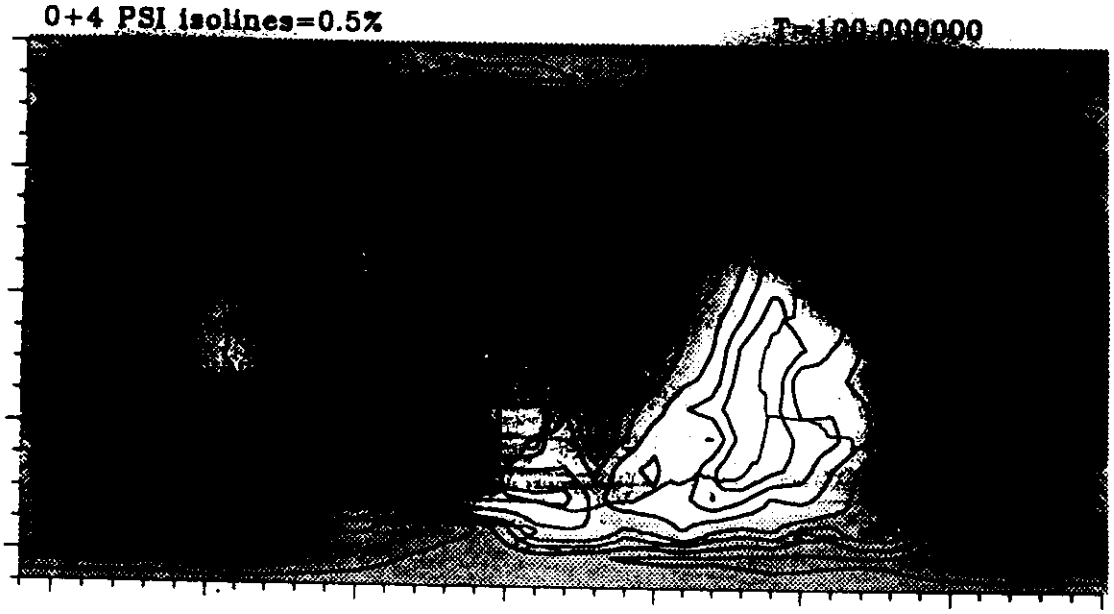

T = 100s

RAYLEIGH 0+2-PSI

AMAX= 2.240

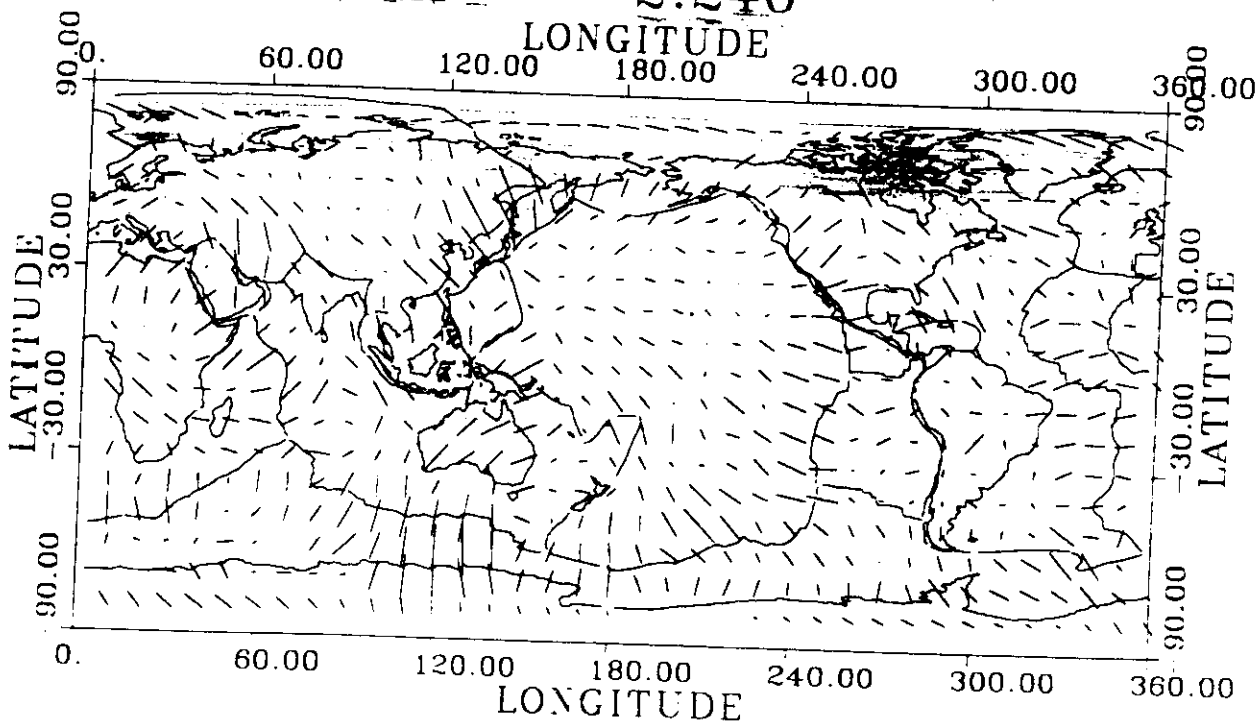

T = 100

Trampert and Woodhouse (1995)

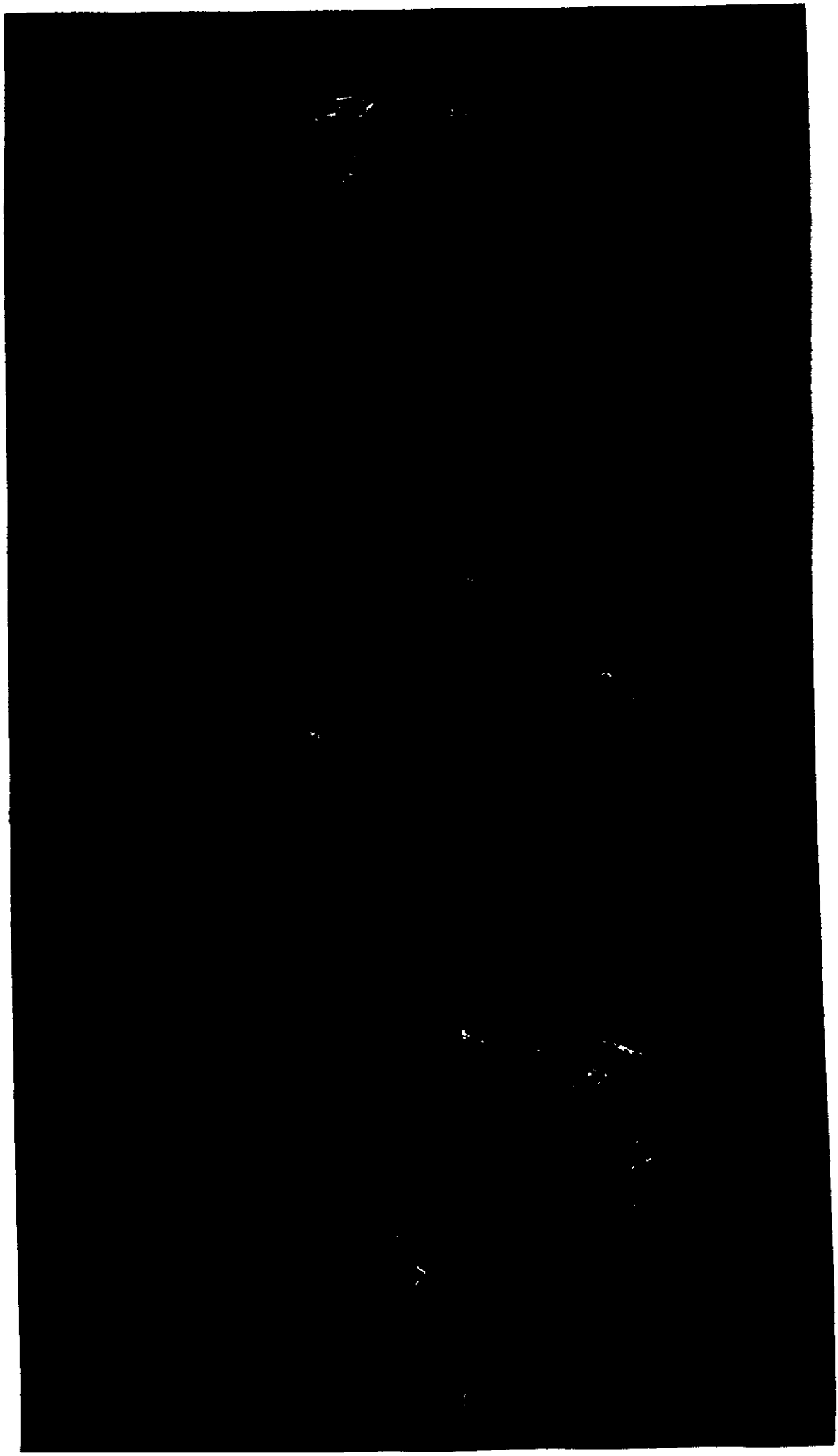

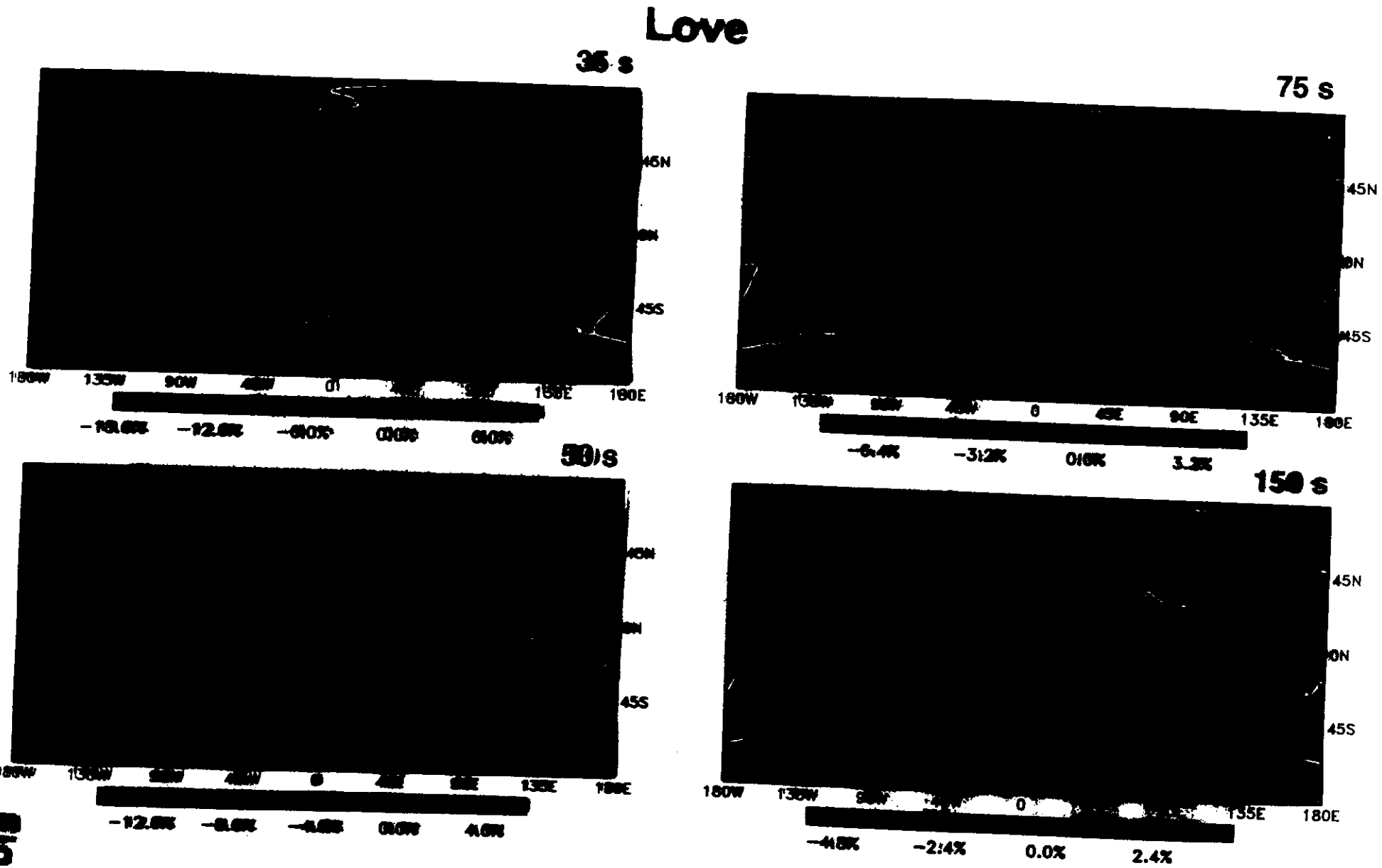

Fig. 12a

(Ekström et al., 1996)

AUM model at depth=100 km

(Montagner & Tanimoto, 1991)

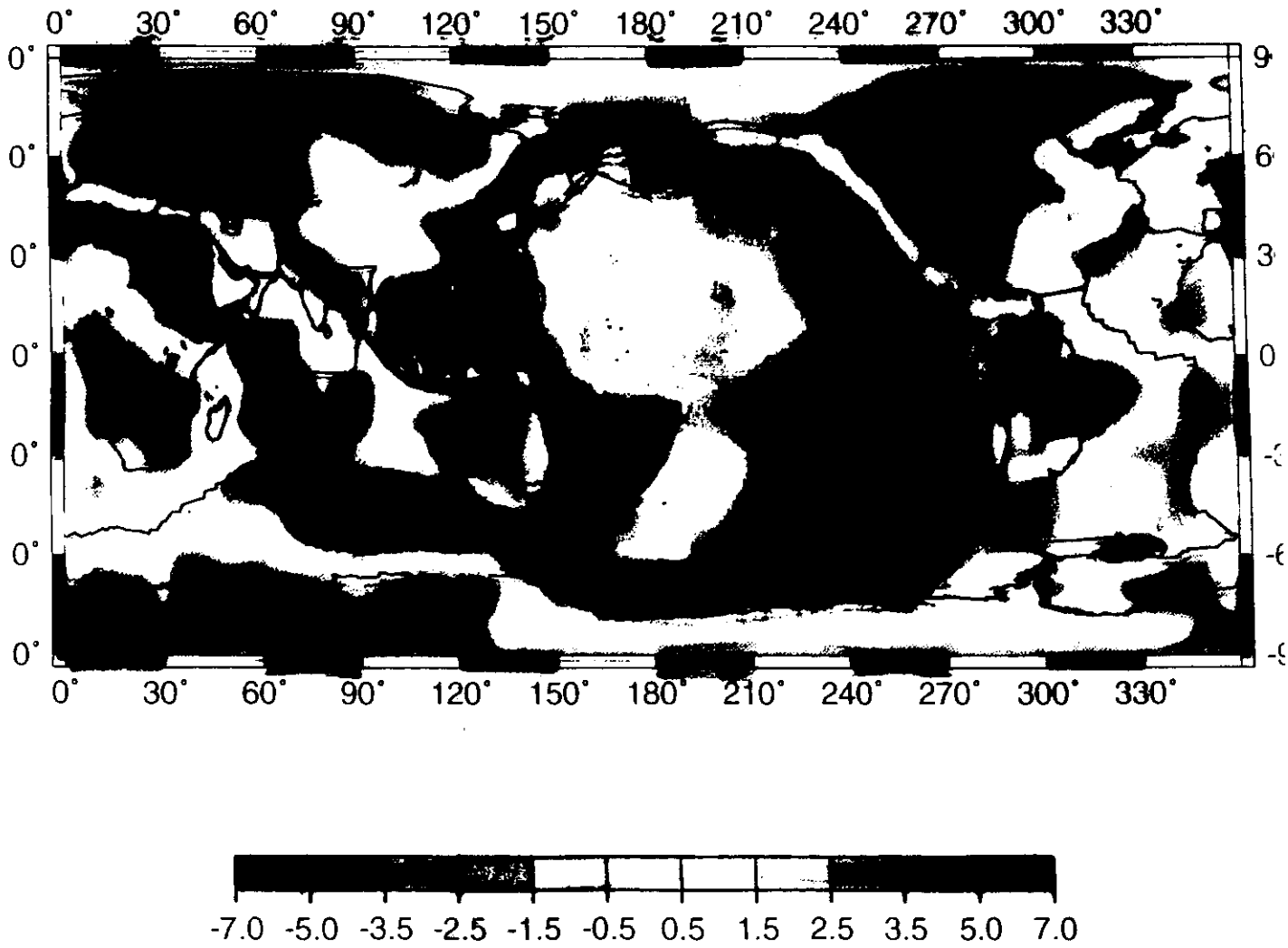

1

AUM model: Radial cross-section for 30 deg. N

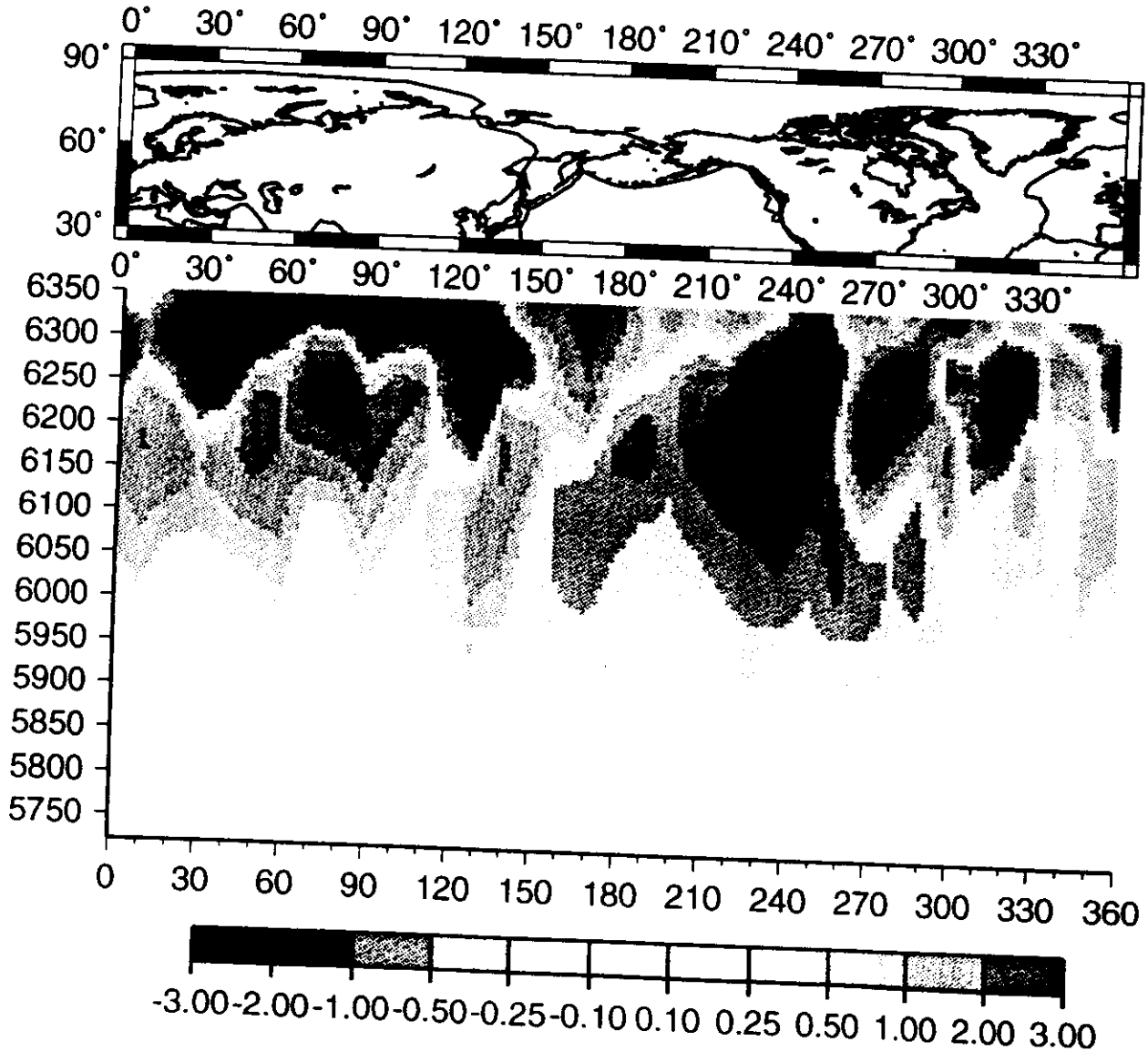

1 Geophysical applications

The number of applications of seismic tomography is very large. Seismic tomography is the most efficient approach to visualize, at the same time, seismic velocities and anisotropy heterogeneities, which can, in turn be related to temperature, petrological anomalies and flow directions. Therefore, the different fields interested in seismic tomography are geodynamics, gravimetry, geochemistry and tectonics. We will briefly review what kind of information can be provided by tomographic models.

• Geodynamics

The most popular application of tomographic models is the understanding of mantle convection, because seismic velocity anomalies can be converted, under some assumptions, into temperature anomalies or into density anomalies. Since *Hager et al.* (1985), numerous studies have been devoted to the correlation between 3D seismic velocity structure, the dynamic topography and the geoid.

Actually, part of seismic anomalies are related to mineralogical heterogeneities, but these ones are very difficult to assess. The main advantage of anisotropy measurements is to provide principal directions of strain, which are related to flow directions (*Anderson*, 1989). Therefore, the simultaneous use of seismic velocity and anisotropy makes it possible to spatially locate temperature and petrological heterogeneities, and their directions of flow. *Montagner and Nataf* (1988) present a method for inverting a local symmetry axis and *Montagner and Jobert* (1988) have been able to plot the 3D-distribution of this axis in the Indian ocean. *Montagner* (1994) presents what can seismic global tomographic tell us about mantle convection and what robust features can be drawn from the different available models.

Most tomographic models agree, that down to about 300km, the deep structure is closely related to plate tectonics and continental distribution. An horizontal cross-section at 30 degree north from model AUM (*Montagner and Tanimoto*, 1991) illustrates the most robust features of the upper mantle models published so far. In this upper depth range, all plate boundaries are slow: ridges and back-arc areas are slow, shields are fast and seismic velocity in oceanic areas is increasing with the age of the seafloor. The amplitude of SV-wave azimuthal anisotropy (G parameter) presents an average value of about 2% below oceanic areas (Figure 4b). It can be noted a good correlation between seismic azimuthal anisotropy and plate velocity directions given by *Minster and Jordan* (1978). As depth is increasing,the amplitude of heterogeneities is rapidly decreasing, some trends tend to vanish, and some distinctive features come up: Fast ridges are still slow but slow ridges are hardly visible and back-arc regions are no longer systematically slow. Large portions of fast ridges are offset with respect to their surface signatures. Below 300km of depth, a high velocity body below western Pacific can be related to subducting slabs.

In order to enable a quantitative comparison with other geophysical observables, tomographic models are usually expanded in spherical harmonics according to:

$$f(r,\theta,\phi) = \sum_{l=0}^{l_{max}} \sum_{m=-l}^{m=l} a_l^m(r) Y_\ell^m(\theta,\phi)$$

where r, θ, ϕ are the spherical coordinates at $\mathbf{r}$ and $Y_\ell^m(\theta,\phi)$ is the spherical harmonic of angular order ℓ and azimuthal order m. Another important parameter is the power spectrum $P_l(r)$, which provides the amplitude of anomalies at different degrees ℓ at different depths r.

In the first 300-400km of depth, the power spectrum regularly decreases with decreasing wavelength. This decrease can be described by a l^{-1} law (*Tanimoto*, 1990).
At greater depth, in the transition zone, degree 2 (*Masters et al.*, 1982) and to a less extent, degree 6 distributions become predominant. It is also found that degree 4 of radial anisotropy (*Roult et al.*, 1991; *Montagner and Tanimoto*, 1991) is the most important degree for this parameter. A simple flow pattern with 2 upgoing and 2 downgoing large-scale flows can be invoked to simply explain the predominance of these different degrees (*Montagner and Romanowicz*, 1993). Therefore, below the apparent complexity of plate tectonics, mantle convection is surprisingly simply organized in the transition zone. Between 400 and 1000km, these large-scale flows are not independent from the circulation in the first 400km but are related to the most tectonically active zones (fast ridges and slabs). This simple flow pattern, usually called degree 2 pattern, is also present in the lower mantle but offset with respect to the one in the transition zone. However, the nature of the power spectrum in the lower mantle is still subject of controversy (*Su and Dziewonski*, 1992).
It is also suggested that tomographic degree 6 is not independent of the deep degree 2 but might be a consequence of this simple flow pattern (*Cazenave et al.*, 1989; *Montagner and Romanowicz*, 1993). Since the hotspot distribution displays a large degree 6 (*Richards and Hager*, 1988), the good correlation between hotspot and seismic degrees 6 might favor an origin of most of hotspots in the transition zone. However, we cannot rule out the possibility of 2 superplumes in Central Pacific and Central Africa. There seems to be a global decoupling between upper structure and lower structure around 800-1000km, but there is some radial continuity of seismic velocity in the whole mantle in some places where slabs are present, and for 2 superplumes in central Pacific and Africa. All these issues are still subject of vigorous debate and call for more reliable tomographic models in the transition zone. However, there seems to be some good consensus that the mantle cannot be divided into independent convecting cells but is characterized by imbricated convection, where different scales coexist and where exchange of matter is possible.

• Geochemistry

The major-element chemistry of basalts erupted at mid-ocean ridges (MORB) is directly influenced by the temperature of the mantle beneath. Since tomography can be used to map lateral temperature variations on a global scale, it is possible to relate global co-variation between MORB chemistry and upper mantle shear wave velocity. The main advantage of this approach is that it can provide a way for locating at depth the reservoirs displayed by geochemists. For instance, *Humler et al.* (1993) found a strong correlation between basalt chemistry and seismic velocity at depths 100-170km, for lateral wavelengths of 1,000- 2,400km, supporting a common thermal origin for the 2 types of signal. This kind of simple approach can be easily generalized to other types of geochemical parameters and *Humler et al.* (in preparation) are applying it to geochemical isotopic elements.

• Petrology

Seismic profiles have long been used to infer the mineralogy of the mantle (*Birch*, 1952). The competing petrological models for the upper mantle and transition zone are pyrolite (*Ringwood*, 1975) and piclogite (*Anderson and Bass*, 1984, 1986). So far, the isotropic seismic velocities can be explained down to 400km by a pyrolite model, but in the transition zone, indifferently by pyrolite or piclogite. *Montagner and Anderson* (1989a) investigated the correlations between anisotropic parameters for realistic mineralogical and petrological models of the up-

per mantle. They show that the anisotropic parameters involved in a radiallly anisotropic medium A, C, F, L, N are strongly correlated but that the 8 other anisotropic parameters $B_c, B_s, G_c, G_s, H_c, H_s, E_c, E_s$ involved in azimuthal anisotropy are less correlated. These correlations have been used in deriving a reference Earth model (ACY400, *Montagner and Anderson*, 1989b). However, a complete exploitation of 3D anisotropic tomographic models such as AUM (*Montagner and Tanimoto*, 1991) has not yet been done. This kind of approach might provide in the future some important constraints on mineralogy in the deep mantle.

• Tectonics

The scientific potential of anisotropy is enormous and still largely unexploited. We have seen so far that the anisotropic parameters make it possible to map convection in the mantle. But only deep anisotropy (below the crust) was considered and related to actual geodynamic processes. The strain field near the surface is probably different from the deep one and could be also related to the strain field prevailing during the setting of materials. This shallow anisotropy could be very useful for understanding the strain field responsible for surficial tectonics. For example, seismic anisotropy could be used for explaining geological observations, such as mountain range building or more generally continental deformation. Such an application is attempted by *Vinnik et al.* (1989a,b; 1992) and *Silver and Chan* (1988, 1991) by using anisotropy derived from SKS splitting. *Nicolas* (1993) and *Vauchez and Nicolas* (1991) are now able relate the geometry of orogenic areas and directions given by SKS-waves splitting. And some quantitative evaluation of the contribution of crustal rocks to the shear-wave splitting is now possible (*Barruol and Mainprice*, 1993).

All these examples show that isotropic seismic tomography is now widely used by the community of Earth scientists and constitutes an invaluable source of information and inspiration but that anisotropic tomography is still largely unexploited.

2 Conclusions

We have presented in this paper some basic first-order asymptotic theories which make it possible to derive a whole family of tomographic models. It was shown that normal modes and surface waves give access not only to isotropic parameters V_P and V_S, but to anisotropic and anelastic parameters as well. It was also shown that the phase information can be more easily interpreted in terms of structural parameters than the amplitude information. That is the reason why seismologists primarily worked on the phase of seismograms rather than on its amplitude. This fundamental distinction between phase and amplitude results from the Fermat's principle (or Rayleigh's principle) which states that the propagation time (directly related to phase) is stationary to second order with respect to path perturbations, contrarily to the amplitude of waves. However, by making some simple assumptions, it is now possible to use amplitude data in Fourier domain, for retrieving the first tomographic models of attenuation. The next steps will consist in taking a simultaneous account of phase and amplitude of seismic waves. By using new theoretical developments, it will be possible to calculate synthetic seismograms in complex *a priori* laterally heterogeneous media and to make a direct comparison with seismic waveform in time domain. And it will be possible to correctly assess the effect of scattering on seismograms. Notwithstanding these theoretical improvements, it should be desirable to increase the lateral resolution of tomographic models, firstly, by installing broad-

band networks at smaller scale (wavelengths smaller than 1000km), secondly by implementing an ocean seismic network, which will provide a better coverage of the whole Earth by seismic waves.

Ackowledgments

CNRS URA 195 - I.U.F. This work was partly supported by 'ATP Tomographie' (1996). This is I.P.G.P. contribution # .

This technique has made it possible to simultaneously explain the "Rayleigh-Love discrepancy" and the azimuhal anisotropy, firstly displayed in the Nazca plate by *Forsyth* (1975). However, the main limitation of this technique applied to the fundamental mode of surface waves is that the radial resolution is limited to the first 500km of the upper mantle. In order to go further, it is necessary to use seismic waves sensitive to deeper structure. Multiple reflected S-waves or higher modes of surface waves are good candidates for doing that. The first approach using body waves obtained by normal mode summation was followed by *Nolet and Kennett* (1978), *Tanimoto* (1990), *Su and Dziewonski* (1991, 1992) and *Woodward and Masters* (1991a,b). On the other hand, *Stutzmann and Montagner* (1993, 1994) showed how to generalize this 2-step tomographic technique to higher modes for retrieving the global structure down to 1500km in the mantle.

APPENDIX: Practical description of a tomographic technique

To solve inverse problems defined in section 3.2, the algorithm of *Tarantola and Valette* (1982) can be used:

$$\mathbf{p} - \mathbf{p_0} = (G^t C_d^{-1} G + C_p^{-1})^{-1} G^t C_d^{-1} (\mathbf{d} - \mathbf{g}(\mathbf{p}) + G(\mathbf{p} - \mathbf{p_0})) \tag{26}$$

where C_d is the covariance matrix of data, C_p the covariance function of parameters $\mathbf{p}$, and G is the Frechet derivative of the operator $\mathbf{g}$ at point $\mathbf{p}(\mathbf{r})$.

This algorithm can be made more explicit by writing it in its integral form:

$$\mathbf{p}(\mathbf{r}) = \mathbf{p_0}(\mathbf{r}) + \sum_i \sum_j \int_V d\mathbf{r}' C_{p_0}(\mathbf{r}, \mathbf{r}') G_i(\mathbf{r}') (S^{-1})_{ij} F_j \tag{27}$$

with

$$S_{ij} = C_{d_{ij}} + \int_V d\mathbf{r_1} d\mathbf{r_2}\, G_i(\mathbf{r_1}) C_{p_0}(\mathbf{r_1}, \mathbf{r_2})\, G_j(\mathbf{r_2})$$

and

$$F_j = d_j - g_j(\mathbf{p} + \int_V d\mathbf{r}''\, G_j(\mathbf{r}'')(\mathbf{p}(\mathbf{r}'') - \mathbf{p_0}(\mathbf{r}''))$$

This algorithm can be iterated and enables to solve slightly non-linear problems, which is the case of the inversion at depth. In case of a large dataset, *Montagner and Tanimoto* (1990) showed how to handle the inverse problem by making a series expansion of the inverse of the matrix S. One of the advantage of this technique is that it can be applied indifferently to regional studies or global studies. In case of imperfect spatial coverage of the area under investigation, it does not display ringing phenomena commonly observed when a spherical harmonics expansion is used (*Tanimoto*, 1985).

The *a posteriori* covariance function is given by:

$$C_p = C_{p_0} - C_{p_0} G^T (C_{d_0} + G C_{p_0} G^T)^{-1} G C_{p_0} = (G^T C_{d_0} G + C_{p_0})^{-1} \tag{28}$$

For the spatial description of the parameter space $\mathbf{p}(\mathbf{r})$, either a discrete basis of functions or a continuous function can be considered. In that case, *Montagner* (1986b) used a Von Mises distribution (*Fisher*, 1953) for the horizontal variations, of parameter $\mathbf{p_0}(\mathbf{r})$ and the *a priori* covariance function of parameters is given by:

$$C_{p_0}(\mathbf{r}, \mathbf{r}') = \sigma_p(\mathbf{r}) \sigma_p(\mathbf{r}') \exp \frac{\cos \Delta_{\mathbf{r}\mathbf{r}'} - 1}{L_{cor}^2}$$

where L_{cor} is the correlation length which will define the smoothness of the final model. This kind of distribution is well suited for studies on a sphere and is asymptotically equivalent to a Gaussian distribution when $L_{cor} \ll a$ (a radius of the Earth).
For the inversion at depth, since the number of physical parameters is very large (13), it is more difficult to make this assumption, and the different terms of the covariance function of parameters C_p between parameters p_1 and p_2 at radii r_i and r_j can be defined as follows:

$$C_{p_1,p_2}(r_i, r_j) = \sigma_{p_1}\sigma_{p_2}\zeta_{p_1,p_2}e^{\frac{(r_i-r_j)^2}{2L_{r_i}L_{r_j}}} \tag{29}$$

Where ζ_{p_1,p_2} is the correlation between physical parameters p_1 and p_2 inferred for instance from different petrological models (*Montagner and Anderson*, 1989a) and L_{r_i}, L_{r_j} are the radial correlation lengths which enable to smooth the inverse model. The resolution R of parameters can be calculated as well. It corresponds to the impulsive response of the system:

$$\mathbf{p} = \tilde{\mathbf{g}^{-1}}\mathbf{d} = \tilde{\mathbf{g}^{-1}}\mathbf{g}\mathbf{p}' = R\mathbf{p}'$$

If the inverse problem is perfectly solved, R is the identity function or matrix. However, the following expression of resolution is only valid in the linear case (*Montagner and Jobert*, 1981):

$$R = C_{p_0}G^T(C_{d_0} + GC_{p_0}G^T)^{-1}G = (G^TC_{d_0}G + C_{p_0})^{-1}G^TC_{d_0}^{-1}G \tag{30}$$

By considering the *a posteriori* covariance function and the resolution, it is possible to assess the reliability of the hypotheses made about the independence of parameters. For example *Tanimoto and Anderson* (1985) and *Montagner and Jobert* (1988) showed that there is a trade-off between azimuthal terms and constant term in case of a poor azimuthal coverage. For the inversion at depth *Nataf et al.* (1986) display as well the trade-off between physical parameters V_{PH}, V_{SV}, ξ, ϕ and η when only Rayleigh and Love wave $0 - \Psi$-terms are used in the inversion process.

EARTH SEISMIC

ANISOTROPY

A BASIC TOOL FOR GEODYNAMICS,

BUT ALSO FOR TECTONICS, MINERAL PHYSICS, PETROLOGY, PROSPECTION...

APPLICATIONS OF ANISOTROPY

GEODYNAMICS - GEOLOGY

Mapping of flow (strain field)

- Radial anisotropy

Degree 4 (below 300-400km) related to "degree 2" pattern in the transition zone.

Base of continental lithosphere

- Azimuthal anisotropy

Comparison with plate velocities

Mountain building

Discrimination heterogeneous versus homogeneous strain field

PETROLOGY - MINERAL PHYSICS

Discrimination between competing models (to be done)

EARTHQUAKE PREDICTION

APPLIED GEOPHYSICS, OIL INDUSTRY

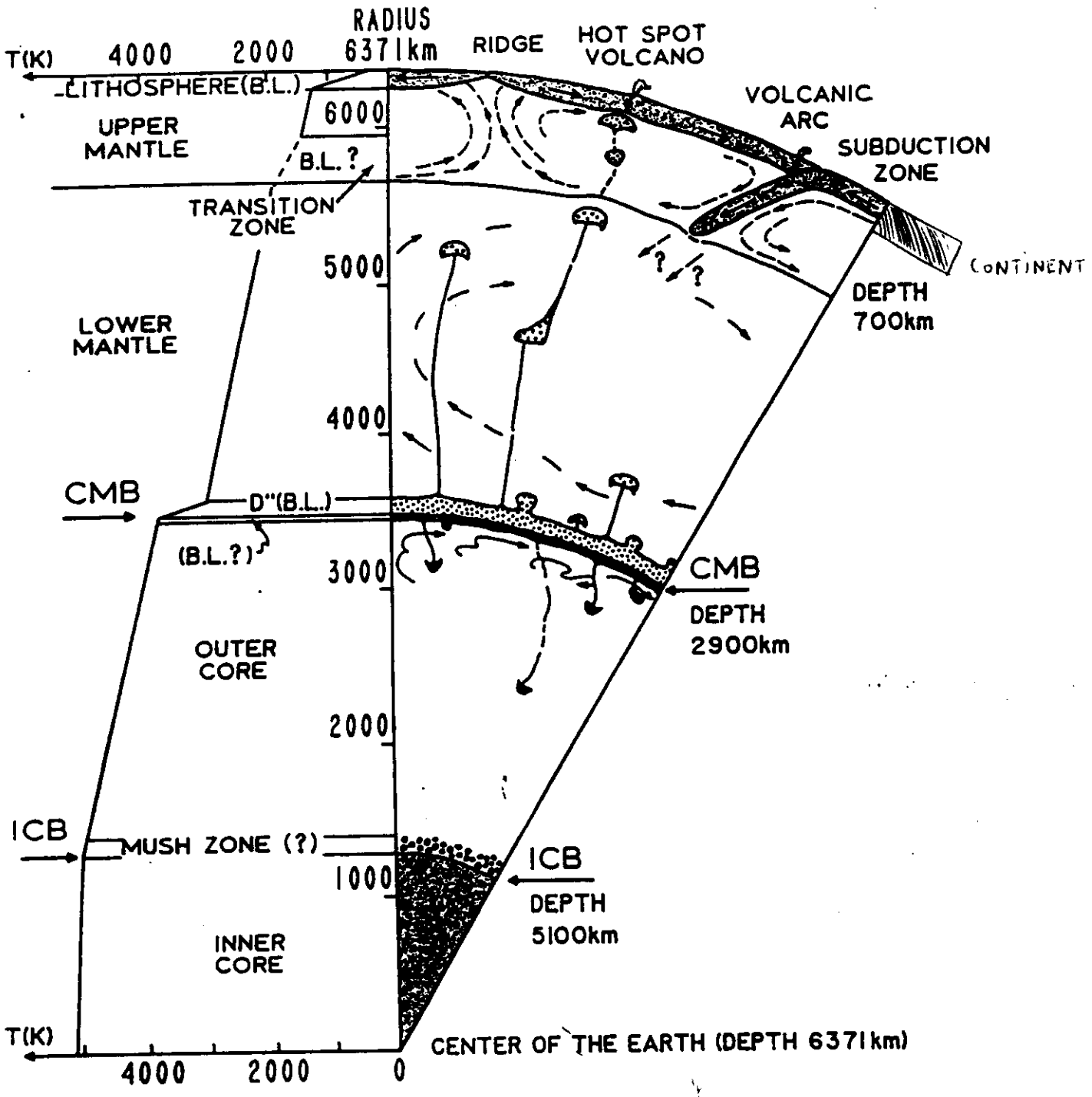
RADIUS
T(K) 4000 2000 6371km
RIDGE
HOT SPOT VOLCANO
LITHOSPHERE(B.L.)
VOLCANIC ARC
UPPER MANTLE
6000
B.L.?
SUBDUCTION ZONE
TRANSITION ZONE
CONTINENT
5000
DEPTH 700km
LOWER MANTLE
4000
CMB
D"(B.L.)
(B.L.?)
3000
CMB
DEPTH 2900km
OUTER CORE
2000
ICB
MUSH ZONE (?)
1000
ICB
DEPTH 5100km
INNER CORE
T(K)
4000 2000 0
CENTER OF THE EARTH (DEPTH 6371km)

fig 1

ANISOTROPY

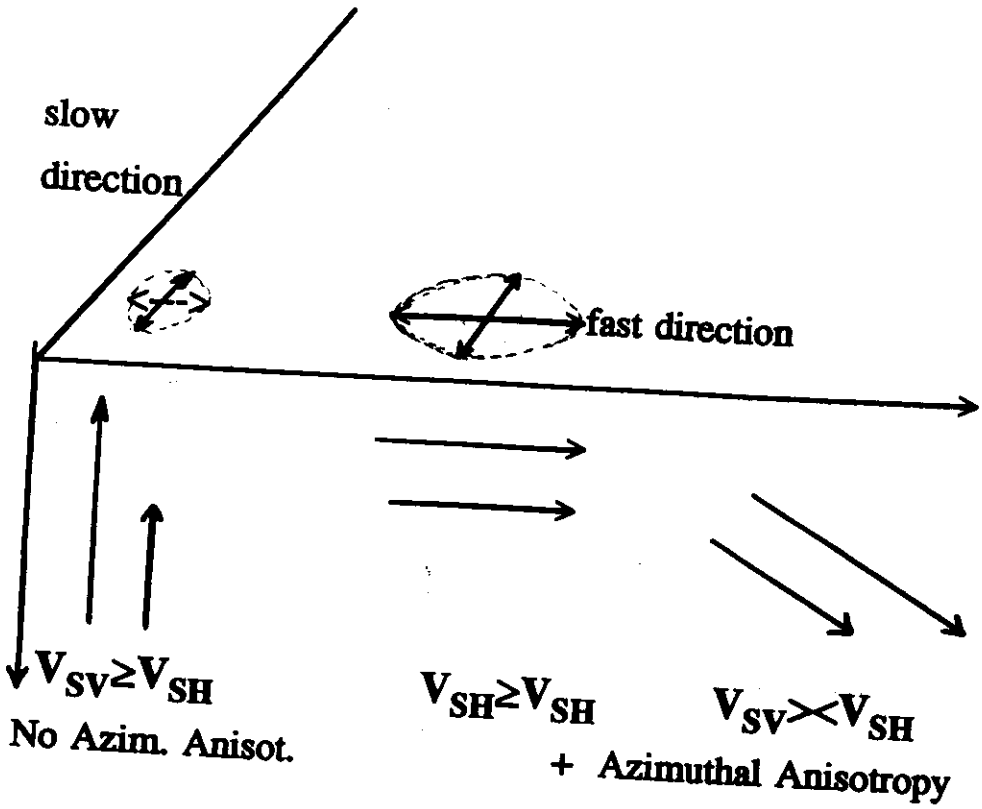

From a seismological point of view, 2 kinds of observable anisotropy:

- Radial Anisotropy: $\frac{(V_{SH}-V_{SV})}{V_{SV}}$
- Azimuthal Anisotropy:

Order of magnitude of anisotropy:

- Olivine: -10% +15%
- Pyrolite: -6% +7%
- Piclogite: -4 +4%

=> IT IS NOT A SECOND ORDER EFFECT.

APPLICATIONS: MAPPING CONVECTION + CONSTRAINING MINERALOGY

V_{SH}

DEPTH=100KM

AVERAGE=2.2%

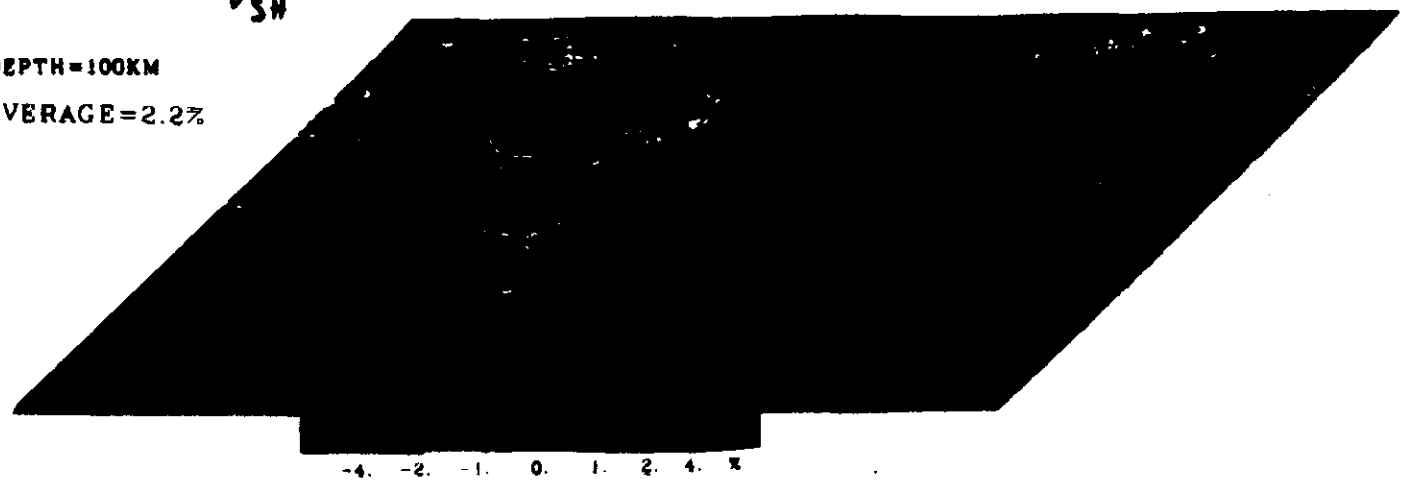

DEPTH=370KM

AVERAGE=-0.6%

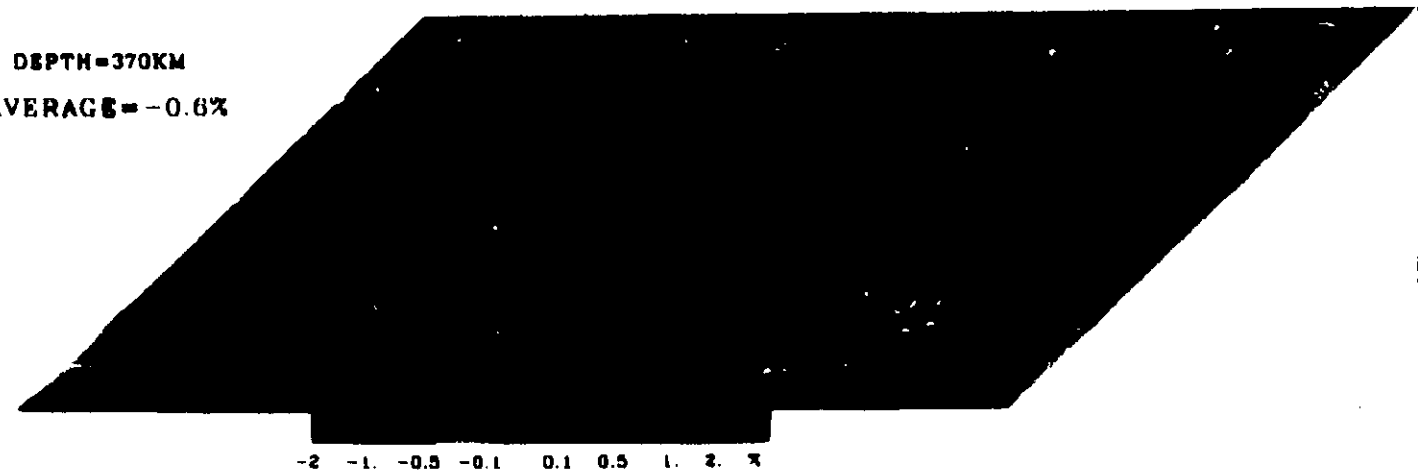

G at depth=200km

V_{SV} AZIMUTHAL ANISOTROPY

AMAX= 2.280

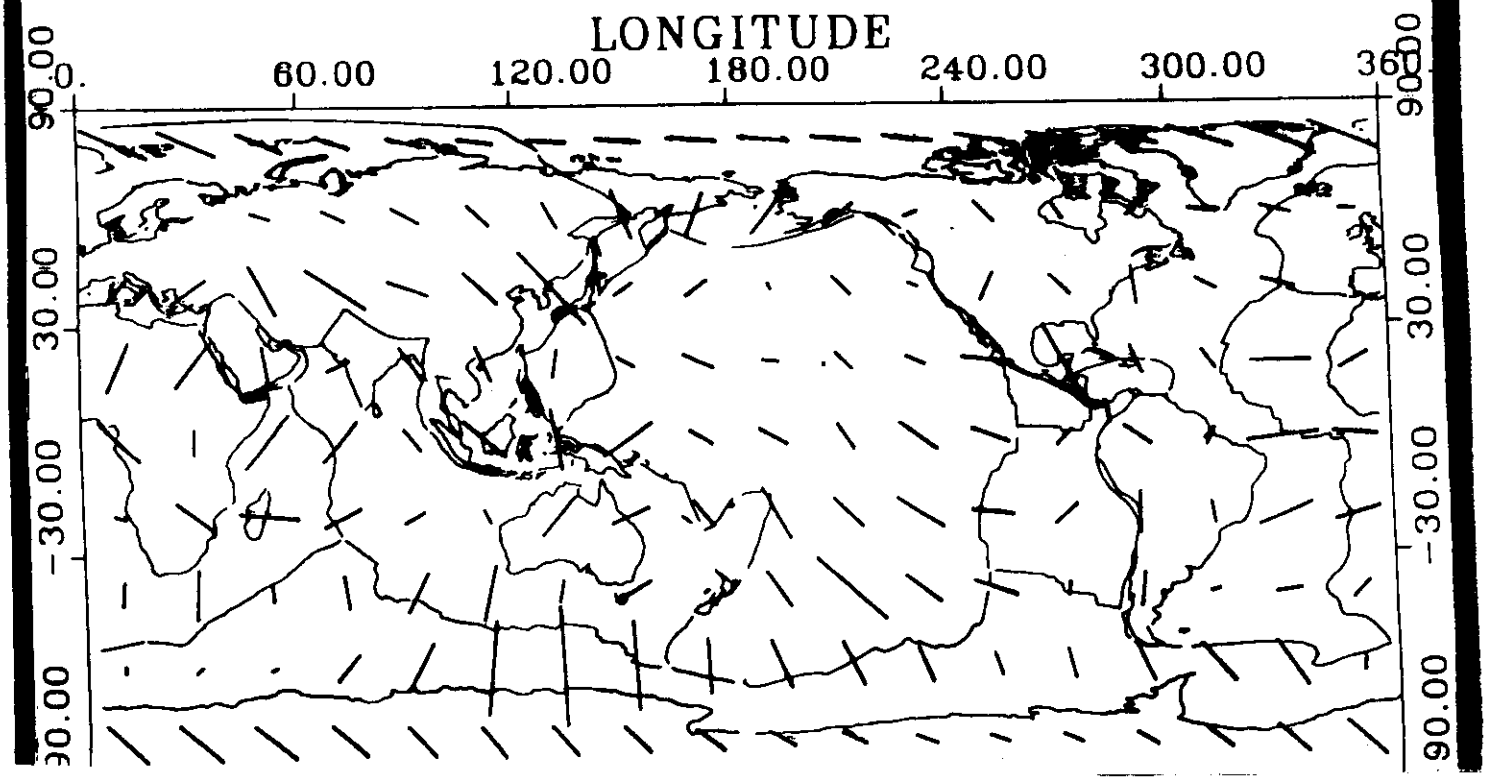

AUM model XI: Radial cross-section 20 deg.

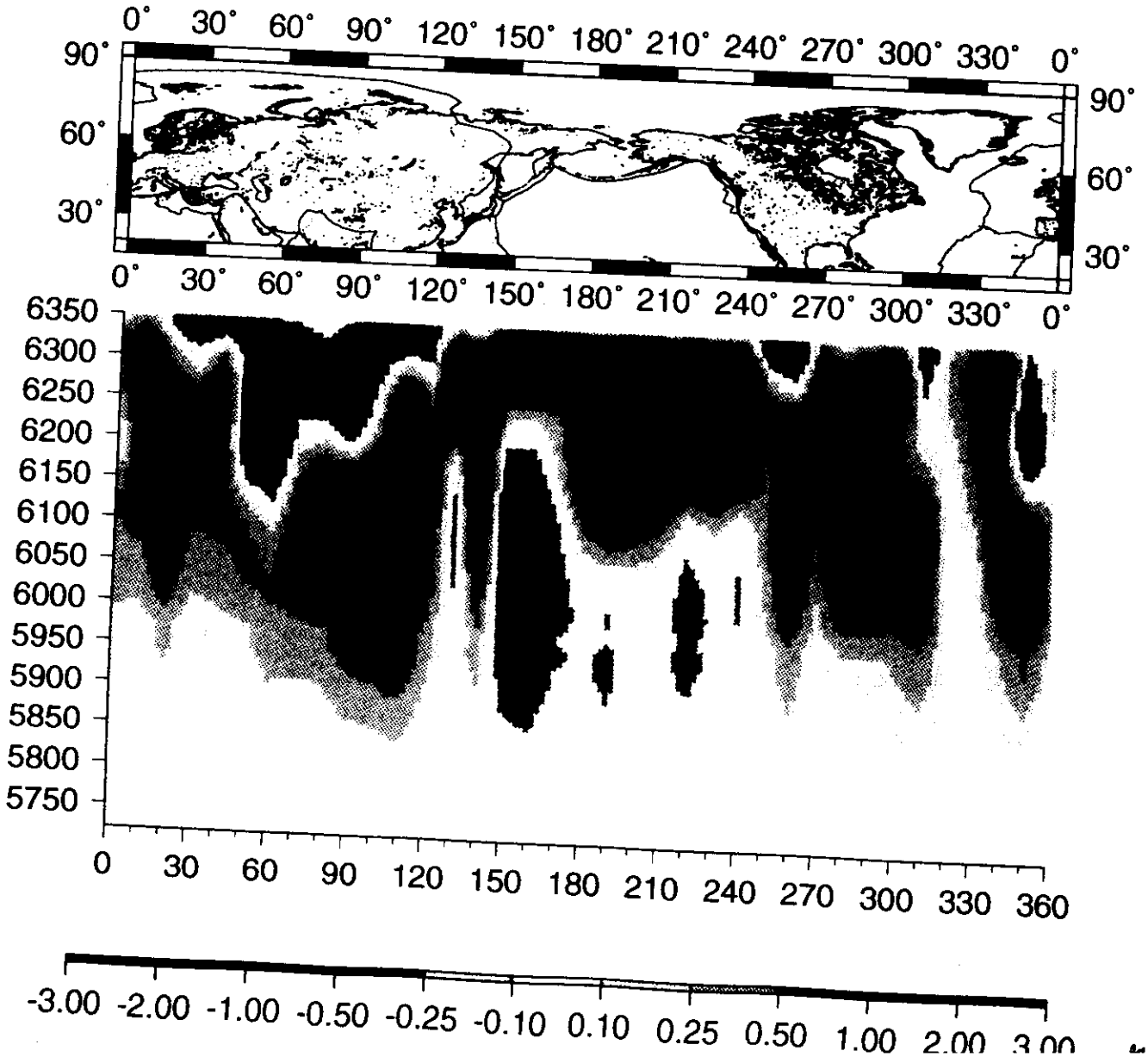

AUM model XI: Radial cross-section -10 deg.

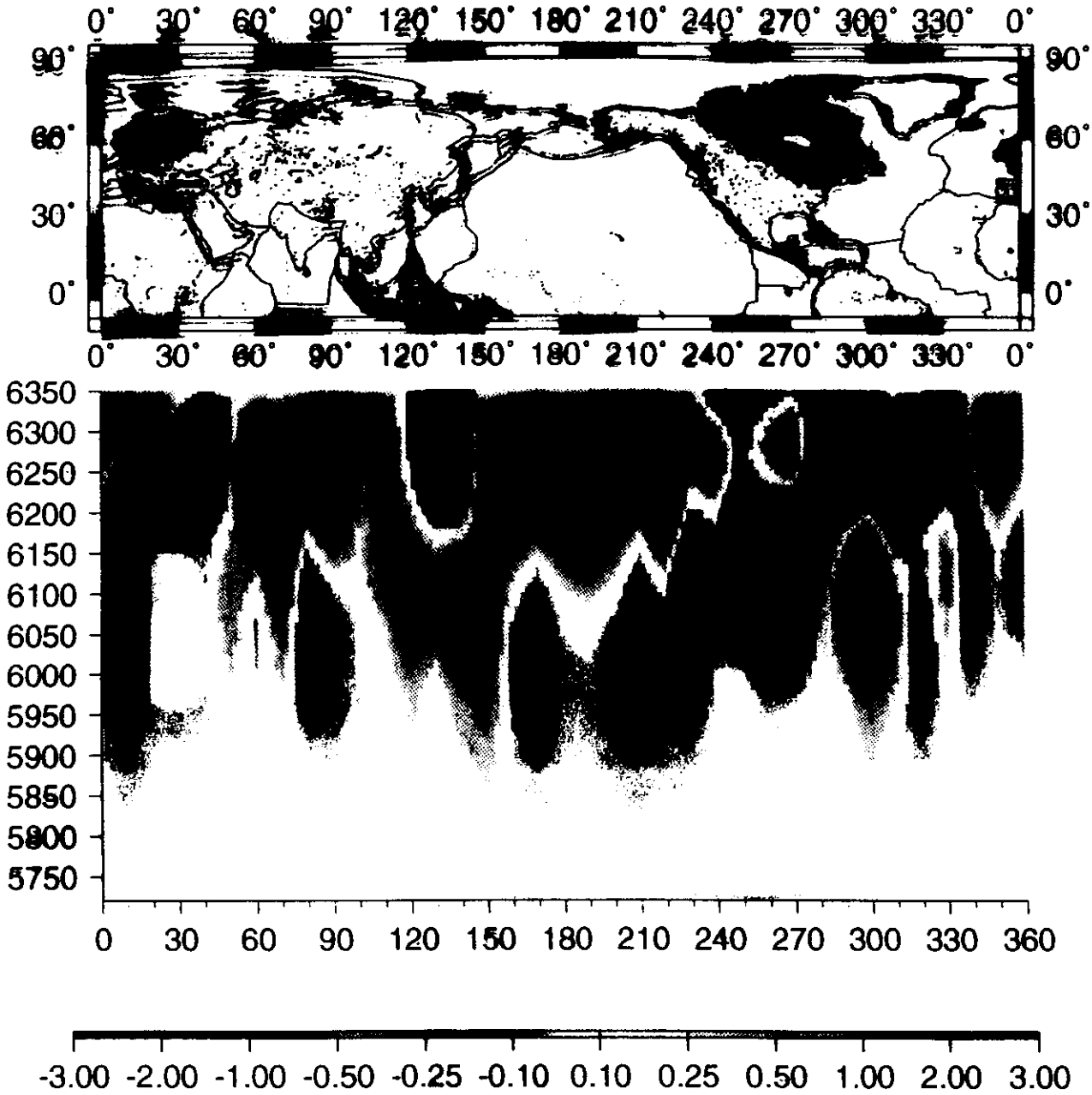

G at depth=200km

V_{SV} **AZIMUTHAL ANISOTROPY**

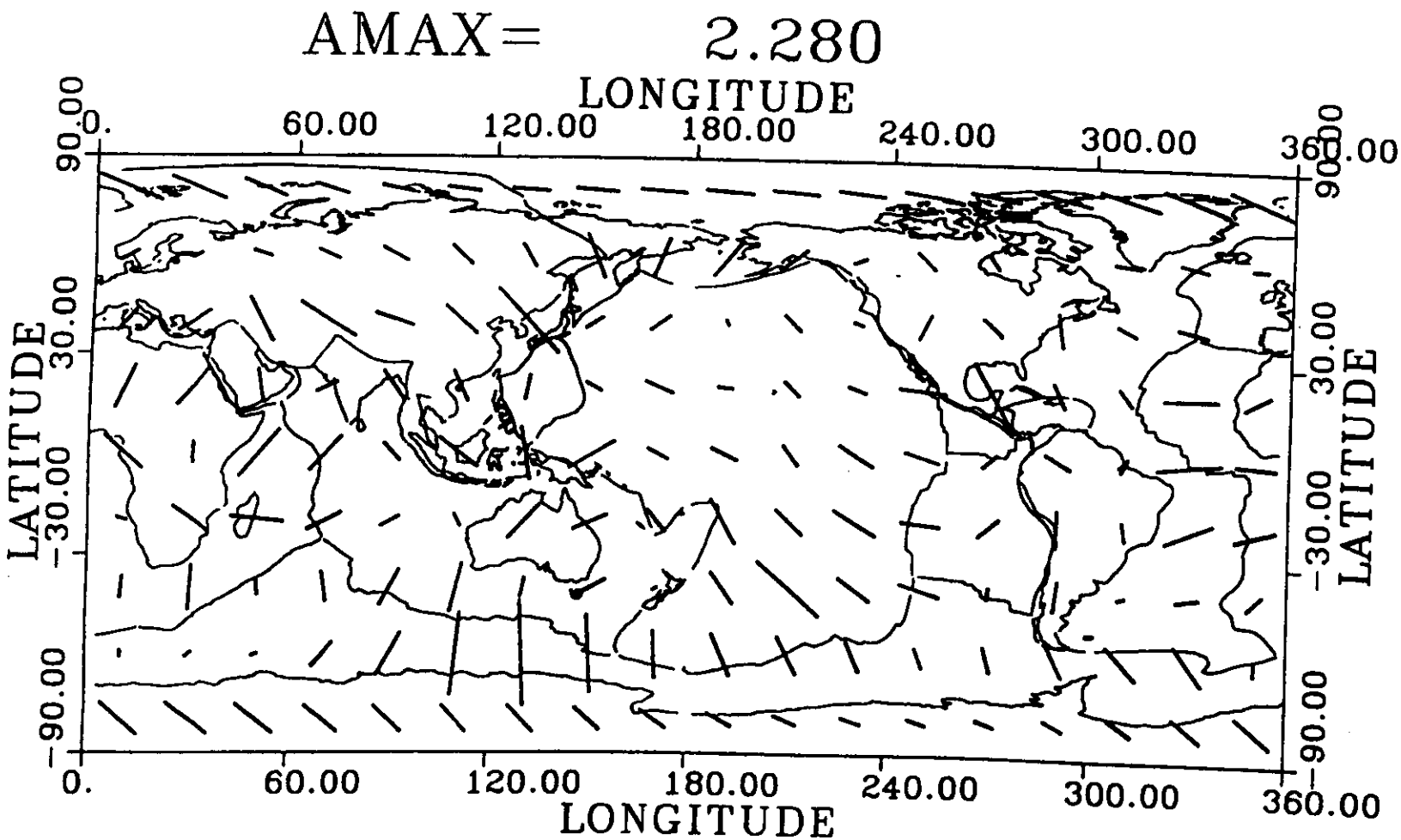

HISTOGRAM:

azimuthal anisotropy - plate velocitie

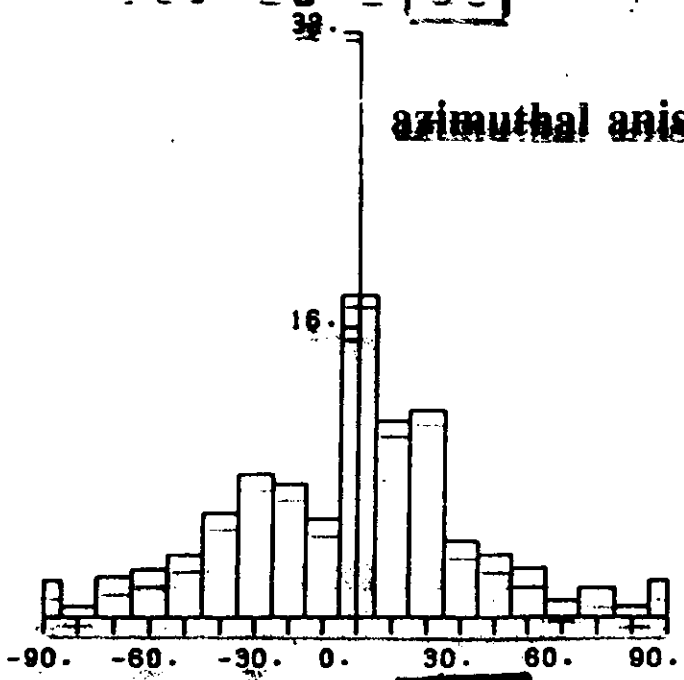

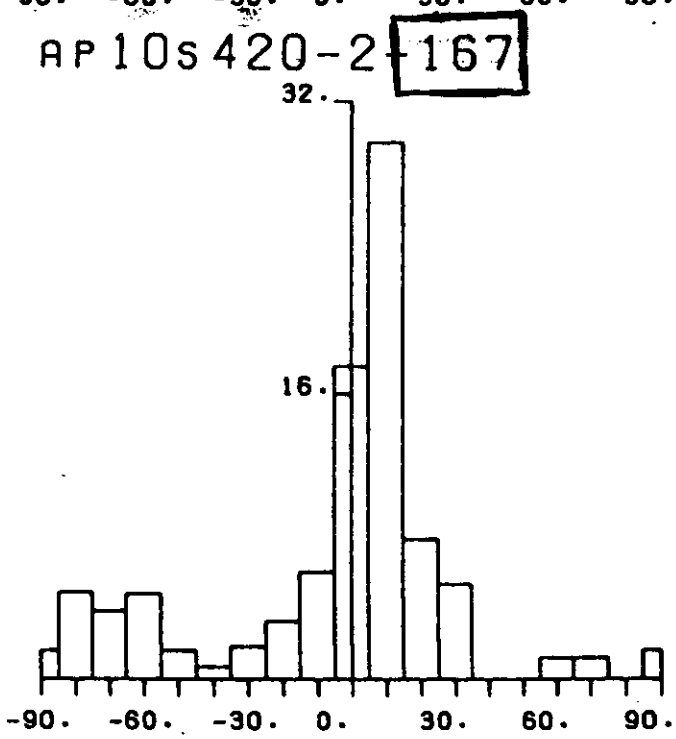

Pacific PLate

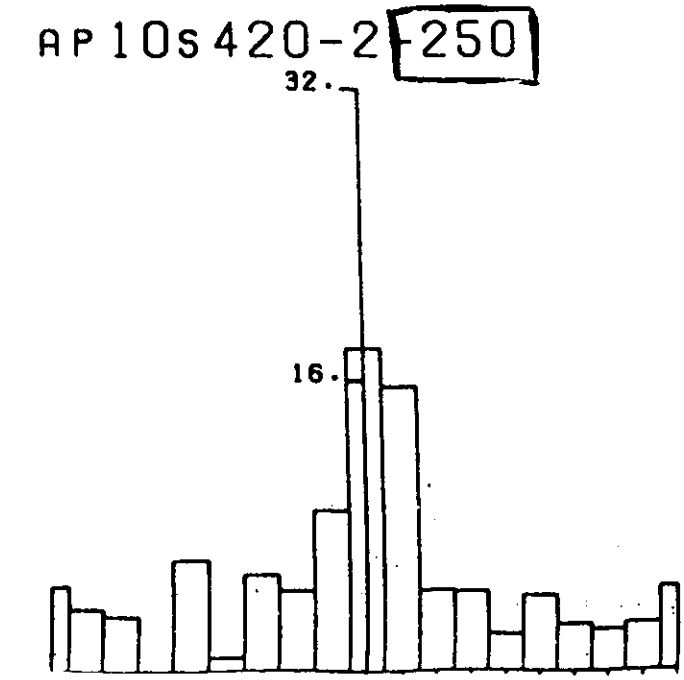

HISTOGRAM: AP10s420-2-83

azimuthal anisotropy - plate velocities

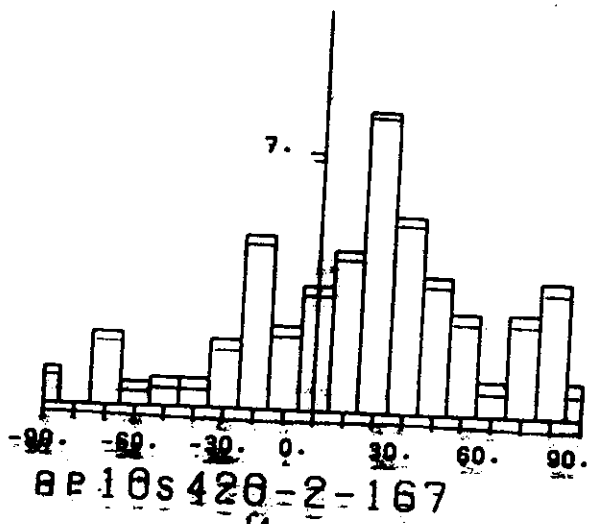

AP10s420-2-167

Australo-Indian Plate

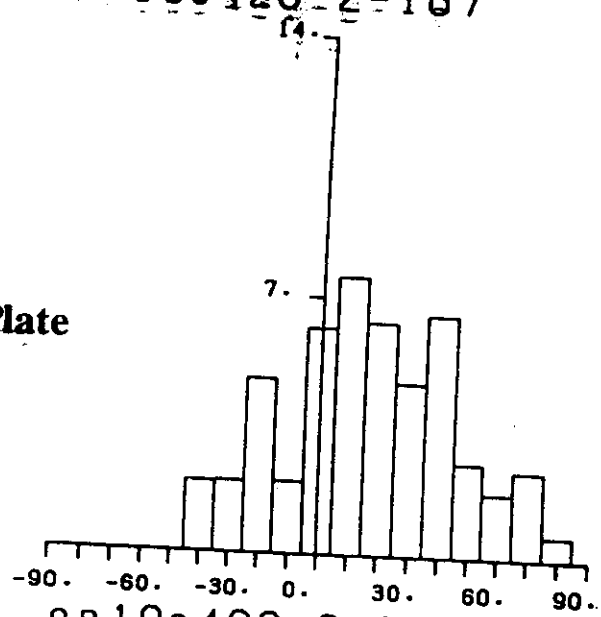

AP10s420-2-250

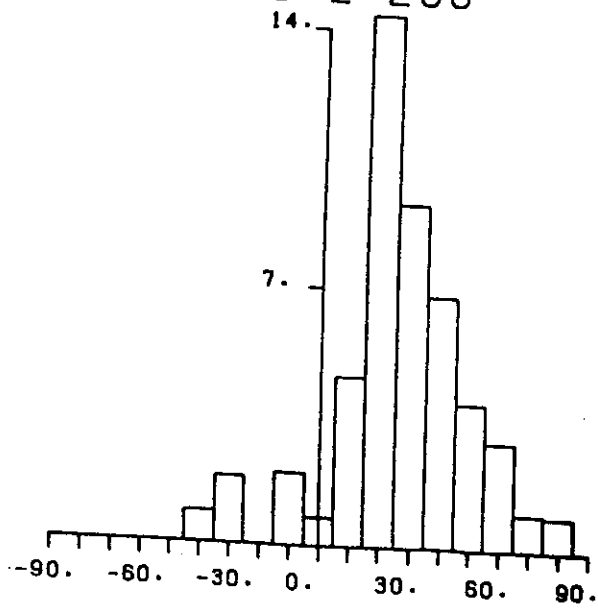

azimuthal anisotropy - plate velocitie

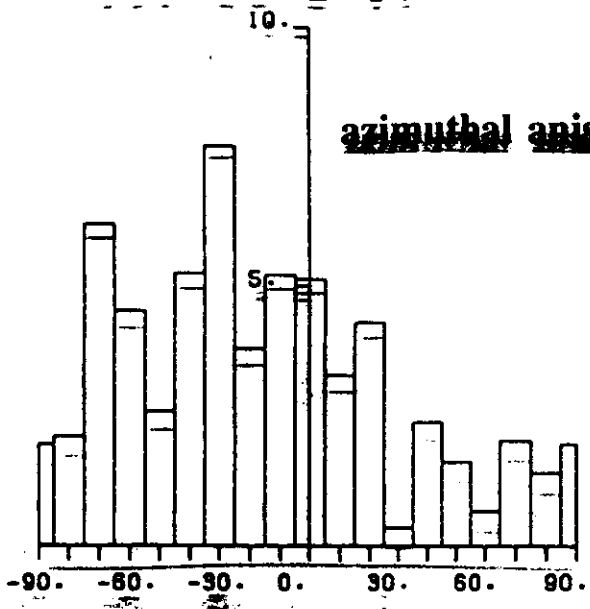

AP10S420-2-167

Eurasian Plate

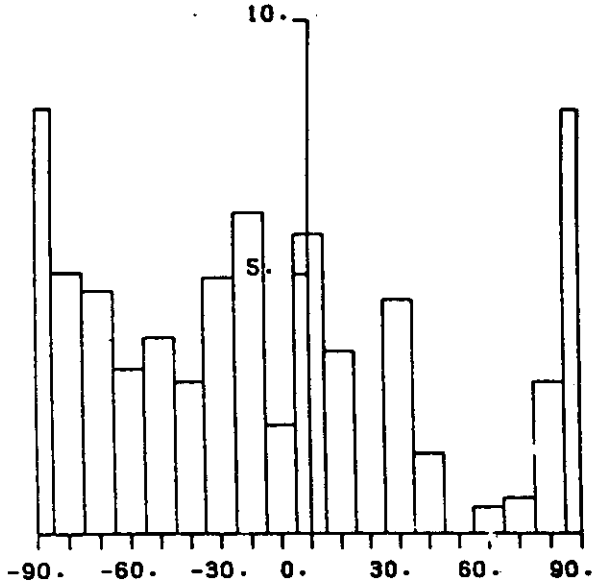

AP10S420-2-250

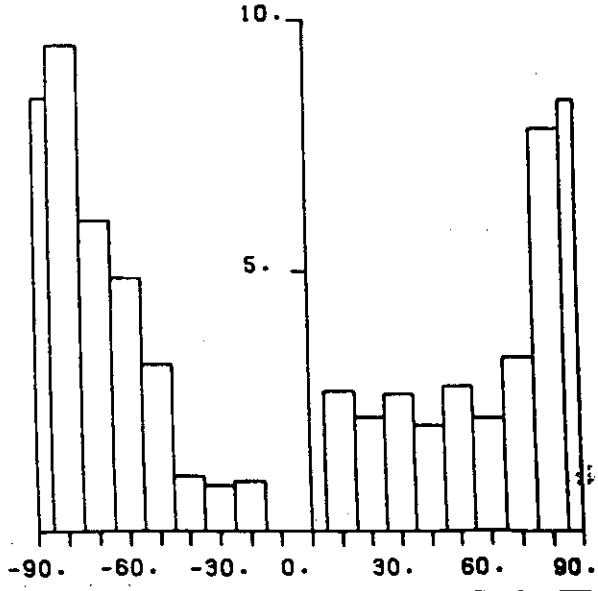

Homogeneous Model

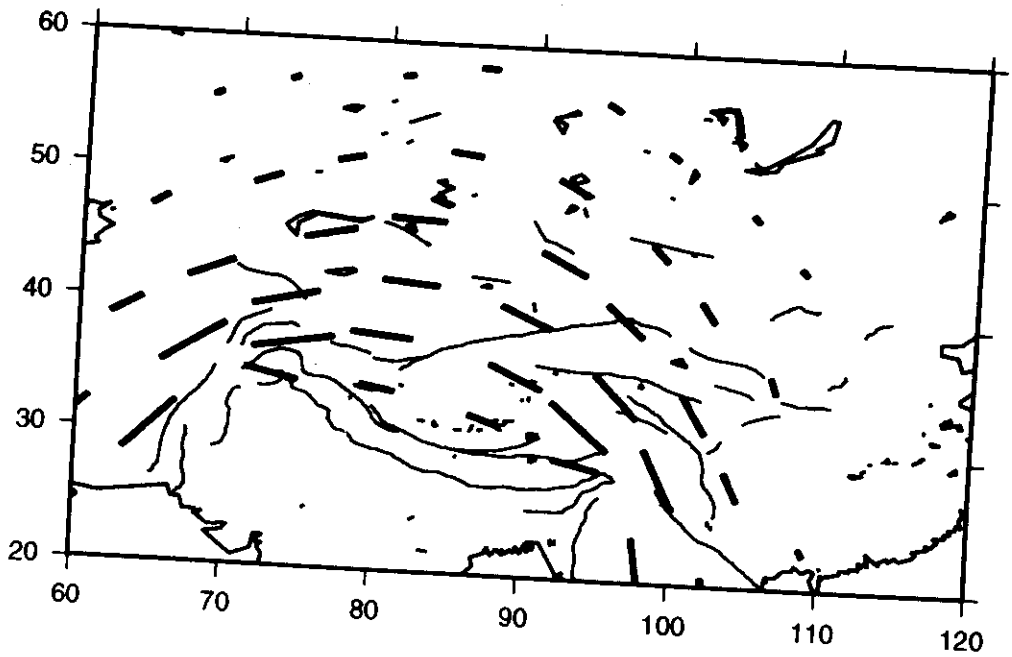

Heterogeneous Model

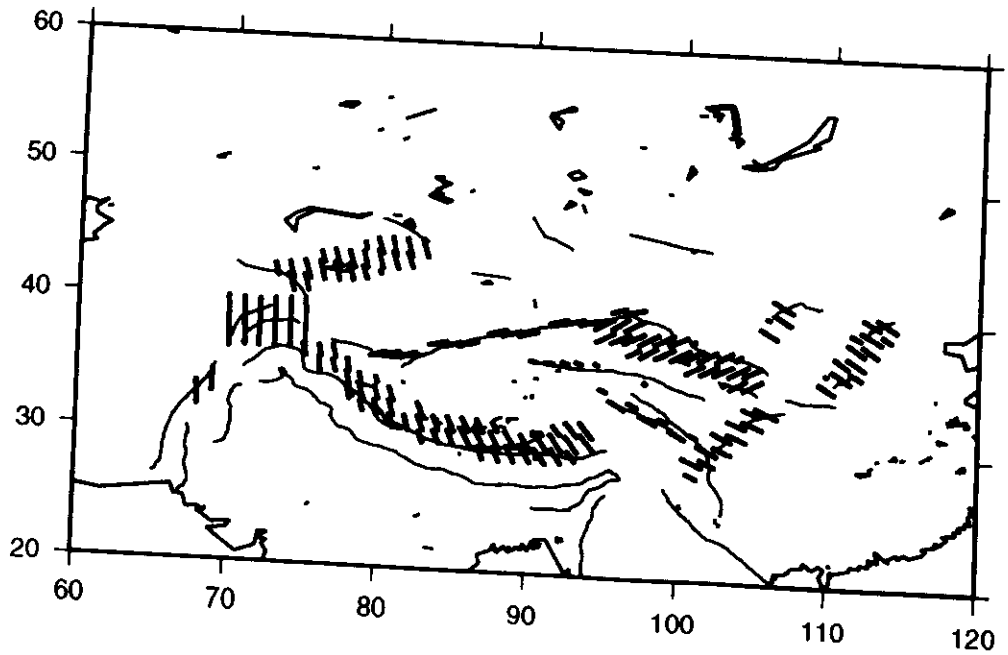

Griot et al. (1996)

Synthetic Anisotropy

Filtered homogeneous model

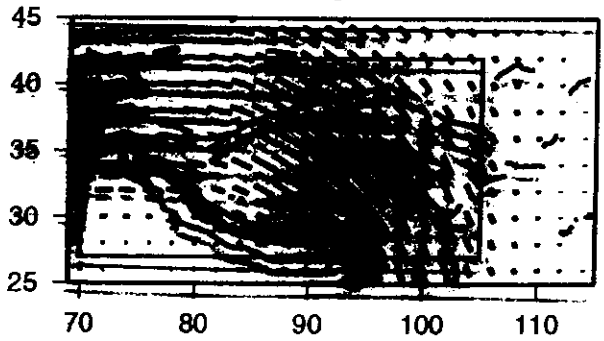

Filtered heterogeneous model

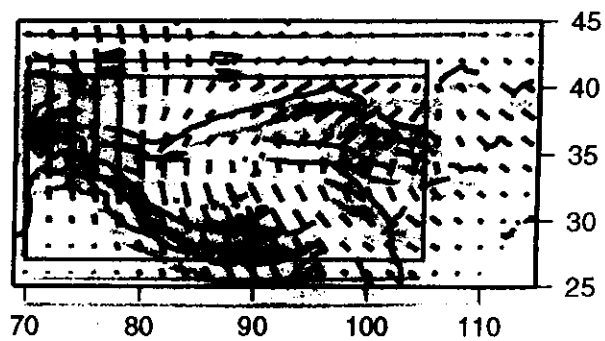

Seismological Anisotropy

Depth=70 km

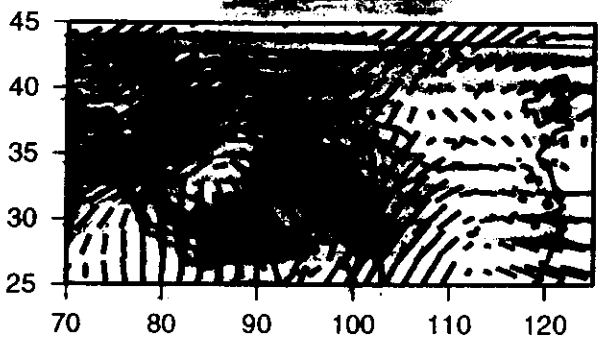

Depth=180 km

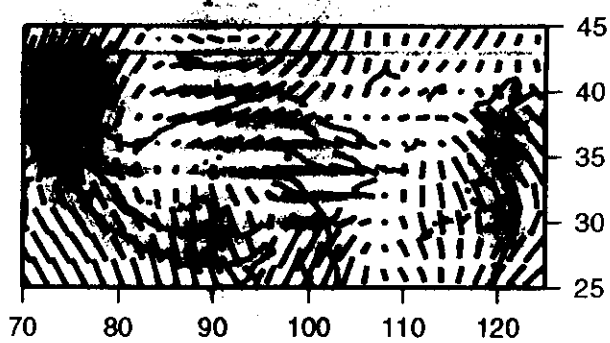

Depth=100 km

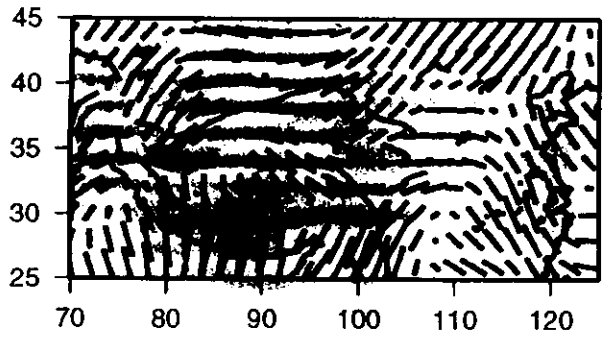

Depth=250 km

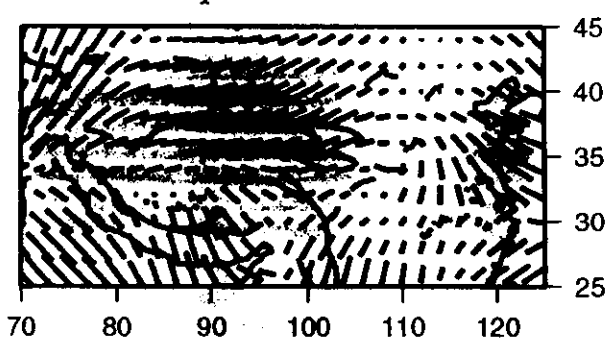

Depth=140 km

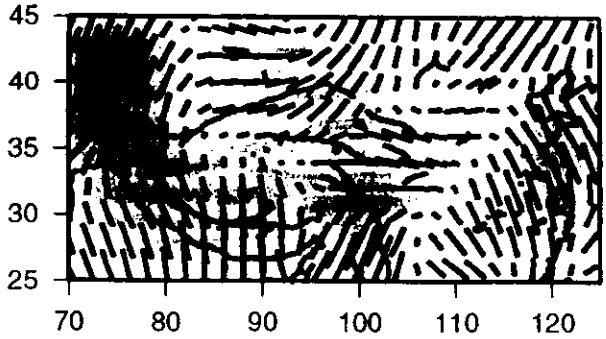

Depth=310 km

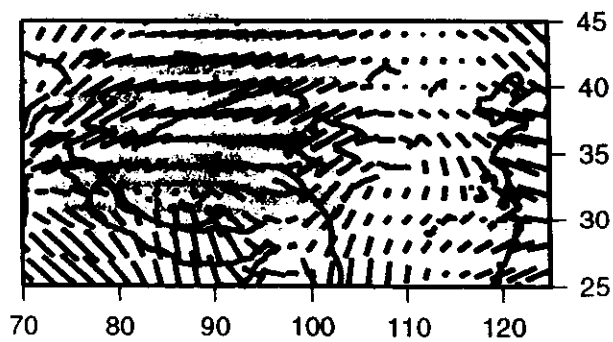

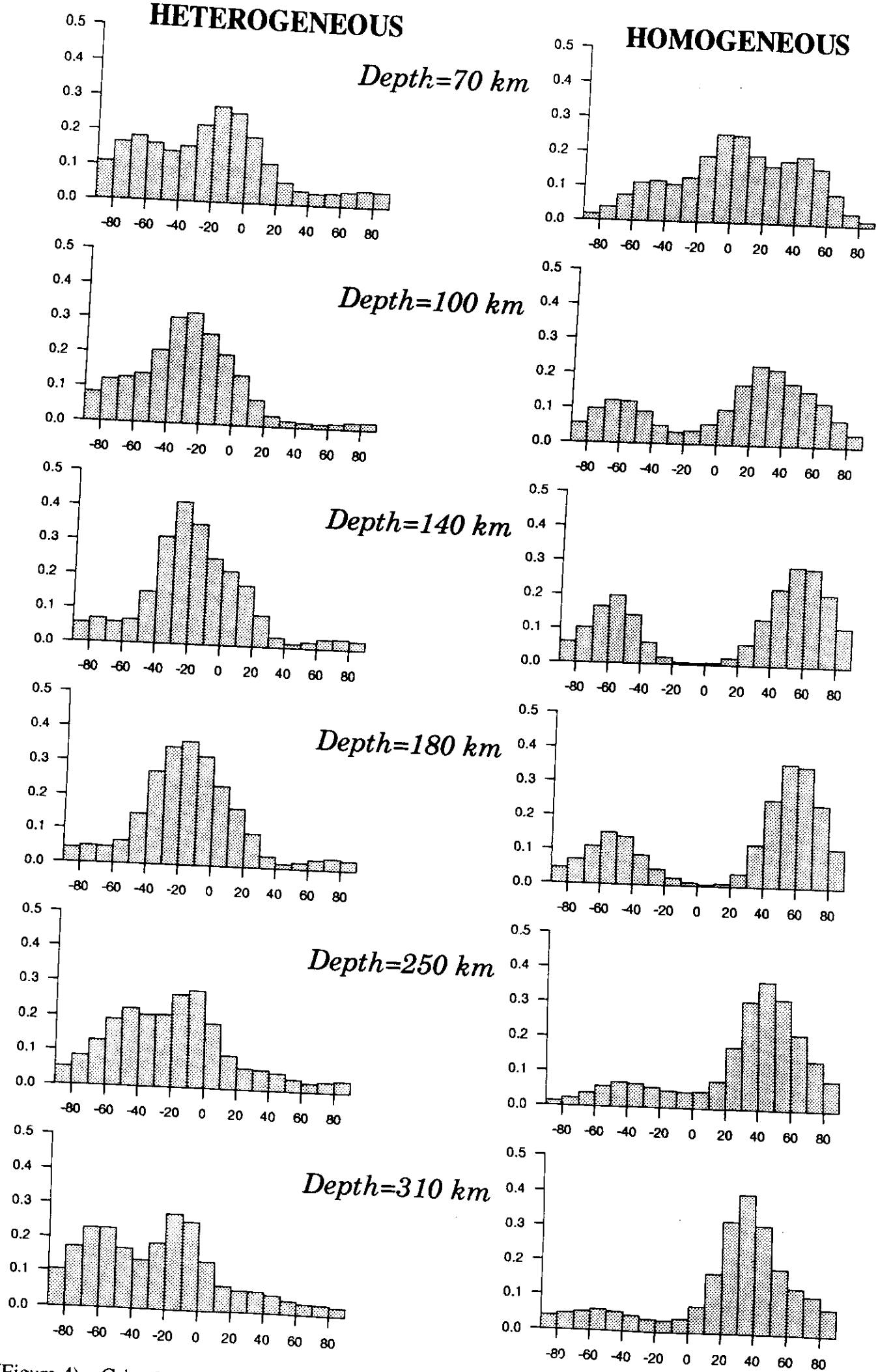

(Figure 4) Griot, D.A., Montagner, J.P. & Tapponnier, P. (1991)

Ackowledgments CNRS URA 195 - I.U.F. This work was partly supported by 'ATP Tomographie' (1996). This is I.P.G.P. contribution # .

References

REFERENCES

Agnew, D., J. Berger, R. Buland, W. Farrell and F. Gilbert, International deployment of accelerometers: A network of very long period seismology, *EOS, Trans. Am. Geophys. Un.*, **57**, 180-188, 1976.

Aki, K., A. Christofferson, and E.S. Husebye, Determination of the three-dimensional seismic structure of the lithosphere, *J. Geophys. Res.*, **82**, 277-296, 1977.

Aki, K., and K. Kaminuma, Phase velocity of Love waves in Japan (part 1): Love waves from the Aleutian shock of March 1957, *Bull. Earthquake Res. Inst.*, **41**, 243–259, 1963.

Aki, K., and P. G. Richards, *Quantitative Seismology: Theory and Methods*, W. H. Freeman, San Fransisco, 1980.

Anderson, D. L., Elastic wave propagation in layered anisotropic media, *J. Geophys. Res.*, **66**, 2953-2963, 1961.

Anderson, D. L., *Theory of the Earth*, Blackwell scientific publications, Oxford, 1989.

Anderson, D. L., and J. D. Bass, Mineralogy and composition of the upper mantle, *Geophys. Res. Lett.*, **11**, 637-640, 1984.

Anderson, D. L., and J. D. Bass, Transition region of the Earth's upper mantle, *Nature*, **320**, 321-328, 1986.

Anderson, D. L., and A. M. Dziewonski, Upper mantle anisotropy: Evidence from fre oscillations, *Geophys. J. R. Astron. Soc.*, **69**, 383-404, 1982.

Anderson, D. L., and J. Regan, Upper mantle anisotropy and the oceanic lithosphere, *Geophys. Res. Lett.*, **10**, 841-844, 1983.

Ando, M., ScS polarization anisotropy around the Pacific Ocean, *J. Phys. Earth*, **32**, 179–196, 1984.

Ando, M., Y. Ishikawa and F. Yamazaki, Shear wave polarization anisotropy in the upper mantle beneath Honshu, Japan, *J. Geophys.Res.*, **88**, 5850–5864, 1983.

Ansel, V., and H.C Nataf, Anisotropy beneath 9 stations of the Geoscope broadband network as deduced from shear wave splitting, *Geophys. Res. Lett.*, **16**, 409–412, 1989.

Backus, G. E., Possible forms of seismic anisotropy of the upper mantle under oceans, *J. Geophys. Res.*, **70**, 3249-3439, 1965.

Backus, G. E., and F. Gilbert, Numerical applications of a formalism for geophysical inverse problems, *Geophys. J. R. Astron. Soc.*, **13**, 247-276, 1967.

Backus, G. E., and J. F. Gilbert, The resolving power of gross earth data, *Geophys. J. R. Astron. Soc.*, **16**, 169-205, 1968.

Backus, G. E., and F. Gilbert, Uniqueness in the inversion of inaccurate gross earth data, *Philos. Trans. R. Soc. London, Ser. A*, **266**, 123-192, 1970.

Barruol, G., and D. Mainprice, A quantitative evaluation of the contribution of crustal rocks to the shear-wave splitting of teleseismic SKS waves, *Phys. Earth Planet. Int.*, **78**, 281-300, 1993.

Birch, F., Elasticity and constitution of the Earth's interior, *J. Geophys. Res.*, **57**, 227-286, 1952.

Bowman, J.R., and M. Ando, Shear-wave splitting in the upper mantle wedge above the Tonga subduction zone. *Geophys. J.R. Astron. Soc.*, **88**, 25–41, 1987.

Bussy, M., J.P. Montagner, and B. Romanowicz, Tomographic model of attenuation in the Pacific Ocean, *Geophys. Res. Lett.*, **20** , 663-666, 1993.

Butkov, E., *Mathematical Physics*, Addison-Wesley Publishinig Company, Reading, Ma, 735PP., 1968.

Canas, J. A., and B. J. Mitchell, Lateral variation of surface wave anelastic attenuation across the Pacific, *Bull. Seism. Soc. Am.*, **68**, 1637-1650, 1978.

Cara, M., Regional variations of Rayleigh-mode velocities: a spatial filtering method, *Geophys. J; R. Astr. Soc.*, **57**, 649-670, 1978.

Cara, M., and J. J. Leveque, Anisotropy of the asthenosphere: The higher mode data of the Pacific revisited, *Geophys. Res. Lett.*, **15**, 205-208, 1988.

Cazenave, A., A. Souriau, and K. Dominh, Global coupling of Earth surface topography with hotspots geoid and mantle heterogeneities, *Nature*, **340**, 54–57, 1989.

Christensen, N.I., and S. Lundquist, Pyroxene orientation within the upper mantle, *Bull. Geol. Soc. Am.*, **93**, 279-288, 1982.

Clayton, R. W., and R. P. Comer, A tomographic analysis of mantle heterogeneities from body wave travel time data, *EOS, Trans. Am. Geophys. Un.*, **64**, 776, 1983.

Clevede, E., and P. Lognonne, Fréchet derivatives of coupled seismograms with to an anelastic rotating Earth, *Geophys. J. Int.*, submitted, 1994.

Cohen-Tannoudji, C., B. Diu, and F. Laloë, *Quantum Mechanics*, Hermann, Paris, and John Wiley & Sons, New-York, 1977.

Crampin, S., An introduction to wave propagation in anisotropic media, *Geophys. J. R. Astron. Soc.*, **76**, 17–28, 1984.

Dost, B., Upper mantle structure under western Europe from fundamental and higher mode surface waves using the NARS array, *Geophys. J; R. Astron. Soc.*, **100**, 131-151, 1990.

Durek, J.J., M.H. Ritzwoller, and J.H. Woodhouse, Constraining upper mantle anelasticity using surface wave amplitude anomalies, *Geophys. J. Int.*, **114**, 249-272, 1993.

Dziewonski, A. M., Mapping the lower mantle: Determination of lateral heterogeneity in P velocity up to degree and order 6, *J. Geophys. Res.*, **89**, 5929-5952, 1984.

Dziewonski, A. M., and D. L. Anderson, Preliminary Reference Earth Model, *Phys. Earth Planet. Int.*, **25**, 297-356, 1981.

Dziewonski, A. M., and J. M. Steim, Dispersion and attenuation of mantle waves from waveform inversion, *Geophys. J. R. Astron. Soc.*, **70**, 503-527, 1982.

Dziewonski, A. M., G. Chou, and J.H. Woodhouse, Determination of earthquake source parameters from waveform modeling, *J. Geophys. Res.*, **86**, 2825-2852, 1981.

Dziewonski, A. M., and J. H. Woodhouse, Global images of the Earth's interior, *Science*, **236**, 37-48, 1987.

Dziewonski, A.M. and Purdy, *proc. Workshop on Broad-Band Downhole Seismometers in the Deep Ocean*, Woods Hole, MA, Apr. 26-28, 1988, Joint Oceanogr. Inst. and U.S. Sci. Advisory Comm., 1989.

Edmonds, A. R., *Angular Momentum and Quantum Mechanics*, Princeton University Press, Princeton, NJ, 1960.

Forsyth, D. W., The early structural evolution and anisotropy of the oceanic upper mantle, *Geophys. J. R. Astron. Soc.*, **43**, 103-162, 1975.

Fukao, Y., Evidence from core- reflected shear waves for anisotropy in the Earth's mantle, *Nature*, **309**, 695–698, 1984.

Futterman, W. I., Dispersive body waves, *J. Geophys. Res.*, **67**, 5279-5291, 1962.

Geller, R. J., and T. Hara, Two efficient algorithms for iterative linearized inversion of seismic waveform data, *Geophys. J. Int.*, **115**, 699-710, 1993.

Gilbert, F., Excitation of normal modes of the Earth by earthquake sources, *Geophys. J. R. Astron. Soc.*, **22**, 223-226, 1971.

Hadiouche, O., N. Jobert and J.P. Montagner, Anisotropy of the African continent inferred from surface waves, *Phys. Earth Planet. Int.*, *58*, 61–81, 1989.

Hager, B., and R. O'Connell, Kinematic models of large-scale flow in the Earth's mantle, *J. Geophys. Res.*, **84**, 1031–1048, 1979.

Hager, B.H., R.W. Clayton, M.A. Richards, R.P. Comer, and A.M. Dziewonski, Lower mantle heterogeneity, dynamic topography and the geoid, *Nature*, **313**, 541-545, 1985.

Hess, H., Seismic anisotropy of the uppermost mantle under the oceans, *Nature*, **203**, 629–631, 1964.

Humler, E., J.L. Thirot, and J.P. Montagner, Global correlations of ocean ridge basalt chemistry with seismic tomographic images, *Nature*, **364**, 225-228, 1993.

Inoue, H., Y. Fukao, K. Tanabe and Y. Ogata, Whole mantle P-wave travel time tomography, *Phys. Earth Planet. Int.*, **59**, 294-328, 1990.

Jobert, N., and G. Roult, Periods and damping of free oscillations observed in France after sixteen earthquakes, *Geophys. J. R. Astron. Soc.*, **45**, 155-176, 1978.

Jordan, T. H., A procedure for estimating lateral variations from low-frequency eigenspectra data, *Geophys. J. R. Astron. Soc.*, **52**, 441-455, 1978.

Kanazawa, T., K. Suyehiro, N. Hirata, and M. Shinohara, Performance of the ocean broadband downhole seismometer at site 794, *Proc. ODP, Scientific Results, 127/128*, 1992.

Lerner-Lam, A.L., and T.H. Jordan, Earth structure from fundamental and higher-mode waveform analysis, *Geophys. J.R. astr. Soc.*, **75**, 759-797, 1983.

Lévêque, J.J., and M. Cara, Inversion of multimode surface wave data: evidence for sub–lithospheric anisotropy, *Geophys. J.R. astr. Soc.*, **83**, 753-773, 1985.

Lévêque, J.J., M. Cara, and D. Rouland, Waveform inversion of surface-wave data: a new tool for systematic investigation of upper mantle structures, *Geophys. J. Int.*, **104**, 565-581, 1991.

Levshin, A., and Ratnikova, Apparent anisotropy in inhomogeneous media, *Geophys. J.R. astr. Soc.*, **76**, 65-69, 1984.

Liu, H.-P., D. L. Anderson and H. Kanamori, Velocity dispersion due to anelasticity; implications for seismology and mantle composition, *Geophys. J. R. Astron. Soc.*, **47**, 41-58, 1976.

Lognonné P., Normal modes and seismograms of an aneleastic rotative Earth, *J. Geophys. Res.*, **96**, 20,309-20,319, 1991.

Lognonné, P., and B. Romanowicz, Modelling of coupled normal modes of the Earth: the spectral method, *Geophys. J.*, **102**, 365-395, 1990.

Love, A. E. H., *A Treatise on the Theory of Elasticity*, 4th edn., Cambridge University Press, 643pp, 1927.

Marquering, H., and R. Snieder, Surface-wave mode coupling for efficient forward modelling and inversion of body-wave phases, *Geophys. J. Int.*, **120**, 186-208, 1995.

Masters, G., and F. Gilbert, Attenuation in the Earth at low frequencies, *Philos. Trans. R. Soc. London, Ser. A*, **308**, 479-522, 1983.

Masters, G., T. H. Jordan, P. G. Silver and F. Gilbert, Aspherical earth structure from fundamental spheroidal mode data, *Nature*, **298**, 609-613, 1982.

Masters, G., and M. Ritzwoller, Low frequency seismology and three-dimensional structure - observational aspects, 1-30, in *Mathematical Geophysics*, eds N.J. Vlaar, G. Nolet, M.J.R. Wortel, and S.A.P.L. Cloetingh, Reidel, Dordrecht, 1988.

Maupin, V., Surface waves in weakly anisotropic structures: on the use of ordinary or quasi-degenrate perturbation methods, *Geophys. J. Int.*, **98**, 553-563, 1989.

Minster, J. B., and T. H. Jordan, Present-day plate motions, *J. Geophys. Res.*, **83**, 5331-5354, 1978.

Mitchell, B. J., Regional Rayleigh wave attenuation in North America, *J. Geophys. Res.*, **80**, 4904-4916, 1975.

Mitchell, B. J., and G.-K. Yu, Surface wave dispersion, regionalized velocity models and anisotropy of the Pacific crust and upper mantle, *Geophys. J. R. Astron. Soc.*, **63**, 497-514, 1980.

Mochizuki, E., Free oscillations and surface waves of an aspherical Earth, *Geophys. Res. Lett.*, **13**, 1478-1481, 1986.

Mochizuki, E., The free oscillations of an anisotropic and heterogeneous Earth, *Geophys. J. R. Astron. Soc.*, **86**, 167-176, 1986.

Montagner, J.-P., Seismic anisotropy of the Pacific Ocean inferred from long-period surface wave dispersion, *Phys. Earth Planet. Int.*, **38**, 28-50, 1985.

Montagner, J.-P., First results on the three dimensional structure of the Indian Ocean inferred from long period surface waves, *Geophys. Res. Lett.*, **13**, 315-318, 1986a.

Montagner J.P., Regional three-dimensional structures using long-period surface waves, *Ann. Geophys.*, **4**, B3, 283–294, 1986b.

Montagner, J.P., Etude du manteau supérieur à partir des ondes de surface sismiques, Thèse d'Etat, Université Pierre and Marie Curie, Paris, 1986c.

Montagner, J.P., What can seismology tell us about mantle convection? *Rev. Geophys.*,**32,2**, 115-137, 1994.

Montagner, J.P., and Anderson D.L., Constraints on elastic combinations inferred from petrological models, *Phys. Earth Planet. Int.*, **54**, 82–105, 1989a.

Montagner J.P., and Anderson D.L., Constrained reference mantle model, *Phys. Earth Planet. Int.*, **58**, 205- 227, 1989b.

Montagner, J.-P., and N. Jobert, Investigation of upper mantle structure under younger regions of the southeast Pacific using long-period Rayleigh waves, *Phys. Earth Planet. Int.*, **27**, 206-222, 1981.

Montagner J.P., and N. Jobert, Vectorial Tomography. II: Application to the Indian Ocean, *Geophys. J.R. astr. Soc.*, **94**, 309–344, 1988.

Montagner, J.-P., and H.-C. Nataf, On the inversion of the azimuthal anisotropy of surface waves, *J. Geophys. Res.*, **91**, 511–520, 1986.

Montagner J.P.and Nataf H.C., Vectorial Tomography. I: Theory. *Geophys. J.R. astr. Soc.*, **94**, 295-307, 1988.

Montagner, J.-P., and T. Tanimoto, Global anisotropy in the upper mantle inferred from the regionalization of phase velocities, *J. Geophys. Res.*, **95**, 4797-4819, 1990.

Montagner J.P., and Tanimoto T., Global upper mantle tomography of seismic velocities and anisotropies, *J. Geophys. Res.*, **96**, 20,337-20,351, 1991.
Montagner, J.P., B. Romanowicz, and J.F. Karczewski, A first step towards an Oceanic Geophysical observatory, *EOS, Trans. Am. Geophys. Un.*, **75**, 150-154, 1994.
Montagner, J.P., J.F. Karczewski, B. Romanowicz, S. Bouaricha, P. Lognonne, G. Roult, E. Stutzmann, J.L. Thirot, D. Fouassier, J.C. Koenig, J. Savary, L. Floury, J. Dupond, A. Echardour, H. Floc'h, The French Pilot experiment OFM/SISMOBS: First scientific results on noise and event detection, *Phys. Earth Planet. Int.*, **84**, 321-326, 1994.
Montagner, J.P., and B. Romanowicz, Degrees 2, 4, 6 inferred from seismic tomography, *Geophys. Res. Lett.*, **20**, 631-634, 1993.
Morgan, W. J., Convection plumes in the lower mantle, *Nature*, **230**, 42-43, 1971.
Nakanishi, I., Phase velocity and Q of mantle Rayleigh waves, *Geophys. J. R. Astron. Soc.*, **58**, 35-59, 1979a.
Nakanishi, I., Regional differences in the phase velocity and the quality factor Q of mantle Rayleigh waves, *Science*, **200**, 1379-1381, 1979b.
Nakanishi, I., and D. L. Anderson, Measurement of mantle wave velocities and inversion for lateral heterogeneity and anisotropy, II. Analysis by the single station method, *Geophys. J. R. Astron. Soc.*, **78**, 573-618, 1984.
Nataf, H.-C., I. Nakanishi and D. L. Anderson, Anisotropy and shear velocity heterogeneities in the upper mantle, *Geophys. Res. Lett.*, **11**, 109-112, 1984.
Nataf, H.-C., I. Nakanishi and D. L. Anderson, Measurement of mantle wave velocities and inversion for lateral heterogeneity and anisotropy, III. Inversion, *J. Geophys. Res.*, **91**, 7261-7307, 1986.
Nicolas, A., Why fast polarization directions of SKS seismic waves are parallel to mountain belts?, *Phys. Earth Planet. Int.*, **78**, 337-342, 1993.
Nishimura, C. E., and D. W. Forsyth, The anisotropic structure of the upper mantle in the Pacific, *Geophys. J.*, **96**, 203-229, 1989.
Nolet, G., Higher Rayleigh modes in Western Europe, *Geophys. Res. Lett.*, **2**, 60-62, 1975.
Nolet, G., Partitioned waveform inversion and two-dimensional structure under the network of autonomously recording seismographs, *J. Geophys. Res.*, **95**, 8499-8512, 1990.
Nolet, G., and B.J. Kennett, Normal-mode representation of multiple ray reflections in a spherical Earth, *Geophys. J. R. Astr. Soc.*, **53**, 219-226, 1978.
Okal, E., and B.-G. Jo, stacking investigation of higher-order mantle Rayleigh waves, *Geophys. Res. Lett.*, **12**, 421-424, 1985.
Park, J., Synthetic seismograms from coupled free oscillations: Effects of lateral structure and rotation, *J. Geophys. Res.*, **91**, 6441-6464, 1986.
Park, J., Asymptotic coupled-mode expressions for multiplet amplitude anomalies and frequency shifts on an aspherical Earth, *Geophys. J. R. Astron. Soc.*, **90**, 129-169, 1987.
Park, J., and F. Gilbert, Coupled free oscillations of an aspherical, dissipative, rotating Earth: Galerkin theory, *J. Geophys. Res.*, **91**, 7241-7260, 1986.
Peselnick, L., A. Nicolas, and P.R. Stevenson, Velocity anisotropy in a mantle peridotite from Ivrea zone: Application to uper mantle anisotropy, *J. Geophys. Res.*, **79**, 1175-1182, 1974.
Peselnick, L., and A. Nicolas, Seismic anisotropy in an ophiolite peridotite. Application to oceanic upper mantle, *J. Geophys. Res.*, **83**, 1227-1235, 1978.
Peterson, J., H. M. Butler, L. G. Holcomb and C. R. Hutt, The Seismic Research Observatory, *Bull. Seism. Soc. Am.*, **66**, 2049-2068, 1977.
Phinney, R. A., and R. Burridge, Representation of the elastic-gravitational excitation of a spherical earth model by generalized spherical harmonics, *Geophys. J. R. Astron. Soc.*, **34**, 451-487, 1973.
Richards, M. A., and B. H. Hager, The Earth's geoid and the large scale structure of mantle convection, in: *The Physics of the Planets*, S. J. Runcorn (Ed.), 247-271, 1988.
Ringwood, A.E., Composition and petrology of the Earth's mantle, McGraw-Hill, New-York, 618pp, 1975.
Ritzwoller, M., G. Masters, and F. Gilbert, Observations of anomalous splitting and their interpretation in terms of aspherical structure, *J. Geophys. Res.*, **91**, 10,203-10,228, 1986.
Ritzwoller, M., G. Masters, and F. Gilbert, Constraining aspherical structure with low frequency interaction coefficients: Application to uncoupled multiplets, *J. Geophys. Res.*, **93**, 6369-6396, 1986.
Robin, L., Fonctions sphériques de Legendre et fonctions sphéroidales, Gauthier-Villars, Paris, 1958.

Romanowicz, B., Multiplet-multiplet coupling due to lateral heterogeneity: asymptotic effects on the amplitude and frequency of the Earth's normal modes, *Geophys. J. R. Astron. Soc.*, **90**, 75-100, 1987.

Romanowicz, B., The upper mantle degree two: Constraints and inferences from global mantle wave attenuation measurements, *J. Geophys. Res.*, **95**, 11,051- 11,071, 1990.

Romanowicz, B., On the measurements of anelastic attenuation using amplitudes of low-frequency surface waves, *Phys. Earth Planet. Int.*, **84**, 179-191, 1994a.

Romanowicz, B., Anelastic Tomography: A new perspective on upper-mantle thermal structure, *Earth Planet. Sci. Lett.*, in press, 1994b.

Romanowicz, B., and G. Roult, First-order asymptotics for the eigenfrequencies of the Earth and application to the retrieval of large-scale lateral variations of structure, *Geophys. J. R. Astron. Soc.*, **87**, 209-239, 1986.

Romanowicz, B., and R. Snieder, A new formalism for the effect of lateral heterogeneity on normal modes and surface waves, II: General anisotropic perturbations, *Geophys. J. R. Astron. Soc.*, **93**, 91-99, 1988.

Romanowicz, B., M. Cara, J. F. Fels, and D. Rouland, GEOSCOPE: a French initiative in long period, three component, global seismic networks, *EOS, Trans. Am. Geophys. Un.*, **65**, 753-754, 1984.

Roult, G., Rouland, D., and J.P. Montagner, Phase velocity distribution of the Indian Ocean inferred from Geoscope records, m Geophys. Res. Lett., **14** 343-346, 1987.

Roult, G., B., Romanowicz, and J.-P. Montagner, 3D upper mantle shear velocity and attenuation from fundamental mode free oscillation data, *Geophys. J.*, **101**, 61-80, 1990.

Roult, G., D. Rouland, and J.P. Montagner, Antarctica II: Upper mantle structure from velocity and anisotropy, *Phys. Earth Planet. Int.*, **84**, 33- , 1994.

Schlue, J.W., and L. Knopoff, Shear–wave polarization anisotropy in the Pacific Ocean, *Geophys. J.R. astr. Soc.*, **49**, 145–165, 1977.

Silver, P.G., and W.W. Chan, Implications for continental structure and evolution from seismic anisotropy, *Nature*, **335**, 34–39, 1988.

Silver, P.G., and W.W. Chan, Shear wave splitting and subcontinental mantle deformation, **J. Geophys. Res.**, **96**, 16,429– 16,454, 1991.

Smith, S. W., IRIS; a program for the next decade, *EOS, Trans. Am. Geophys. Un.*, **67**, 213-219, 1986.

Smith, M. L., and F. A. Dahlen, The azimuthal dependence of Love and Rayleigh wave propagation in a slightly anisotropic medium, *J. Geophys. Res.*, **78**, 3321-3333, 1973.

Smith, M. L., and F. A. Dahlen, Correction to 'The azimuthal dependence of Love and Rayleigh wave propagation in a slightly anisotropic medium', *J. Geophys. Res.*, **80**, 1923, 1975.

Snieder, R., 3D linearized scattering of surface waves and a formalism for surface wave holography, *Geophys. J. R. Astron. Soc.*, **84**, 581-605, 1986.

Snieder, R., Large-scale waveform inversions of surface waves for lateral heterogeneity, 1. Theory and numerical examples, *J. Geophys. Res.*, **93**, 12,055-12,066, 1988a.

Snieder, R., Large-scale waveform inversions of surface waves for lateral heterogeneity, 2. Application to surface waves in Europe and the Mediterranean, *J. Geophys. Res.*, **93**, 12,067-12,080, 1988b.

Snieder, R., Global inversions using normal modes and long-period surface waves, 23-63, in *Seismic Tomography* Eds. H.M. Iyer and K. Hirahara, Chapman and Hall, London, 1993.

Snieder, R., Surface wave inversions on a regional scale, *lecture notes for the International School of Solid Earth Geophysics*, Erice, 1994.

Snieder, R., and G. Nolet, Linearized scattering of surface waves, *J. Geophys.*, **61**, 55-63, 1987.

Snieder, R., J. Beckers, and F. Neele, The effect of small-scale structure on normal mode frequencies and global inversions, *J. Geophys. Res.*, **96**, 501-515, 1991.

Snieder, R., and B. Romanowicz, A new formalism for the effect of lateral heterogeneity on normal modes and surface waves, I: Isotropic perturbations, perturbations of interfaces and gravitational perturbations, *Geophys. J. R. Astron. Soc.*, **92**, 207-222, 1988.

Stutzmann, E., and J.P. Montagner, An inverse technique for retrieving higher mode phase velocity and mantle structure, *Geophys. J. Int.*, **113**, 669-683, 1993.

Stutzmann, E., and J.P. Montagner,Tomography of the transition zone from the inversion of higher-mode surface waves, *Phys. Earth Planet. Int.*, **86**, 99-116, 1994.

Su, W.J., and A.M. Dziewonski, Predominance of long-wavelength heterogeneity in the mantle, *Nature*, **352**, 121-126, 1991.

Su, W.J., and A.M. Dziewonski, On the scale of mantle heterogeneity, *Phys. Earth Planet. Inter.*, **74**, 29-54, 1992.

Su, W.J., R.L. Woodward, and A.M. Dziewonski, *Nature*, **360**, 149-152, 1992.

Su, L., J. Park, and Y. Yu, Born seismograms using coupled free oscillations: the effect of strong coupling and anisotropy, *Geophys. J. Int.*, **115**, 849-862, 1993.

Suda, N., Shibata, N., and Y. Fukao, degree 2 pattern of attenuation structure in the upper mantle from apparent complex frequency measurements of fundamental spheroidal modes, *Geophys. Res. Lett.*, **18**, 1119-1122, 1991.

Suetsugu, D., and I. Nakanishi, Regional and azimuthal dependence of phase velocities of mantle Rayleigh waves in the Pacific Ocean, *Phys. Earth Planet. Int.*, **47**, 230–245, 1987.

Takeuchi, H., and M. Saito, Seismic surface waves, *Methods Comput. Phys.*, **11**, 217-295, 1972.

Tanimoto, T., A simple derivation of the formula to calculate synthetic long period seismograms in a heterogeneous earth by normal mode summation, *Geophys. J. R. Astron. Soc.*, **77**, 275-278, 1984a.

Tanimoto, T., Waveform inversion of mantle Love waves: The Born seismogram approach, *Geophys. J. R. Astron. Soc.*, **78**, 641-660, 1984b.

Tanimoto, T., The Backus-Gilbert approach to the three-dimensional structure in the upper mantle, 1. Lateral variation of surface wave phase velocity with its error and resolution, *Geophys. J. R. Astron. Soc.*, **82**, 105-123, 1985.

Tanimoto, T., Free oscillations in a slightly anisotropic Earth, *Geophys. J. R. Astron. Soc.*, **87**, 493-517, 1986.

Tanimoto, T., Long-wavelength *S*-wave velocity structure throughout the mantle, *Geophys. J. Int.*, **100**, 327-336, 1990.

Tanimoto, T., and D. L. Anderson, Lateral heterogeneity and azimuthal anisotropy of the upper mantle: Love and Rayleigh waves 100–250s, *J. Geophys. Res.*, **90**, 1842-1858, 1985.

Tarantola, A., and B. Valette, Generalized non-linear inverse problems solved using the least squares criterion, *Rev. Geophys. Space Phys.*, **20**, 219-232, 1982.

Tromp, J., and F.A. Dahlen, Free oscillations of a spherical anelastic earth, *Geophys. J. Int.*, **103**, 707-723, 1990.

Vauchez, A., and A. Nicolas, Mountain building: strike-parallel motion and mantle anisotropy, *Tectonophys.*, **185**, 183-191, 1991.

Vinnik, L.P., G.L. Kosarev and L.I. Makeyeva, Anisotropiya litosfery po nablyudeniyam voln SKS and SKKS, *Doklady Akademii Nauk USSR*, **278**, 1335–1339, 1984.

Vinnik, L.P., R. Kind, G.L. Kosarev, and L.I. Makeyeva, Azimuthal Anisotropy in the lithosphere from observations of long–period S–waves, *Geophys. J. Int.*, **99**, 549–559, 1989a.

Vinnik, L.P., V. Farra, and B. Romanowicz, Azimuthal anisotropy in the earth from observations of SKS at GEOSCOPE and NARS broadband stations, *Bull. Seism. Soc. Am.*, **79**, 1542–1558, 1989b.

Vinnik, L., L.I. Makayeva, A. Milev, A.Y. Usenko, Global patterns of azimuthal anisotropy and deformations in the continental mantle, *Geophys. J. Int.*, *111*, 433-447, 1992.

Widmer, R., G. Masters, and F. Gilbert, Spherically symmetric attenuation within the Earth from normal mode data, *Geoph. J. Int.*, **104**, 541-553, 1993.

Wong, Harvard PhD Thesis, 1989.

Woodhouse, J. H., The joint inversion of seismic waveforms for lateral variations in Earth structure and earthquake source parameters, Proc. "Enrico Fermi" Int. Sch. Phys. *LXXXV* (H. Kanamori and E. Boschi, eds.), 366-397, 1983.

Woodhouse, J. H., and F. A. Dahlen, The effect of a general aspherical perturbation on the free oscillations of the Earth, *Geophys. J. R. Astron. Soc.*, **53**, 335-354, 1978.

Woodhouse, J. H., and A. M. Dziewonski, Mapping the upper mantle: Three dimensional modelling of Earth structure by inversion of seismic waveforms, *J. Geophys. Res.*, **89**, 5953-5986, 1984.

Woodhouse, J. H., and T. P. Girnius, Surface waves and free oscillations in a regionalized Earth model, *Geophys. J. R. Astron. Soc.*, **68**, 653-673, 1982.

Woodhouse, J. H., and Y. K. Wong, Amplitude, phase and path anomalies of mantle waves, *Geophys. J. R. Astron. Soc.*, **87**, 753-773, 1986.

Woodward, R. L., and G. Masters, Global uppper mantle structure from long-period differential travel-times, *J. Geophys. Res.*, **96**, 6351-6377, 1991a.

Woodward, R., and G. Masters, Lower-mantle structure from long period differential travel times, *Nature*, **352**, 231-233, 1991b.

Yu, Y., and J. Park, Anisotropy and coupled long-period surface waves, *Geophys. J. Int.*, **114** , 473-489, 1993.

Zhang, Y., and T. Tanimoto, High resolution global upper mantle structure; plate tectonics, *J. Geophys. Res.*, **98**, 9793-9823, 1993.

Zielhuis, A., and G. Nolet, Deep seismic expression of an ancient plate boundary in Europe, *Science*, **265**, 79-81, 1994.